AD-A047 386 WEIDLINGER ASSOCIATES MENLO PARK CALIF F/G 13/13
NUMERICAL SIMULATION OF FORCED VIBRATION TESTS ON A BURIED ARCH--ETC(U)
MAR 77 J ISENBERG, H S LEVINE, S H PANG DNA001-76-C-0110
UNCLASSIFIED 7712 DNA-4281F NL

1 OF 2
AD
A047386

(12) AD-E300021

DNA 4281F

NUMERICAL SIMULATION OF FORCED VIBRATION TESTS ON A BURIED ARCH

Weidlinger Associates
Suite 245, Building 4
3000 Sand Hill Road
Menlo Park, California 94025

1 March 1977

Final Report for Period March 1976—March 1977

CONTRACT NO. DNA 001-76-C-0110

APPROVED FOR PUBLIC RELEASE;
DISTRIBUTION UNLIMITED.

THIS WORK SPONSORED BY THE DEFENSE NUCLEAR AGENCY
UNDER RDT&E RMSS CODE B344076462 L19GAXSX33802 H2590D.

Prepared for
Director
DEFENSE NUCLEAR AGENCY
Washington, D. C. 20305

Destroy this report when it is no longer needed. Do not return to sender.

UNCLASSIFIED

SECURITY CLASSIFICATION OF THIS PAGE (When Data Entered)

REPORT DOCUMENTATION PAGE

READ INSTRUCTIONS BEFORE COMPLETING FORM

1. REPORT NUMBER: DNA 4281F

2. GOVT ACCESSION NO.

3. RECIPIENT'S CATALOG NUMBER

4. TITLE (and Subtitle): NUMERICAL SIMULATION OF FORCED VIBRATION TESTS ON A BURIED ARCH.

5. TYPE OF REPORT & PERIOD COVERED: Final Report, for Period Mar 76—Mar 77,

6. PERFORMING ORG. REPORT NUMBER: 7712

7. AUTHOR(s): J. Isenberg, H. S. Levine, S. H. Pang

8. CONTRACT OR GRANT NUMBER(s): DNA 001-76-C-0110

9. PERFORMING ORGANIZATION NAME AND ADDRESS: Weidlinger Associates, Suite 245, Building 4, 3000 Sand Hill Road, Menlo Park, California 94025

10. PROGRAM ELEMENT, PROJECT, TASK AREA & WORK UNIT NUMBERS: Subtask L19GAXSX338-02

11. CONTROLLING OFFICE NAME AND ADDRESS: Director, Defense Nuclear Agency, Washington, D.C. 20305

12. REPORT DATE: 1 March 1977

13. NUMBER OF PAGES: 104

14. MONITORING AGENCY NAME & ADDRESS (if different from Controlling Office): 98p.

15. SECURITY CLASS (of this report): UNCLASSIFIED

15a. DECLASSIFICATION/DOWNGRADING SCHEDULE

16. DISTRIBUTION STATEMENT (of this Report): Approved for public release; distribution unlimited.

DNA, SBIE

4281F, AD-E [illegible] 021

17. DISTRIBUTION STATEMENT (of the abstract entered in Block 20, if different from Report)

18. SUPPLEMENTARY NOTES: This work sponsored by the Defense Nuclear Agency under RDT&E RMSS Code B344076462 L19GAXSX33802 H2590D.

19. KEY WORDS (Continue on reverse side if necessary and identify by block number)

Structure-medium Interaction
Finite Element Simulation
Radiation Damping
Friction Damping

20. ABSTRACT (Continue on reverse side if necessary and identify by block number)

Finite element simulation of a buried arch structure shows that the effective damping depends on backfill conditions. This information is used to explain the occurence of resonance in forced vibration tests of buried rectangular structures and its absence in tests of the arch. Implications of the findings for developing single degree of freedom models of complex structures are examined.

DD FORM 1 JAN 73 1473 EDITION OF 1 NOV 65 IS OBSOLETE

UNCLASSIFIED

SECURITY CLASSIFICATION OF THIS PAGE (When Data Entered)

392 150

1B

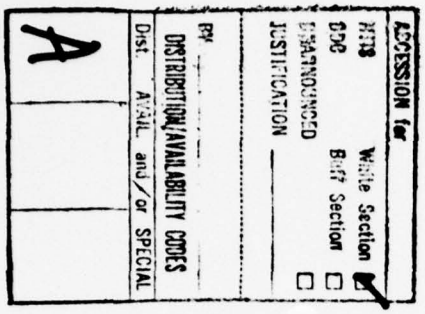

TABLE OF CONTENTS

LIST OF ILLUSTRATIONS

LIST OF ILLUSTRATIONS (continued)

LIST OF ILLUSTRATIONS (continued)

LIST OF TABLES

PREFACE

The work reported below is related to forced vibration testing which was performed on approximately one-third scale model reinforced concrete structures. The tests were performed at Fort Polk, Louisiana, in the Summer and Autumn of 1975 in connection with Event ESSEX-V by personnel of Waterways Experiment Station, Vicksburg, Mississippi. Those at WES who have been especially helpful in obtaining data needed to prepare this report include Dr. J. P. Balsara, Mr. Robert Walker, Dr. Sam Kiger, Mr. Roger Crowson and Mr. Jim Ball. Their cooperation is greatly appreciated.

Acknowledgment is also due Mr. J. P. Wright of Weidlinger Associates, New York, New York, whose suggestions led to pursuing the effect of backfill stiffness on radiation damping. The authors are also indebted to Professor H. H. Bleich, consultant to Weidlinger Associates, who pointed out the possibility that friction at the soil-structure interface is a significant mechanism of energy absorption. The authors are also grateful to Dr. T. L. Geers of Lockheed Palo Alto Research Laboratory who made available results of analytic solutions for vibrations of a cylindrical shell in an infinite elastic domain.

NOTATION

a	radius of shell
A	tributary surface area associated with nodal point
c	wave speed (in general)
c_o, c_s, c_p	bar, shear and dilatational wave speeds, respectively
C	viscous friction coefficient
d	depth of a point on a buried structure below ground surface
E_o, E_m	Young's modulus of structure and idealized soil medium, respectively
F	matrix of friction forces
F_{max}	maximum harmonically-applied force
g	acceleration due to gravity
h	thickness of structure wall
I	area moment of inertia
k	stiffness of single degree-of-freedom oscillator
K	stiffness matrix
l	width of an element
M	mass matrix
n	cycle number (subscript)
N	typical nodal normal force
p	frequency of excitation
P	matrix of externally applied forces
r	radius of arch
t	time
v	particle velocity
V_{max}	maximum velocity
w	weight density
W	weight
x, $\dot{x}$, $\ddot{x}$	displacement, velocity, acceleration
X	maximum displacements in successive cycles of oscillation
X_o	maximum displacement of single degree-of-freedom system

X_{stat}	maximum displacement under statically applied load
α, β_s, μ_o	non-dimensional shell parameters
β_o	ratio of bar wave velocity to dilatational wave velocity
δ	log decrement
Δ	angle subtended by two radii from arch centerline to two adjacent element centroids
ε	strain
η	fraction of critical damping
μ	coefficient of friction
ν_o, ν_m	Poisson's ratio for the structure and soil, respectively
ρ_o, ρ_m	mass density of structure and soil, respectively
σ_h, σ_v	horizontal and vertical components of overburden stress
σ_n	normal stress on surface of structure due to overburden
τ_{max}	maximum friction stress
ϕ	angle of a node on the surface of the arch (positive clockwise from horizontal)
ω	natural frequency of single degree-of-freedom oscillator

SECTION 1

INTRODUCTION

1.1. BACKGROUND

Forced vibration tests were conducted on a 1:3.7 scale buried arch and on two buried rectangular structures at the site of ESSEX-V near Fort Polk, Louisiana. The objective of the tests was to determine stiffness and damping characteristics of the structures before and after backfill was placed. This information is needed in order to develop single degree-of-freedom models of structures for use in target evaluation.

The geometry of the arch and backfill are shown in Figure 1-1. The arch was first tested in the excavation without backfill cover. Then backfill was added and compacted (98-100 pcf) up to original grade level and vibration tests repeated. All vibration testing on the arch was completed before the main ESSEX-V event. The tests and results are described in detail in Ref. 1. Typical results of the tests are shown in Figure 1-2 in the form of impedance (F_{max}/V_{max}) and quadrature (F_{max} times peak acceleration times sine of the phase angle between them) versus frequency. The valleys in the impedance curves and the peaks in the quadrature curves for the uncovered structure show that the peak velocity becomes large (resonance) when the driving frequency approaches a natural frequency of the structure. The curves for the covered structure do not show such peaks or valleys. This is interpreted as absence of resonance. The covered structure was tested three times at peak force levels of 50, 150 and 500 pounds, respectively, and the impedance versus frequency plots were almost identical. This result is considered to confirm the absence of resonance in the covered structure.

Forced vibration tests were also conducted on two 1:3.7 scale rectangular structures, which are illustrated in Figure 1-3. Unlike the arch, these structures were subjected to forced vibration testing after ESSEX-V. The original backfill was excavated, the structures were inspected and were found to be undamaged, and sand backfill was placed by raining from a height of 5 feet.

The plots of impedance and quadrature versus frequency for the stiffer structure (Structure 3D, L/h = 4) with and without backfill, Figure 1-4, exhibit distinct resonances. Similar plots for the more flexible structure (Structure 3B, L/h = 10), Figure 1-5, show resonances for the uncovered structures. Some evidence of weak resonance was also found in the covered structure, but this is somewhat a matter of interpretation of the data.

The observations that resonance did not appear in the arch after backfilling and that resonance was weak in one rectangular structure (L/h = 10) were unexpected. The results cast doubt on the usefulness of forced vibration testing to develop parameters for SDOF models of buried structures. The results also point out a deficiency in fundamental knowledge of soil-structure interaction.

1.2. OBJECTIVE

The objective of the present study is to explain why resonance was suppressed in the buried arch and to determine what changes, if any, should be made in SDOF models of buried arches. The results of the tests on the buried rectangular structure which clearly exhibited resonance were kept in mind when various hypotheses were evaluated. A secondary objective was to study methods of estimating the equivalent percentage of critical viscous damping from the forced vibration test data and also from the various finite element simulations.

1.3. SCOPE

An investigation was made of factors governing the behavior of the arch before and after emplacement of backfill using three-dimensional elastic finite element simulation techniques. The scope of the studies included obtaining mode shapes and frequencies, performing dynamic modal analysis and dynamic step-by-step analysis.

The chief hypothesis of the analytic studies was that adding backfill to the arch increased the effective damping to the point where resonance was significantly reduced or suppressed altogether. This type of effect occurs

in a single degree-of-freedom oscillator with even modest amounts of viscous damping. Figure 1-6 shows that at 12.5 percent critical damping, forced vibration of a SDOF oscillator at its resonant frequency produces only four times the displacement produced by the same peak force applied statically; at 50 percent critical damping, peak dynamic and static displacements are equal (Ref. 2).

Possible sources of damping for the buried arch were identified as follows:

a. Radiation damping

b. Friction between soil and structure

c. Hysteresis in soil adjacent to the structure

Structural damping in the concrete structure was another possible source of damping; it was assumed to be small and was therefore not considered.

The amount of radiation damping for each structure depends on the natural frequencies of the soil-structure system, its geometry and the wave speeds in the soil and structural materials. Differences in geometry between the arch and rectangular structures and in the respective backfill materials may account for different amounts of radiation damping. This is considered to be a significant effect.

Friction must be considered because overburden stresses (σ) of 2 to 10 psi allow maximum friction stresses (τ_{max}) of between .5 psi to 3 psi to develop, based on an assumed coefficient of friction (μ) of .25 to .3 (Ref. 3). Summing these stresses over the surface area of the structure indicates a potential for energy absorption which is comparable to the total of kinetic and potential energy of the structure during the forced vibration tests. Since the geometry of the arch structure is more conducive to generating motions tangent to the soil-structure interface, which enables the friction forces to do work, and since the soil is probably in more effective contact with the arch than with the vertical walls of the rectangular structures, dissipation due to friction may be greater for the arch. Friction is therefore a second possible source of damping which may effect the arch and rectangular structures to different degrees.

Hysteresis in stress-strain relations causes energy to be absorbed by cycles of load-unload or reload which are produced in the soil by oscillation of the structure. The effective hysteretic damping depends on the amount of energy absorbed in each cycle. Although no measurements of soil strains were made during the forced vibration tests, the order of magnitude can be estimated (Ref. 4) from

$$\varepsilon = \frac{v}{c}$$

where

ε = representative strain parameter in the soil

v = peak particle velocity in the soil (.05 in./sec. to .5 in./sec. for 500 pounds maximum force

c = wave speed in the soil (approximately 12,000 in./sec. for backfill.

This leads to estimates of order 5×10^{-6} to 5×10^{-5} in./in. in a small volume of soil adjacent to the structure, and smaller values at greater distances. It is difficult to estimate the energy loss associated with these strain levels because no accurate measurements were made on the backfill material in this range. Earthquake-related research has developed a concept of equivalent critical viscous damping for soil subjected to shear waves (Refs. 5 and 6). The problem of converting this information into fractions of equivalent critical viscous damping for the present soil-structure system is formidable and beyond the scope of the present study; however, an upper bound can be determined by assuming that the structure experiences as much damping as the adjacent elements of soil, which is that associated with the strain range given above. This appears to be about 3 to 4 percent of critical damping.

The present study concentrates on radiation damping and friction. Preliminary estimates suggested that radiation damping is the dominant effect and major emphasis was placed on investigating it. The final results confirmed that radiation effects outweigh friction by 4 or 5 to 1.

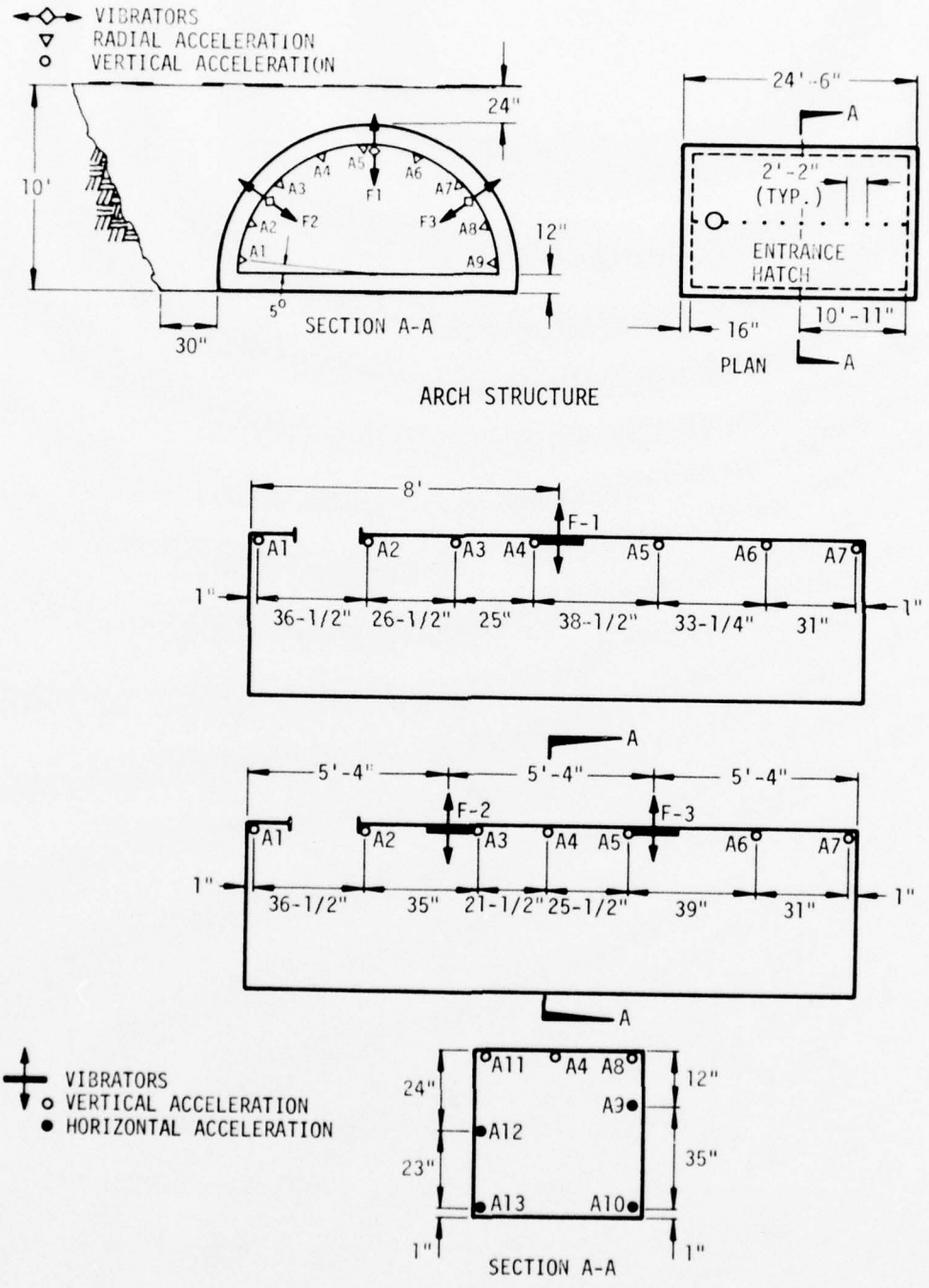

Figure 1-1. Geometry and Instrumentation for Arch and Rectangular Structures.

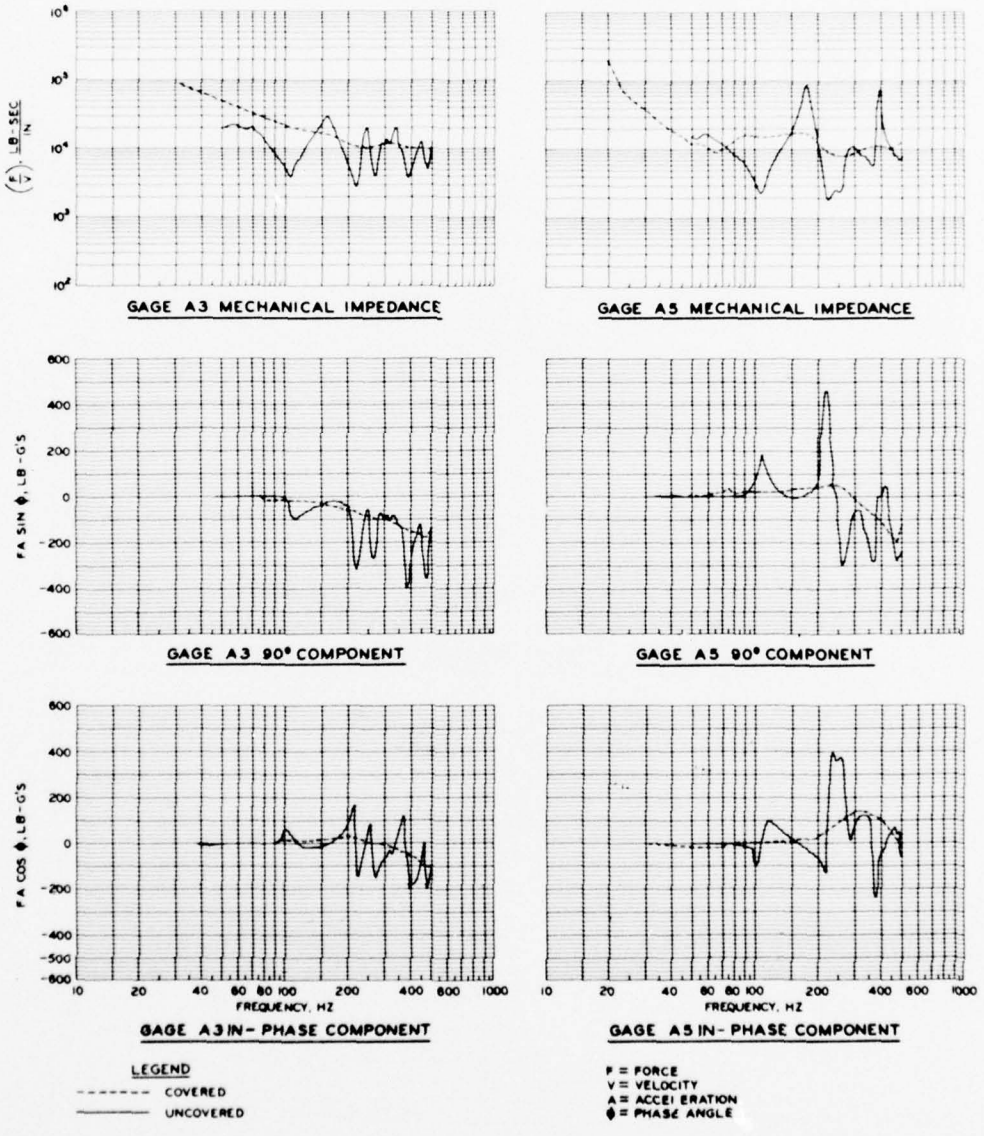

Peak Force F = 500 Pounds

Figure 1-2. Impedance and Quadrature for Arch Before and After Placement of Backfill Determined from Tests with Vibrators In Phase.

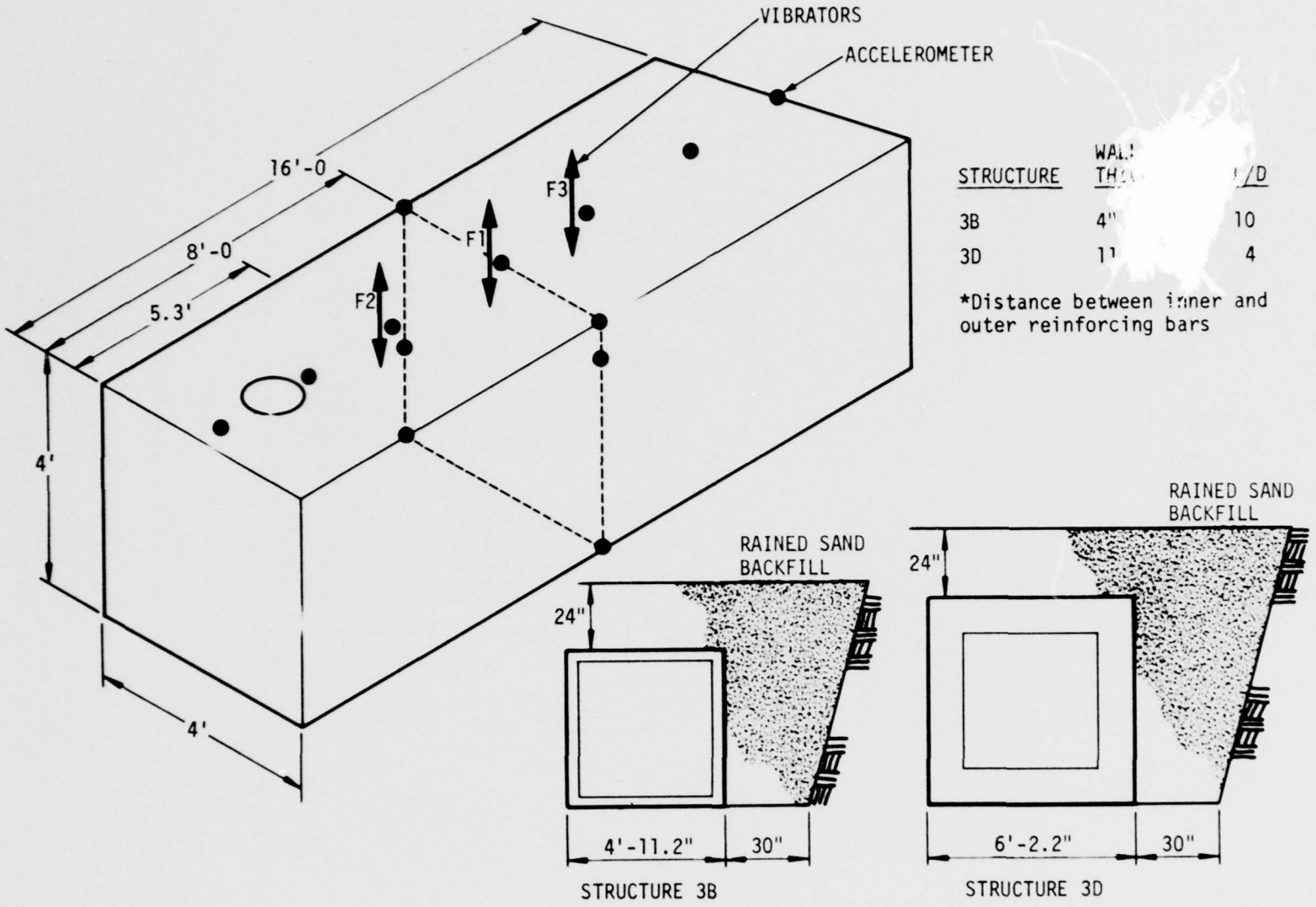

STRUCTURE	WALL THICKNESS	*/D
3B	4"	10
3D	11	4

*Distance between inner and outer reinforcing bars

Figure 1-3. Rectangular Structure and Backfill Geometry.

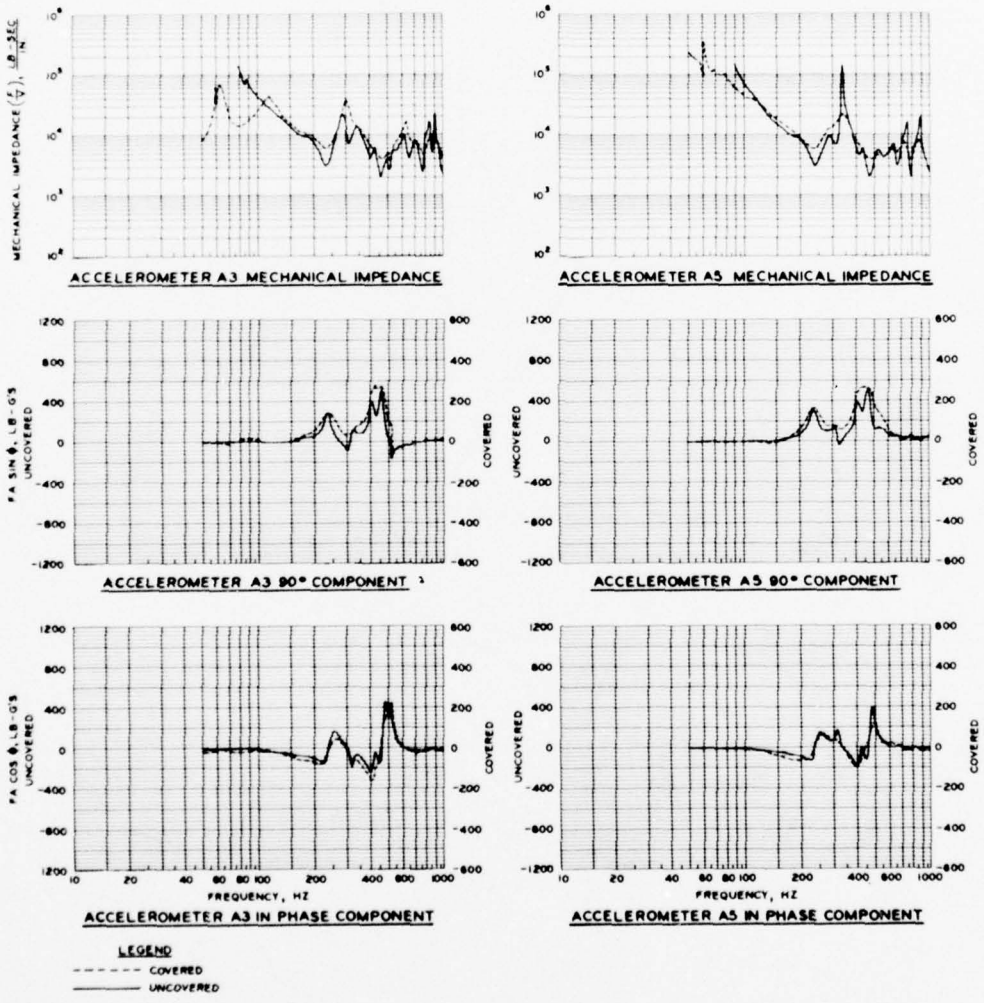

Peak Force F = 500 Pounds

Figure 1-4. Impedance and Quadrature for Rectangular Structure 3D Before and After Placement of Backfill Determined From Tests With Vibrators In Phase.

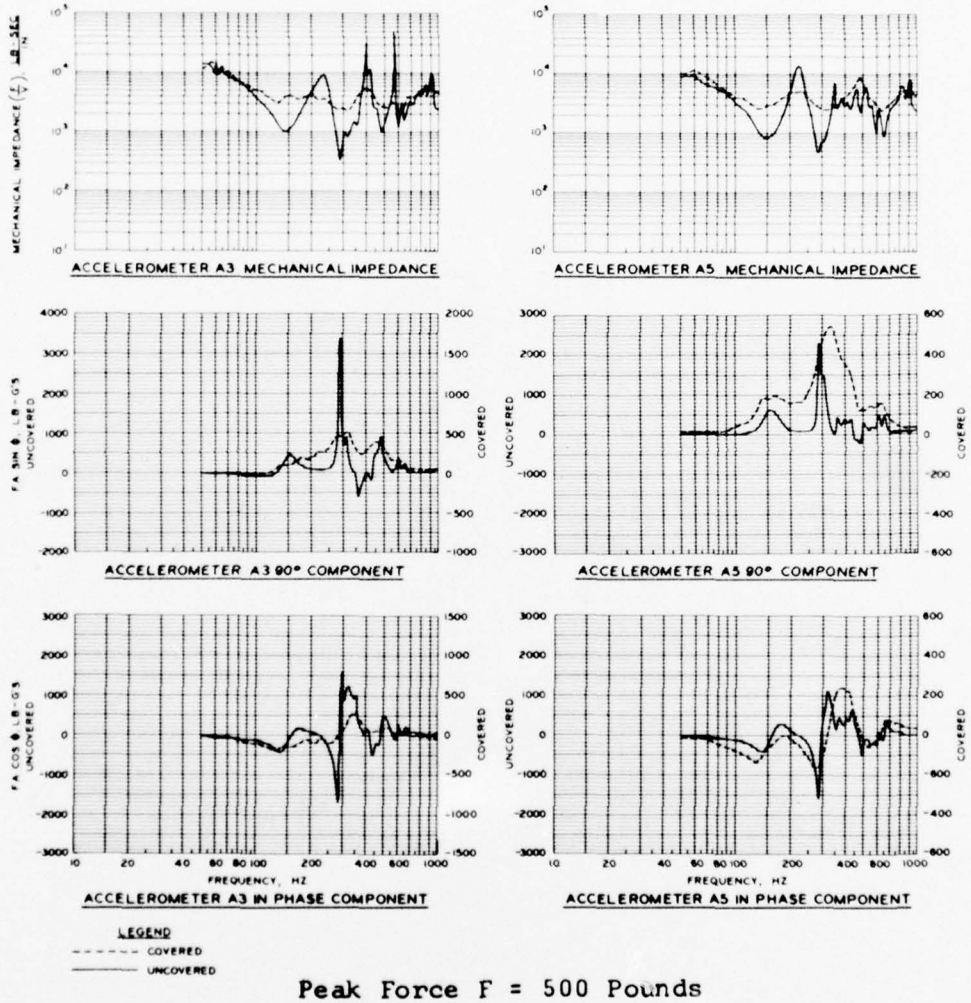

Peak Force F = 500 Pounds

Figure 1-5. Impedance and Quadrature for Rectangular Structure 3B Before and After Placement of Backfill Determined From Tests With Vibrators In Phase.

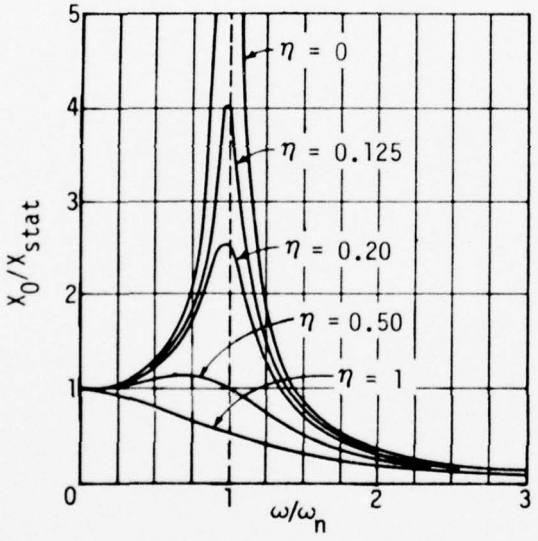

Figure 1-6. Response of Damped, Single Degree-of-Freedom System to Harmonic Forcing for Various Ratios of Critical Viscous Damping (η) (Ref. 2).

SECTION 2

FINITE ELEMENT SIMULATION OF BURIED ARCH

2.1. INTRODUCTION

The first step in simulating the forced vibration tests on the arch is to obtain natural frequencies and mode shapes associated with deformations of the structure. Those of the uncovered structure were compared with measured quantities in order to qualify the dynamic model. Modes and frequencies of the covered structure were compared with those from the uncovered structure to indicate the extent of soil participation. Next, a normal mode analysis was performed using the results of the modal extraction. The loading was a frequency sweep in which 25 cycles of a harmonic load were applied at the crown, following which the frequency of the force was increased by roughly 5 percent and held for another 25 cycles. Undamped modal analysis was conducted for both covered and uncovered models, and a parametric study of the effects of modal damping on resonance in the covered structure was made in which 12.5, 25 and 50 percent critical damping in all modes were assumed. The third step was to clarify the role of radiation damping by investigating the properties of the structure in a semi-infinite soil deposit. Since such a system does not possess classical normal modes, the harmonic modal analysis was abandoned in favor of transient analysis using direct integration, and a non-reflecting boundary condition of the Lysmer-Kuhlemeyer type (Ref. 7) was used at the subsurface edges of the soil island in order to simulate a semi-infinite soil domain. A parametric study was made to study the effect of variation in wave speeds in soil on radiation damping. The final step reported here is to investigate the contribution of friction at the soil-structure interface to damping of the covered structure. The linear finite element code GENSAP was amended to apply damping forces at interface nodes. After executing several check problems, a three-dimensional transient analysis of the covered structure, including nonlinear effects of friction, was performed.

2.2. RESULTS OF MODAL EXTRACTION

The geometry of the finite element simulation used throughout the present study is shown in Figure 2-1. A plane of symmetry is assumed perpendicular to the long axis of the structure, with the result that only half the structure is represented. A second geometric plane of symmetry exists which lies along the axis but this was not assumed in the model. In order to preserve the option to consider anti-symmetrical modes and unsymmetrical loading it was necessary to include both sides of the structure. However, this option was not used during the phase of the study reported here. The finite element discretization of the structure is shown in Figure 2-2. Thin plate elements (four node, linear curvature compatible) are used for the structure. Hexahedral continuum elements are used for the soil.

The material properties of the soil assumed in the analysis were based on secant moduli in uniaxial strain from 0 to 1-2 percent strain (Ref. 8). This was based on a preliminary upper bound estimate of the stresses which could be induced by the forced vibration. The properties derived in this way are shown in Table 3-1. As is discussed below, subsequent transient response analysis showed that this strain level is probably much too high. Although the transient analyses showed the radiation damping to be sensitive to changes in the assumed moduli, previous numerical experiments indicate that the effect of soil stiffness on mode shapes and frequencies is much weaker (Ref. 9). A detailed parameter study was therefore deemed necessary, and the modes reported below are obtained on the basis of lower bound soil moduli.

The natural frequencies and mode shapes were obtained with a Rayleigh-Ritz procedure in which the initial shape functions were a set of harmonic displacement functions suggested by the theory of cylindrical shells. Modes of the uncovered structure were extracted by placing the structure in the excavation without any backfill. Modes of the covered structure were extracted by adding soil elements having properties of backfill. Table 2-2 compares natural frequencies of the covered and uncovered models with measured frequencies of the uncovered structure. The range of measured frequencies is somewhat above

those calculated. This is partly because the calculations reveal lower modes which are strongly influenced by rigid body motion whereas the measurements tend to miss these. The calculations could have been extended to higher modes, but this would have required finer discretization of both structure and soil. This was unnecessary because only a few deformational modes are needed to investigate the influence of damping on response. The range from mode 5 to mode 10 of the models is rich in deformations. Measured mode shapes and natural frequencies for modes 1 and 2 compared favorably with values calculated for modes 5 and 7 of the finite element model of the uncovered arch. This is shown in Figures 2-2 and 2-3. Measurements of the deflected shape for mode 3 were not reported by WES. Hence, it is not certain whether the mode shape is the same as that of mode 9 of the uncovered analytic model. The calculated mode shapes of the covered and uncovered structure are given in Appendix I.

Previous studies (Ref. 9) have correlated mode shapes of a structure with and without soil cover by summing the dot product of eigenvectors from the two analyses. This correlation was part of an effort to develop in vacuuo models which would have the same frequency characteristics as buried structures. The present study investigates the damping associated with free vibration of an embedded structure. This information may eventually be combined with the previous data to develop an in vacuuo model with approximately the same frequency and damping characteristics as the embedded structure.

2.3. SIMULATION OF FORCED VIBRATION MODAL ANALYSIS

Simulation of forced vibration at the crown of both covered and uncovered structures was performed using the natural frequencies and mode shapes described above. The crown of the arch was driven with a sinusoidally varying force whose peak magnitude was 250 pounds (500 pounds for full structure). Starting at a frequency of 75 Hz, the frequency of the forcing function was held fixed for 25 cycles. The frequency was then increased by 5 percent (to 78.75 Hz) and held for another 25 cycles. This procedure was continued until a frequency of 141 Hz was reached. Damping was assumed to be zero apart from a small amount present in the linear acceleration method used to integrate the

modal equations. The results are shown in Figures 2-4 and 2-5 in terms of velocity-time histories at the drive point. Each discrete frequency and the interval during which it is applied is shown on the time axis. Each natural frequency of the finite element simulation is marked by an arrow pointing to the time interval (and hence, frequency) where resonance might be expected.

Figure 2-4 shows the velocity-time history for the uncovered arch at the crown (excitation point). There are three natural frequencies that occur within the range of the sweep and which may appear as a resonant peak. The ones at 84.2 and 100.5 Hz (modes 6 and 7) can be recognized because of the relatively high amplitudes reached as the forcing function sweeps through them. However, mode 8 (119.9 Hz) is not detected at all. This is apparently because it involves predominantly floor deformations.

The corresponding velocity-time history at the crown of the covered arch, Figure 2-5, contains three natural frequencies within the frequency range swept and range of modes extracted. The first natural frequency in this range is 83.8 Hz. However, this is the same floor mode that did not exhibit resonance at the crown of the uncovered arch and it is believed that it goes undetected again for the same reasons. However, modes 9 and 10 are observed. These are at 100.5 and 110.8 Hz. Because of their close spacing extra care must be taken in examining and interpreting the results.

The occurrence of resonance in both models indicates that much greater damping was needed to simulate the physical experiment. In order to estimate the equivalent viscous damping required to suppress resonance, which would agree qualitatively with the observations on the covered arch, three modal analyses were made in which the percentage of critical damping was 12.5, 25 and 50 percent. In each case the damping was assumed to be constant in all modes. The calculations are thus similar to the one whose results are shown in Figure 2-4, except that the damping is greater. The results show that resonance occurs at 12.5 percent and that it is suppressed at 50 percent. At 25 percent critical viscous damping there are only slight remnants of resonance. There is motion in both the 25 and 50 percent cases, but the amplitude is, to first order, independent of frequency of the forcing function.

The result described above indicates that an effective damping of 20 to 30 percent is required to bring the analytic model into qualitative agreement with the test data. The questions to be addressed next are: What are the sources of damping and is their aggregate effect great enough to suppress resonance?

2.4. TRANSIENT ANALYSIS OF COVERED ARCH

Three damping mechanisms have been postulated in Section 1 as contributing to the total damping of the arch:

a. Radiation damping

b. Friction

c. Hysteresis in backfill material

Radiation damping is associated with wave propagation in an infinite or semi-infinite domain and is not correctly represented in a bounded domain such as the one analyzed by modal extraction methods. To represent a semi-infinite soil domain, a Lysmer-Kuhlemeyer non-reflecting boundary condition (Ref. 7) was applied to the subsurface boundaries of the soil island. This model no longer possesses classical normal modes, and hence resort is made to a direct, step-by-step integration method. The possibility that friction between the soil and structure may absorb a significant amount of vibrational energy arises from the significant confining stresses (2-10 psi, depending on depth) due to overburden. Sliding friction introduces nonlinearity into the system of equations, which is another reason for using direct, step-by-step integration methods. As is explained above, soil hysteresis is omitted for lack of experimental data on which to base a constitutive model and structural damping is omitted because it is small.

In the following analysis, damping is investigated by observing decay in the amplitude of free vibration. Motion is induced by applying a triangular pulse whose duration is about equal to .005 second (approximately the half period of the 100.7 Hz mode). The total duration of the calculation is .108 second, or about 21 times the duration of the load; case 2 is an exception due to being terminated prematurely by the computer center operator.

2.4.1. EFFECT OF SOIL STIFFNESS ON RADIATION DAMPING

Calculations were made to investigate radiation damping and the influence of wave speed in the backfill and surrounding soil on the amount of radiation damping. The finite element simulation showed that the amount of radiation damping is sensitive to variations in the assumed wave speeds which are within the range of experimental uncertainty. All of the analyses were based on measurements of uniaxial stress-strain properties performed on undisturbed samples taken from the ESSEX test site. The site profile and representative stress-strain data are given in Ref. 8. Among the most important data is the uniaxial stress-strain curve for the tamped backfill surrounding the arch, which is shown in Figure 2-6.

In interpreting the data for use in the calculations, attention was given to possible differences between the actual stress-strain curves for backfill in the field and the representative curve given in Figure 2-6. There is the possibility of disturbance during sampling; the effects of sampling procedures on moduli are not well known at the exceptionally low stress levels of interest in the present study. This problem is reflected in the observation that in situ seismic wave speeds are in some cases (Ref. 10) higher than laboratory stress-strain measurements would lead one to expect. Also, there is variability in such properties as the extent of compaction of the backfill, which is reflected neither in the stress-strain curve in Figure 3-5 nor in the calculation.

A second question is whether the secant or the initial tangent moduli of the experimental stress-strain curves should be used as a basis for the elastic moduli of the finite element model. A parametric study was performed to investigate how backfill and in situ soil stiffness influence radiation damping. A lower bound on moduli in the backfill and other soil layers was established on the basis of the secant modulus from 0 to 1-2 percent strain. The secant modulus in the backfill is about 6,700 psi, which leads to a dilitational wave speed of about 533 psi. The wave speeds assumed for the backfill and the other soil layers are summarized in Table 2-3. The results of the

calculation using these properties are illustrated by a velocity-time history at the crown in Figure 2-7. The response is lightly damped and is unlike the response of the physical arch. Suspecting that this is due to ineffective transfer of energy in deformational modes to the soil, a second calculation was made in which the soil properties were based on the initial tangent moduli, which are about four times stiffer. The justification for this is that the stress levels developed in the backfill during the tests were probably of order 0.1 psi (order .01 bars), so that the initial tangent modulus is more representative of the stiffness governing radiation damping effects in the forced vibration tests (though not necessarily under weapons effects loading) than is the secant modulus. The results of the second calculation, shown as velocity-time history of the crown in Figure 2-8, indicate a substantial increase in radiation damping. Since this result is central to the purpose of the present study, it was decided to perform another calculation which would establish a reasonable upper limit on the radiation damping. In this calculation, the initial tangent moduli were doubled. This is a modest increase in the recommended values which in the opinion of the authors could have occurred. The results, shown in Figure 2-9, confirm the trend toward increasing radiation damping with increasing wave speeds in the soil.

It appears that, as the impedance of the soil approaches that of the concrete, coupling improves between deformational modes of the structure and the soil. In the extreme case of a perfect impedance match between structure and medium, the radiation damping would be very high; in the opposite extreme case of a structure in vacuuo, there would be no damping. In case 3 (2 X tangent moduli) where the impedance ratio of concrete to backfill is about 1 to 15, the damping is estimated to be the equivalent of 12 to 21 percent critical viscous damping, depending on interpretation of the response of the crown. In order to confirm the trend obtained from the finite element calculations, Dr. T. L. Geers of Lockheed Palo Alto Research Laboratory was asked to compute analytically the equivalent fraction of critical viscous damping for an infinite cylinder having roughly the same geometric and material properties as the arch

and which is embedded in an infinite medium having roughly the same properties as those assumed for the backfill in the finite element calculations. In spite of significant differences between the arch and the cylinder, the trends substantially agree. Results of the cylinder analysis are shown in Appendix II.

2.4.2. EFFECT OF FRICTION ON DAMPING

The energy of vibration which is absorbed by friction between the soil and the surface of the structure was investigated. An ideal computer simulation of friction would include three-dimensional geometry, non-reflecting boundaries and the capability for slip at the soil-structure interface and a Coulomb-type friction slip criterion in which the direction and magnitude of the friction force depend on the relative velocity between the soil and structure. A step was taken toward this ideal simulation by modifying the existing GENSAP model to include frictional forces tangential to the interface and in the direction opposite to the absolute velocity of the structure. It is believed that this simulation is adequate for purposes of this study. The maximum frictional stress which can be applied was assumed to be proportional to the normal stress acting on the structure, which depends on the depth of each nodal point below the surface. The relationship between the overburden and frictional stresses is shown in Figure 2-10. The frictional shear stress was multiplied by the tributary area for each node and the resulting force was included in the discretized equation of motion as follows:

$$M\ddot{x} + Kx = P - F$$

where

M, K = global mass and stiffness matrices

$\ddot{x}$, x = acceleration, displacement vectors, respectively

P = externally applied load (forcing function)

F = friction force (applied only to soil-structure interface nodes)

An initial attempt was made to compute F according to a simple Coulomb-friction law in which the maximum magnitude of friction force was applied whenever the absolute velocity of a node on the structure exceeded a threshold value.

The direction of the force was assumed always to be opposite to the velocity of the structure. This attempt was unsuccessful because the system was too strongly nonlinear for the integration algorithm to handle it correctly. The results depended on the time step used. Consequently a nonlinear viscous friction model, in which the frictional force was assumed to be proportional to velocity, was used.

The nonlinear viscous friction model used was adapted from the work of Den Hartog (Ref. 2); a viscous single degree-of-freedom model in which the work per cycle done by the friction force is equivalent to a constant force Coulomb model. In the viscous model, it is assumed that

$$F = C\dot{x} \tag{2-1}$$

where

$$C = \frac{4f}{\pi\omega x_o} \tag{2-2}$$

and

f = peak friction force

ω = frequency of the SDOF system

x_o = peak displacement of the SDOF system

This model exaggerates the effects of friction by assuming that the friction forces are related to the absolute rather than to the relative velocity. It is believed that, because the loading is from inside the structure, the absolute motion of the structure is reasonably close to the relative motion. This would not necessarily be the case for engulfment by a shock wave.

The implementation of this type of model in GENSAP required numerous coding changes, and two check problems were devised to test the new model. These are described in Appendix III.

An analysis of the covered arch was performed which was aimed at producing an upper bound estimate for damping including the effects of friction and radiation damping. The friction parameter f in Equation 2-2 was calculated for each node as follows:

$$f = \mu \sigma_n A \qquad (2\text{-}3)$$

where

σ_n = normal stress at each surface node due to overburden

A = tributary surface area associated with the node

μ = coefficient of friction

The nodal friction force is applied tangentially to the arch in the direction opposite to the tangential component of velocity. It is the large cumulative area which magnifies the friction force and which makes friction potentially a significant effect. In the present example $\mu = 0.4$ was assumed on the basis of data presented in Ref. 3.

The wave speeds in the soil are based on two times the initial tangent moduli (see Table 2-3); hence, radiation damping is maximum for the range of parameters considered in this study. This is not a situation which maximizes dissipation due to friction because large radiation damping reduces velocities which in turn reduce friction forces. However, the total damping is maximum, or nearly so.

The results of the calculation are best interpreted when compared with the response without friction, which is done in Figure 2-11 for the crown. Friction reduces the amplitudes of oscillations at intermediate and late times, but the effect is not dramatic. The response of the model also contains higher frequency motions at intermediate and late times. This is due to the assumption that the friction force is proportional to the absolute velocity and has the opposite direction. High frequency oscillations are even more characteristic of Coulomb than of viscous damping (Ref. 2). Another aspect of the response with friction is that the first downward motion is greater than in the case without friction. The reason for this is apparently discretization error in space, time or both. The frictional forces are applied tangentially to the true curve of the arch, which is only approximated at each node by the two intersecting flat plate elements. Thus, the lines of action of the internal resisting forces are not exactly correct, and this error is compensated in the inertia terms in order to achieve equilibrium. Also, at early times the friction forces are the same order as the inertia forces, which means that nonlinearity is

strong. The integration algorithm is not capable of handling strongly non-linear systems perfectly, and some errors undoubtedly occur. For the main part of the calculation, the friction forces are smaller than the inertia forces and the conditions for accurate integration are more nearly met.

2.5. EVALUATION OF PERCENTAGE OF EQUIVALENT CRITICAL VISCOUS DAMPING FROM CALCULATIONS

Evaluation of an equivalent fraction of critical viscous damping from the results of free vibration computations is necessary to decide whether the damping mechanisms considered analytically can account for the suppression of resonance in the physical vibration tests. It is difficult to arrive at a clear and unambiguous fraction of critical damping because the response of the arch involves several modes. It is therefore hard to apply the conventional log decrement interpretation to the displacement-time history because it is difficult to identify successive maxima in the same mode. It is also probable that the fraction of critical damping varies from mode to mode, as is shown by the results given in Appendix II. In the following, the log decrement approach is applied to successive maxima according to the expression

$$-\ell n \frac{X_{n+1}}{X_n} = \delta = \frac{2\pi\eta}{\sqrt{1-\eta^2}} \qquad (2\text{-}4)$$

where

X_n, X_{n+1} = successive maximum amplitudes

η = fraction of critical viscous damping

δ = log decrement

Pairs of successive maxima are obtained from each calculation and Equation 2-4 is solved for η. To try to reduce bias in selecting maxima for each case, two pairs of maxima are chosen wherever possible. The pairs selected here are the first and second and the second and third.

Displacement-time histories at the crown from the four cases considered are shown in Figures 2-12a through 2-12d. In each case, the points chosen for

successive maxima are indicated by the numbers 1, 2 and, in most cases, 3. Table 2-4 shows the fractions of critical damping for each case. The trend is in the direction of greater damping for stiffer soils; it is increased further by accounting for friction. However, not all damping values are consistent with this pattern; it is necessary to select the values marked by an asterisk to obtain the trend described above. However, visual inspection of the displacement-time histories supports the interpretation that the cases are ranked in Table 2-4 in order of decreasing damping.

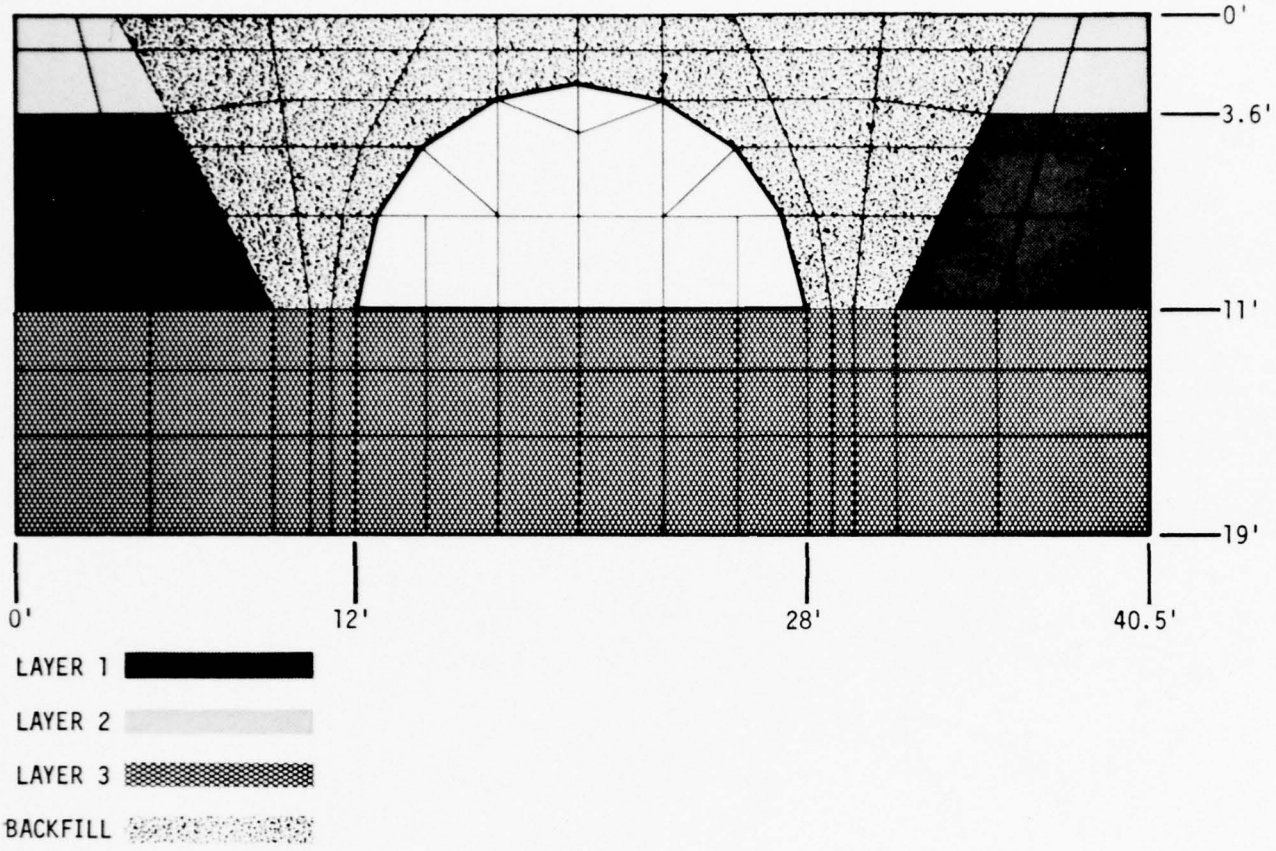

Figure 2-1. Discretization for Finite Element Mesh.

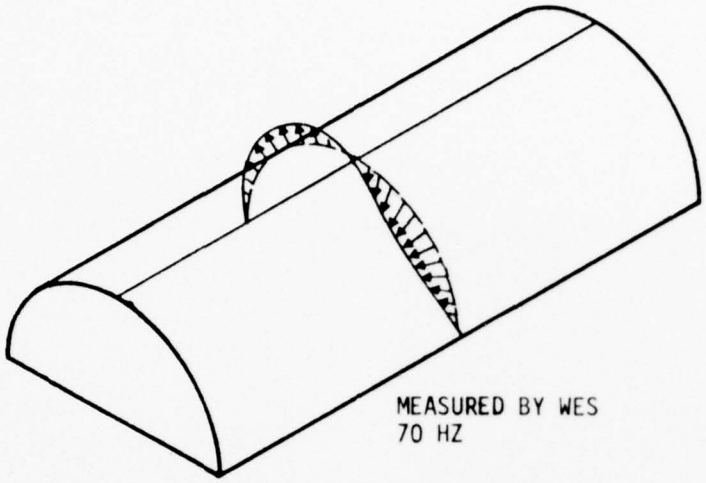

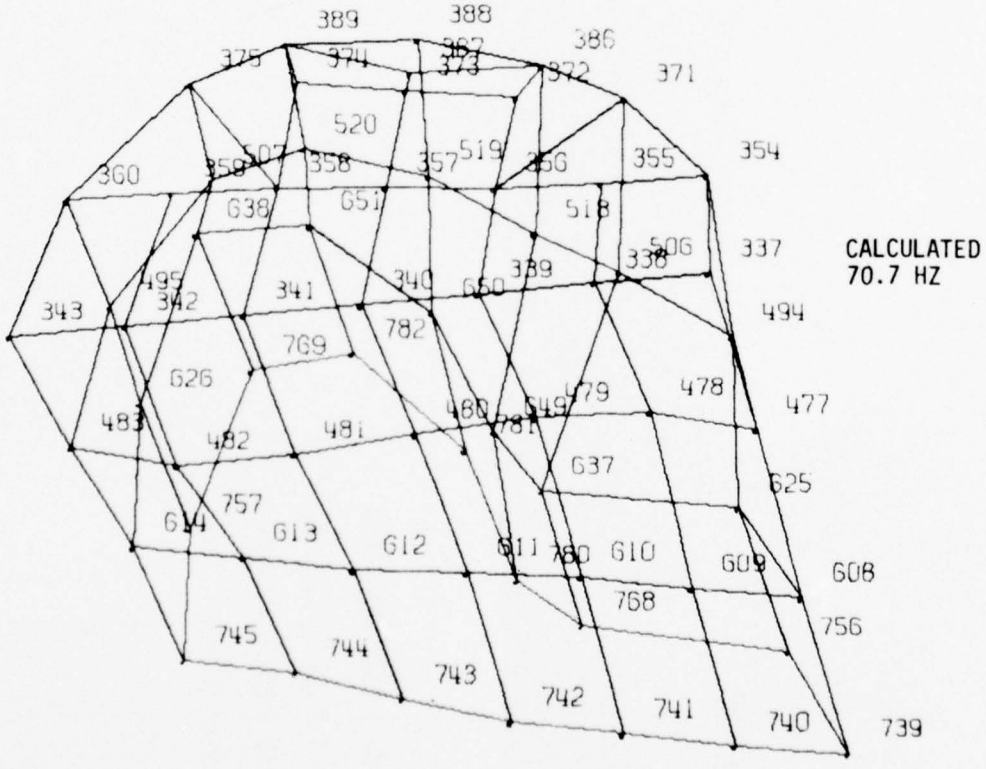

Figure 2-2. Comparison of Calculated and Measured Mode Shapes and Natural Frequencies for Uncovered Arch-Sway Mode.

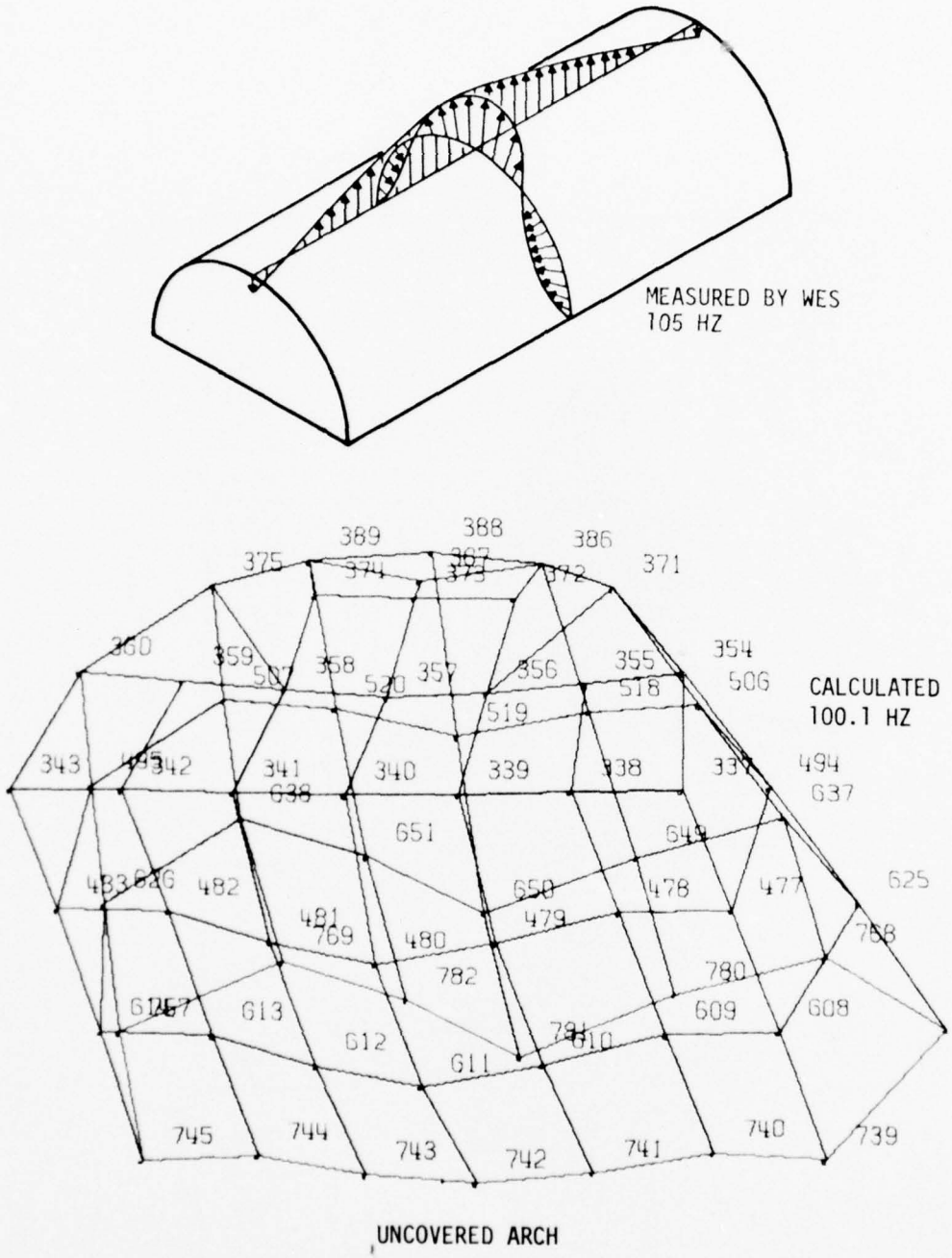

Figure 2-3. Comparison of Calculated and Measured Mode Shapes and Natural Frequencies for Uncovered Arch-Roof Sagging Mode.

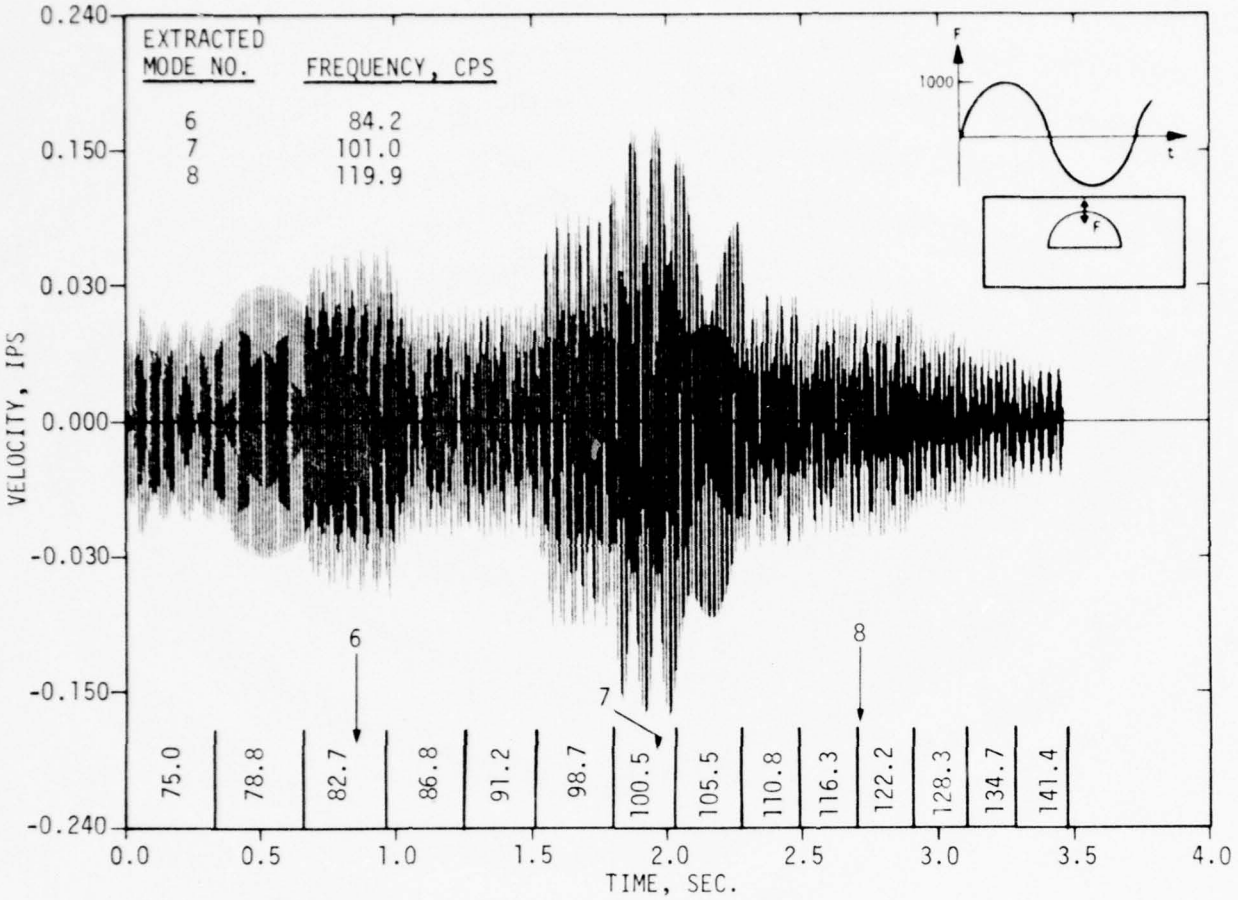

Figure 2-4. Response at Crown of Uncovered Arch Due to Harmonic Loading of the Crown with Continuously Increasing Frequency. Modal Analysis.

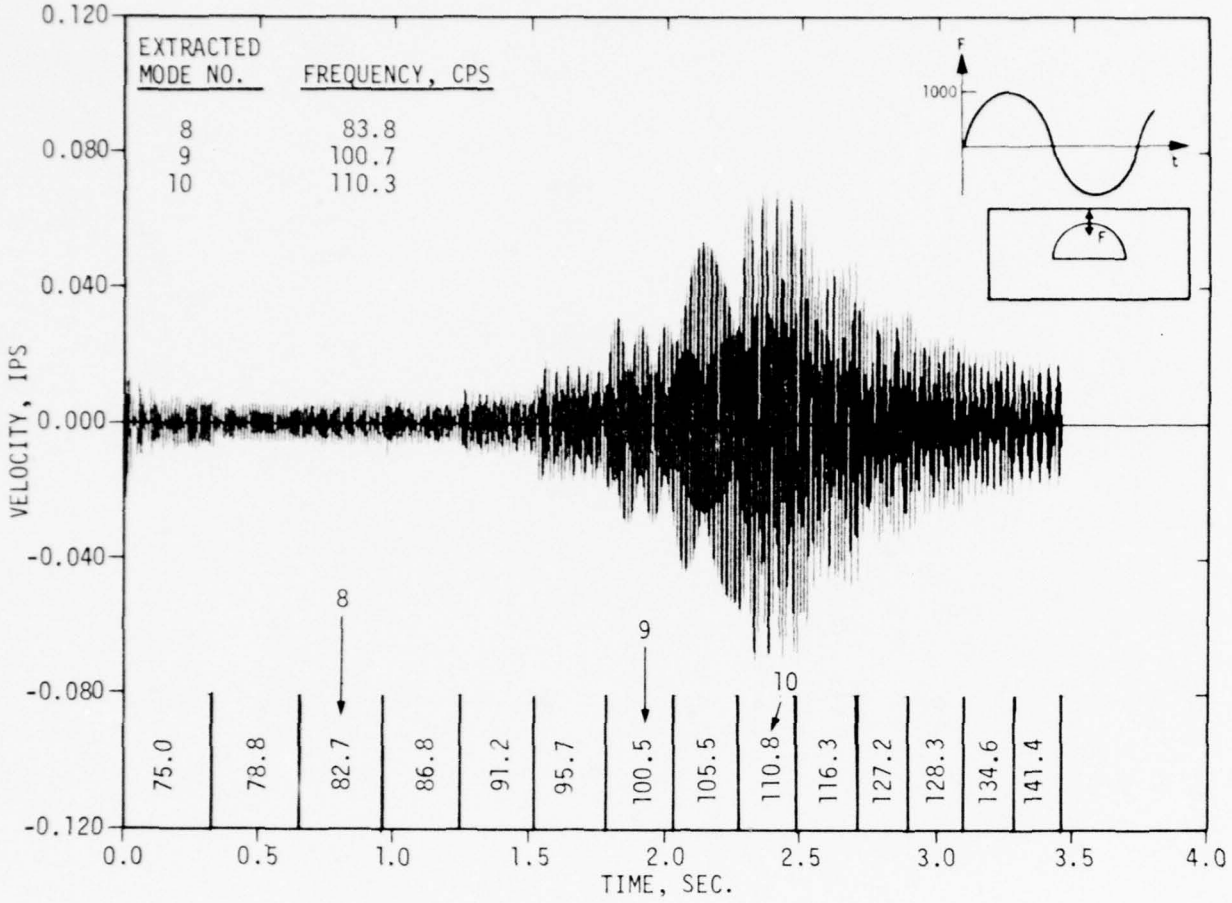

Figure 2-5. Response at Crown of Covered Arch Due to Harmonic Loading of the Crown with Continuously Increasing Frequency. Modal Analysis.

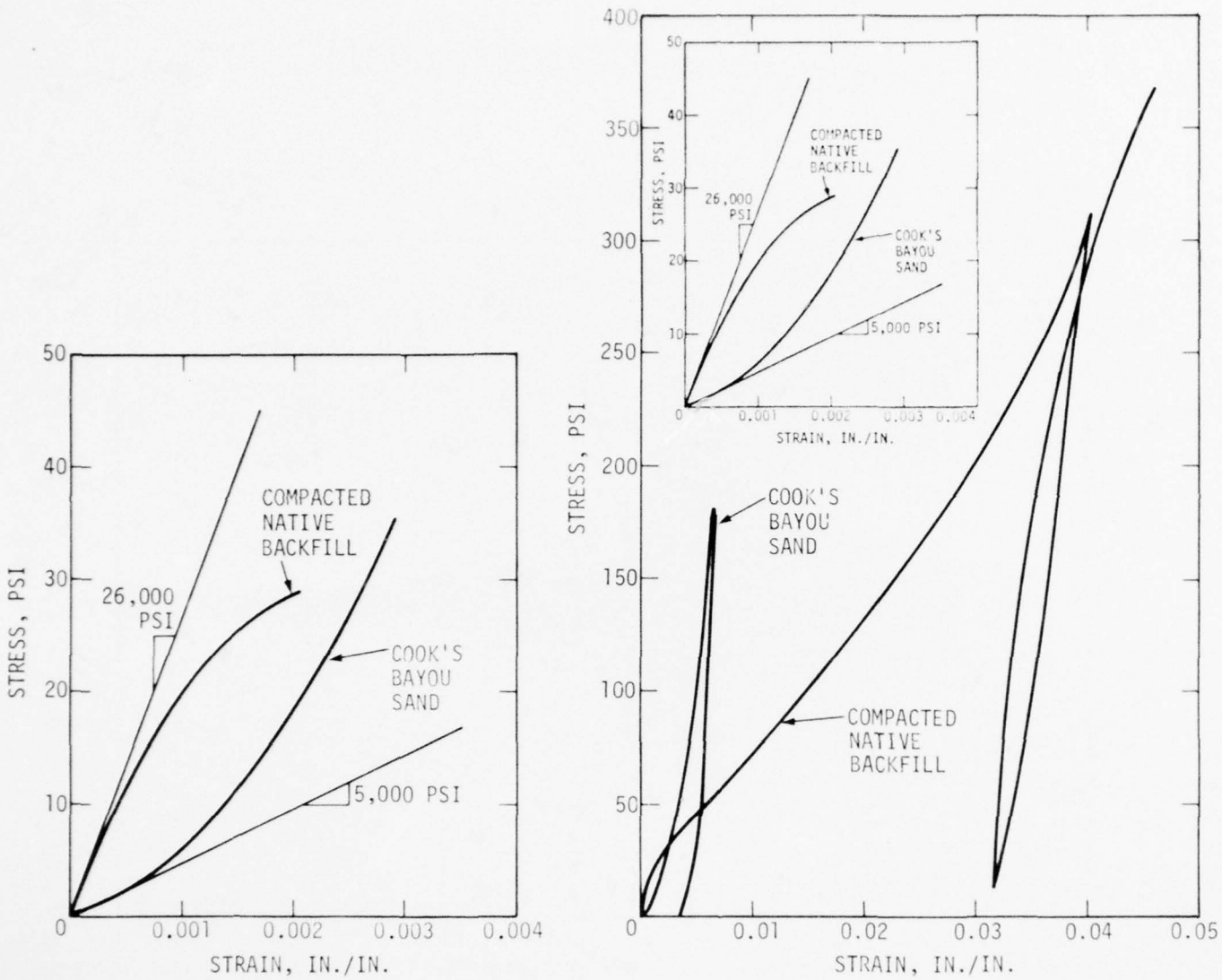

Figure 2-6. Uniaxial Stress-Strain Properties of Compacted Native Backfill (Arch) and Cook's Bayou Sand (Rectangular Structures).

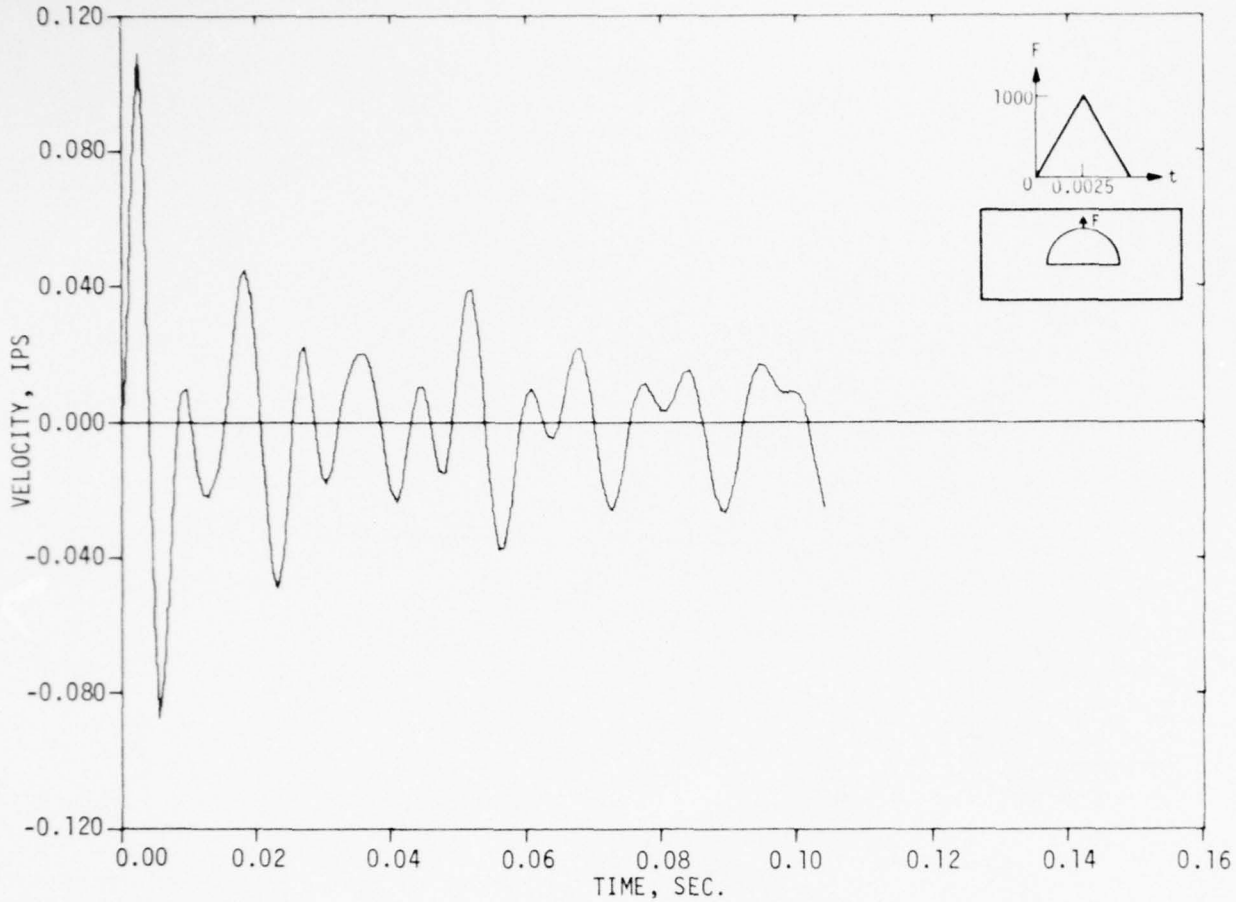

Figure 2-7. Velocity-Time History at Crown of Covered Arch. Backfill and Soil Properties Based on Secant Moduli.

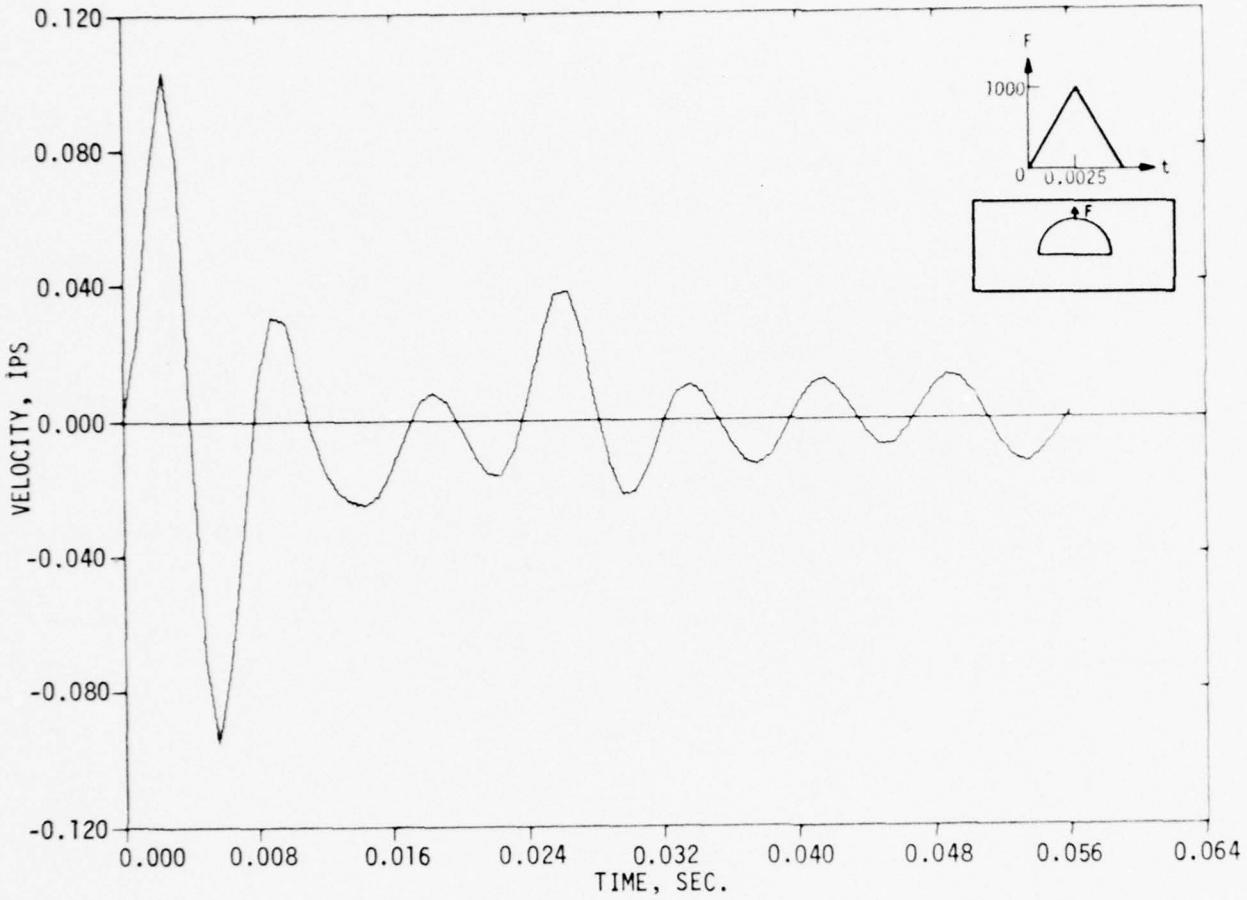

Figure 2-8. Velocity-Time History at Crown of Covered Arch. Backfill and Soil Properties Based on Initial Tangent Moduli.

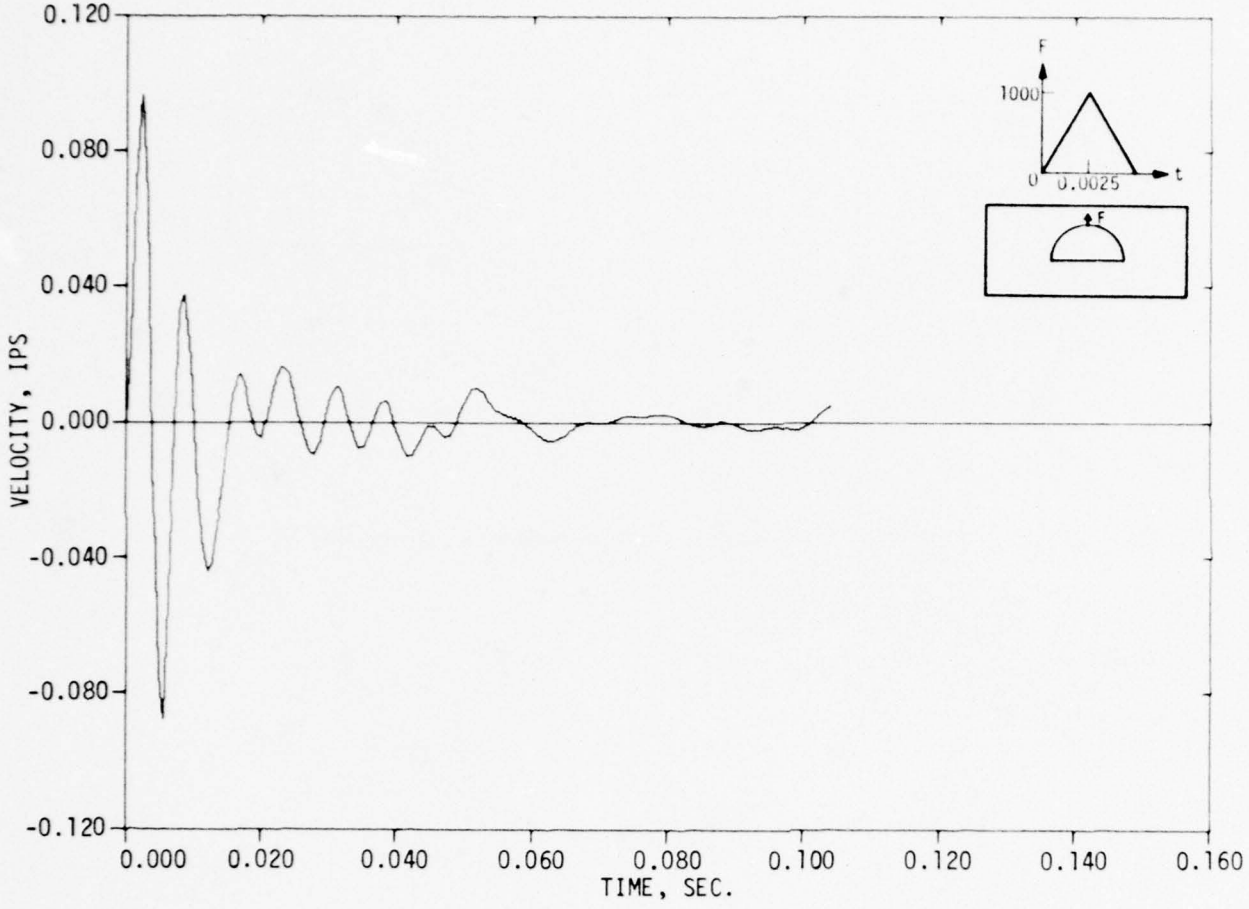

Figure 2-9. Velocity-Time History at Crown of Covered Arch. Backfill and Soil Properties Based on Two Times Initial Tangent Moduli.

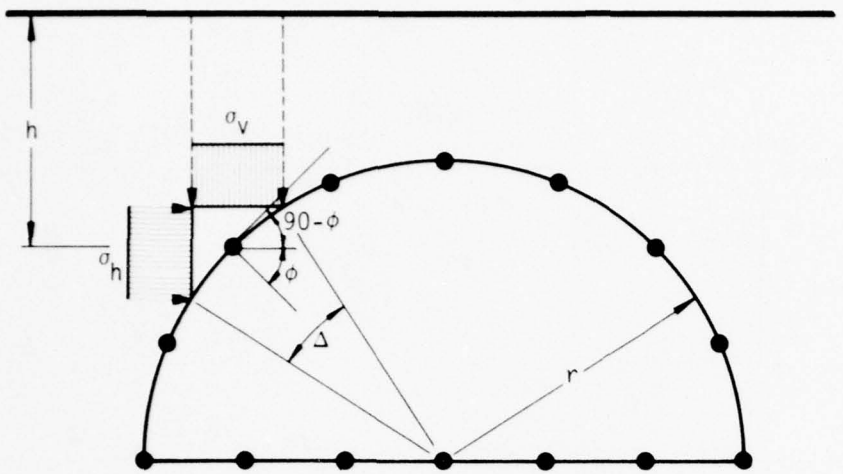

$$\sigma_n = \frac{\sigma_h + \sigma_v}{2} + \frac{\sigma_h - \sigma_v}{2} \cos 2\phi$$

$A = \Delta r \ell$

WHERE ℓ IS THE WIDTH OF THE ELEMENT

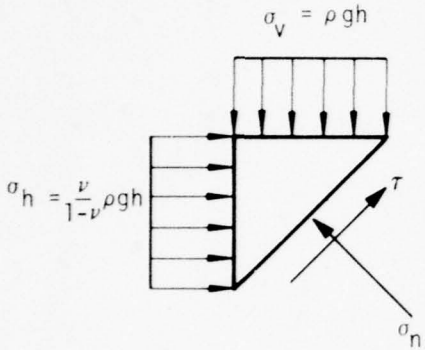

Figure 2-10. Computation of Normal Stresses and Tributary Areas Used in Evaluating Friction Forces.

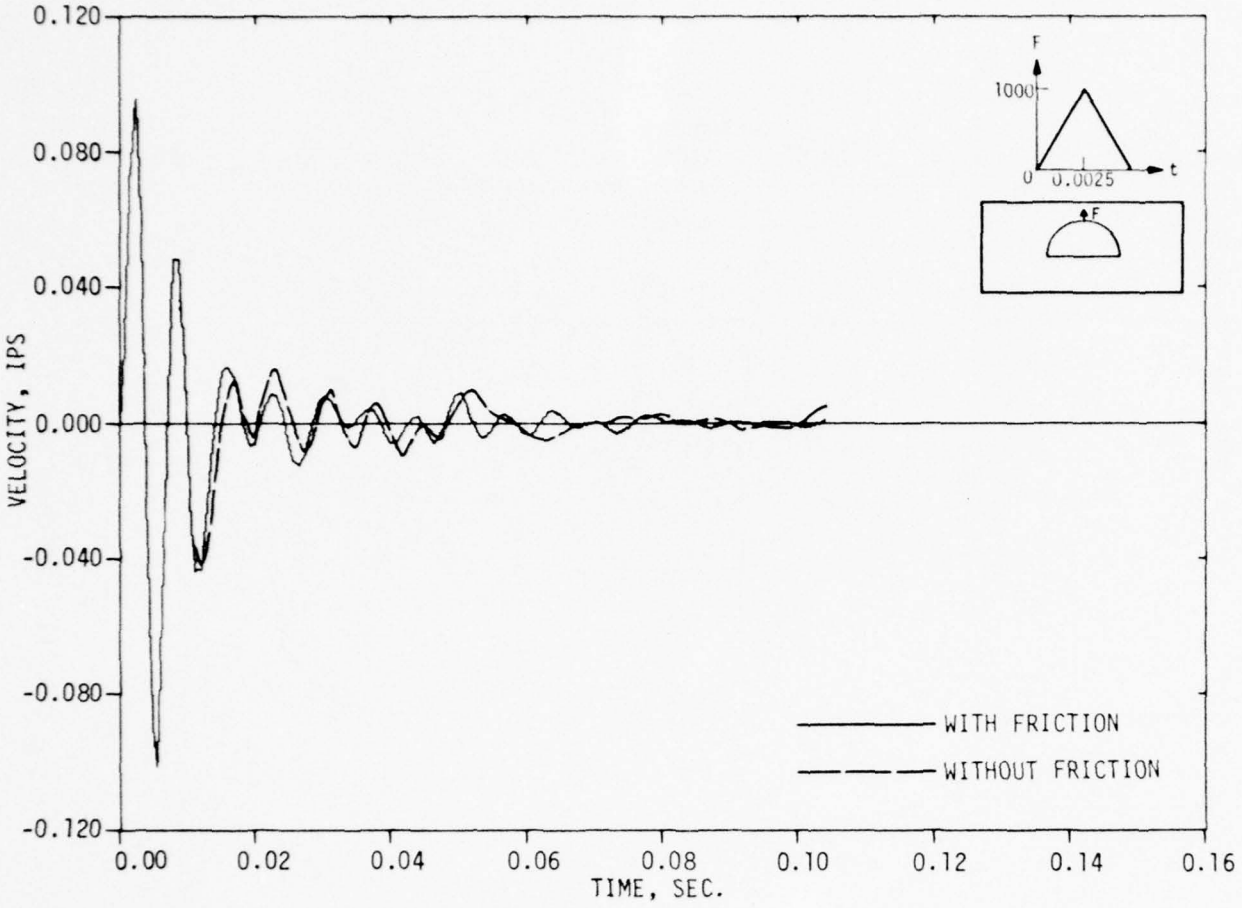

Figure 2-11. Velocity-Time History at Crown of Model Structure Embedded in High Wave Speed Backfill, With and Without Friction.

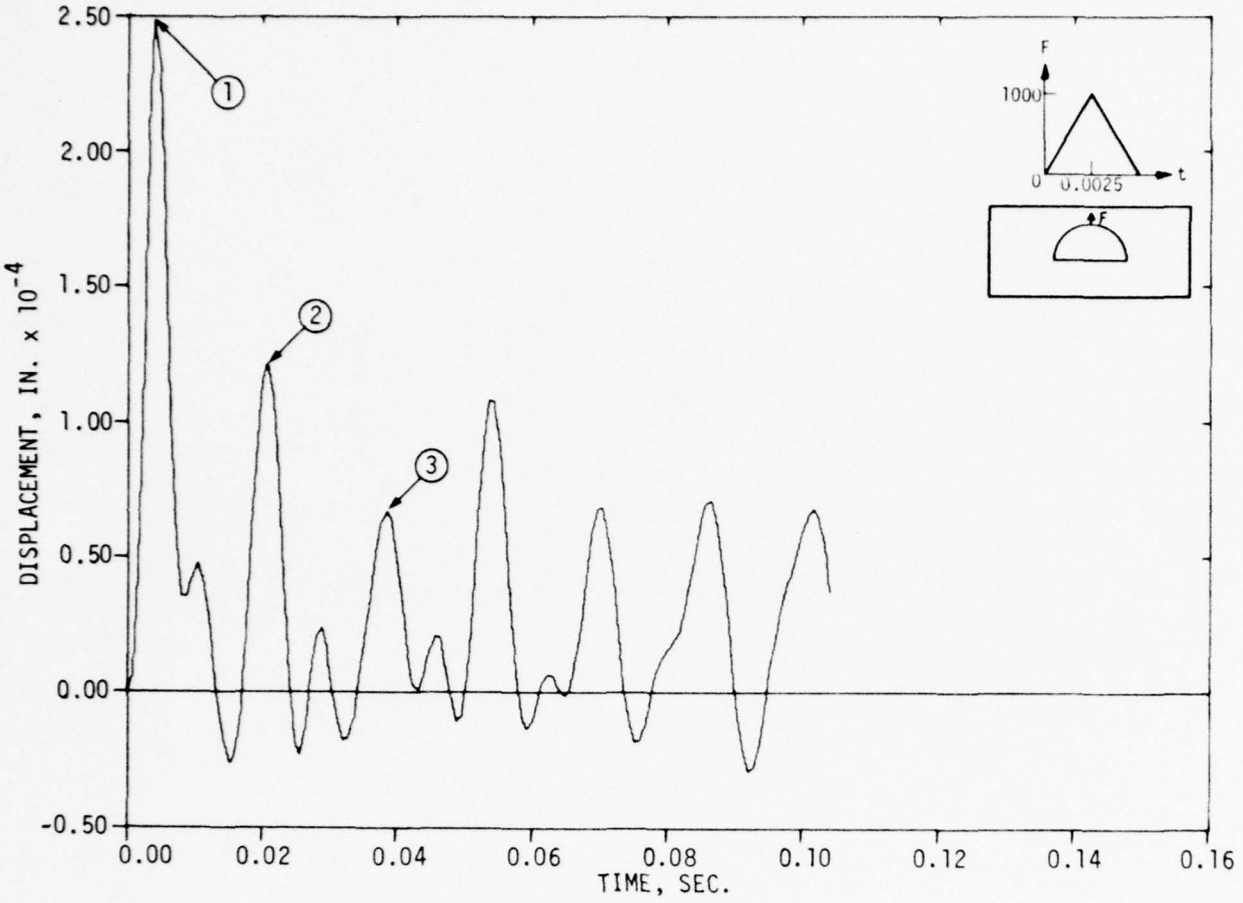

Figure 2-12a. Displacement-Time History at Crown of Buried Arch. Backfill and Soil Properties Based on Secant Moduli.

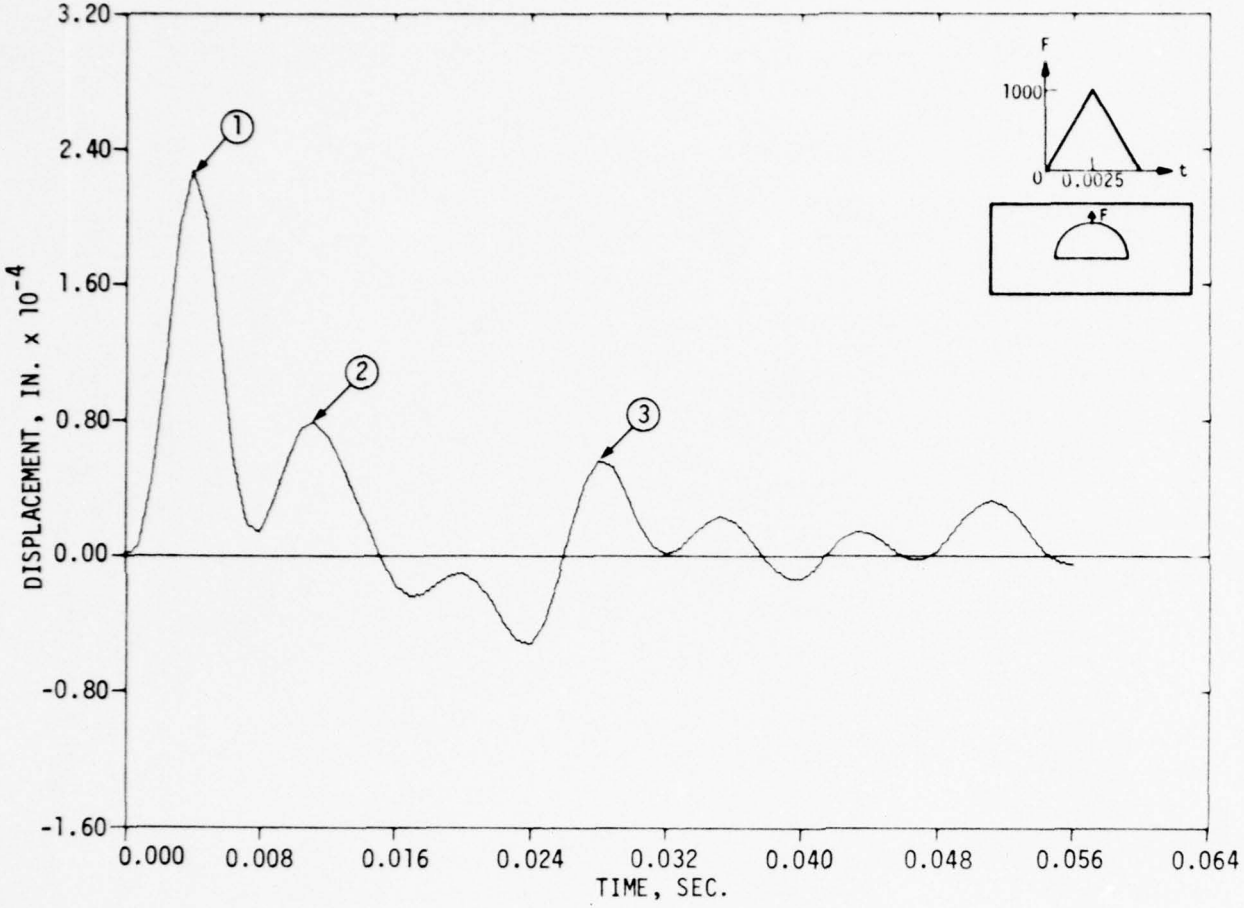

Figure 2-12b. Displacement-Time History at Crown of Buried Arch. Backfill and Soil Properties Based on Initial Tangent Moduli.

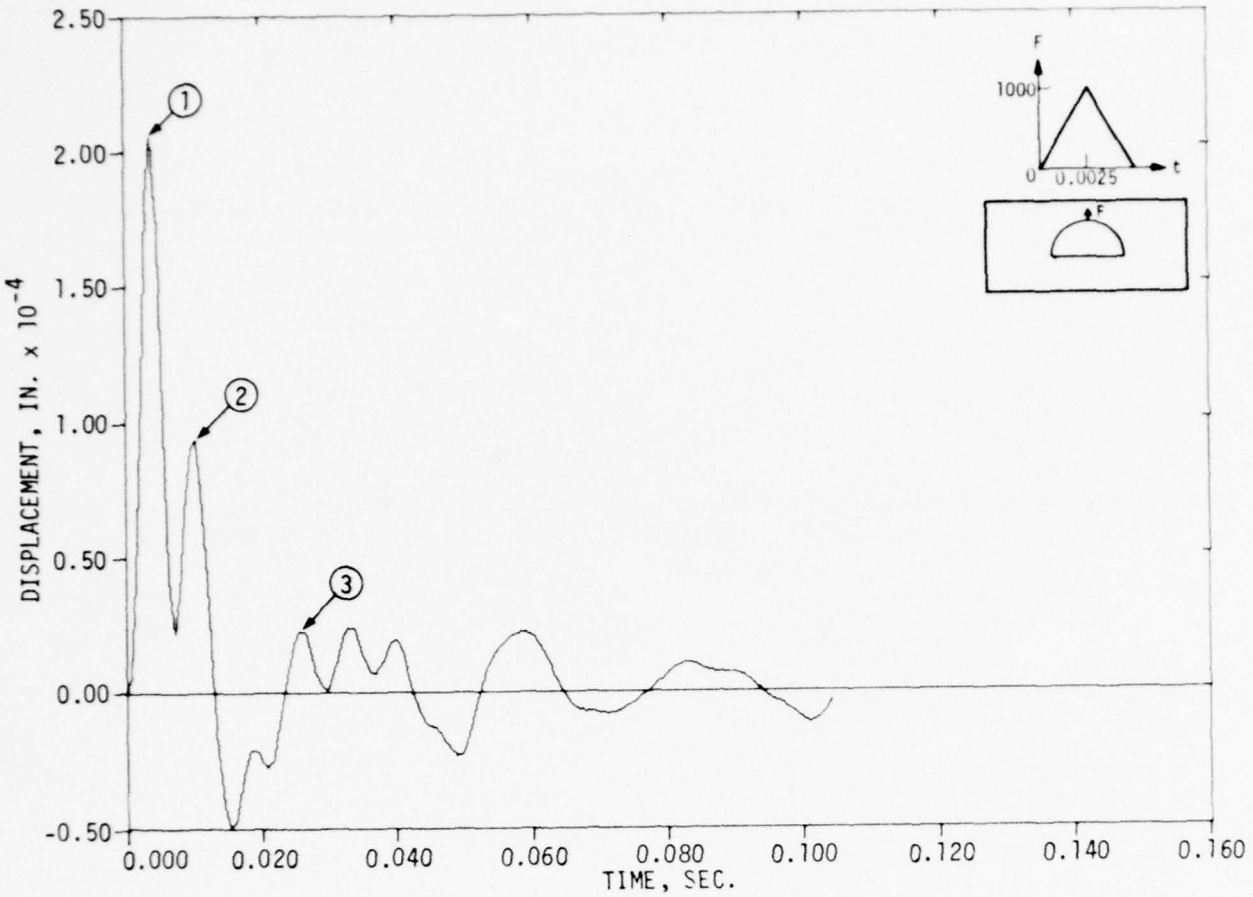

Figure 2-12c. Displacement-Time History at Crown of Buried Arch. Backfill and Soil Properties Based on Two Times Initial Tangent Moduli.

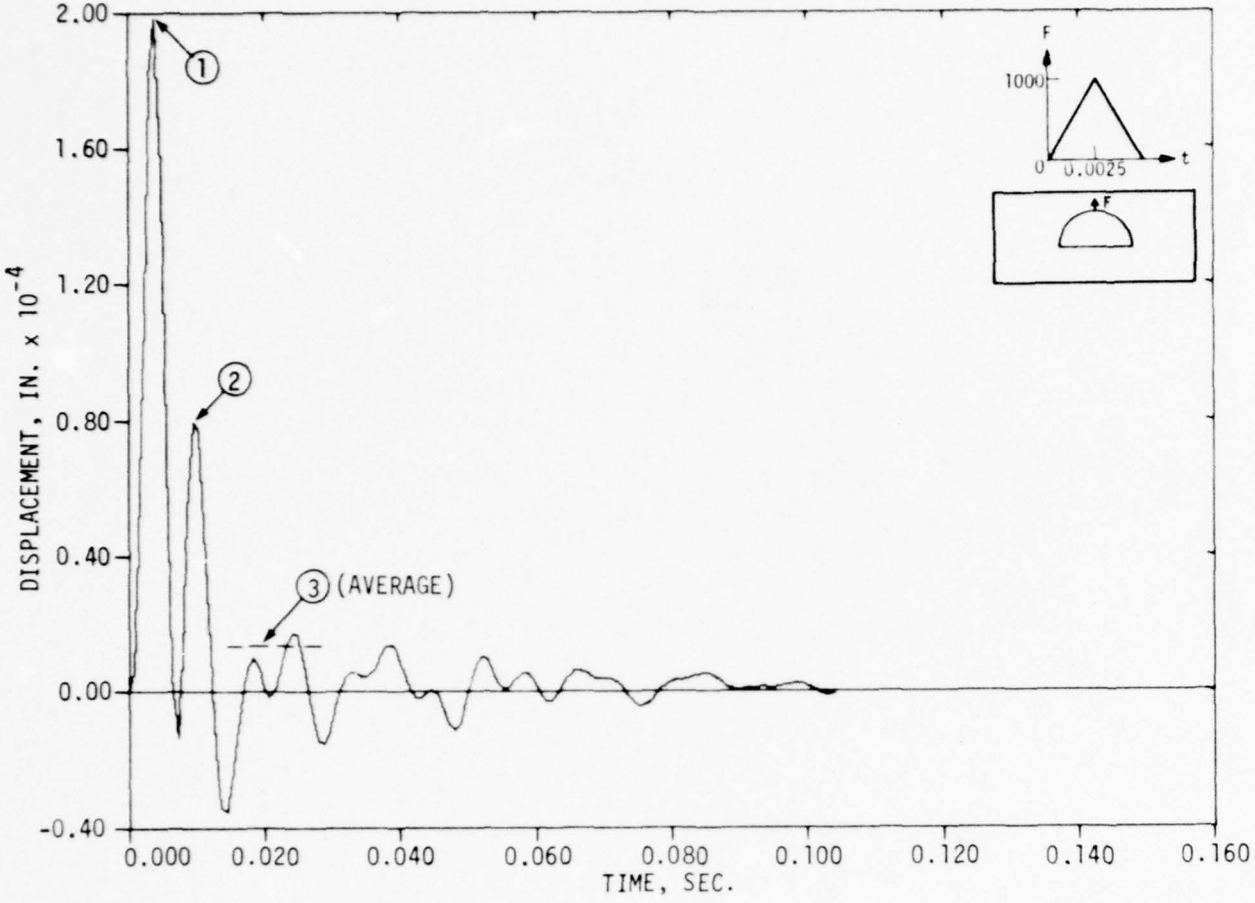

Figure 2-12d. Displacement-Time History at Crown of Buried Arch. Backfill and Soil Properties Based on Two Times Initial Tangent Moduli. Friction at Soil-Structure Interface Included.

TABLE 2-1.

MATERIAL PROPERTIES USED IN ANALYSIS OF ARCH

Soil

Layer	Depth (ft.)	E_m (psi)	ν_m	ρ_m $\frac{(lb.-sec.^2)}{in.^4}$
1	3.6	4,700.	.25	$.1820 \times 10^{-3}$
2	11.0	8,800.	.33	$.1780 \times 10^{-3}$
3	19.0	4,930.	.33	$.1780 \times 10^{-3}$
Backfill	11.0	4,900.	.33	$.1880 \times 10^{-3}$

Structure

Component	E_o (psi)	ν_o	ρ_o $\frac{(lb.-sec.^2)}{in.^4}$	h (in.)
Roof	3.77×10^6	.176	$.225 \times 10^{-3}$	11.0
Floor	3.77×10^6	.176	$.225 \times 10^{-3}$	12.0
Endwalls	3.77×10^6	.176	$.225 \times 10^{-3}$	16.0

TABLE 2-2.

NATURAL FREQUENCIES OF ARCH STRUCTURE, COVERED AND UNCOVERED

Mode No.	Measured (Uncovered) (Hz)	Mode	Calculated (Uncovered) (Hz)	(Covered) (Hz)
		1	10.8	10.1
		2	13.7	10.4
		3	16.1	13.8
		4	33.0	29.3
1	70	5	70.7	42.1
		6	84.2	51.8
2	105	7	100.1	62.5
		8	119.9	83.8
3	155	9	148.7	100.7
		10	185.4	110.3
4	222			
5	260			
6	450			

TABLE 2-3.

SOIL PROPERTIES USED IN PARAMETRIC STUDY OF RADIATION DAMPING

ASSOCIATED WITH FREE VIBRATION OF BURIED ARCH

	Depth (Ft.)	c_s (fps)	c_ρ (fps)
Secant Moduli (1-2% Strain)			
Layer 1	0- 3.6	269	533
2	3.6-14.6	359	713
3	14.6-18.6	268	464
Backfill	0-10.6	261	522
Tangent Moduli			
Layer 1	0- 3.6	654	1296
2	3.6-14.6	983	1953
3	14.6-18.6	941	1630
Backfill	0-10.6	519	1039
2 X Tangent Moduli			
Layer 1	0- 3.6	925	1833
2	3.6-14.6	1390	2762
3	14.6-18.6	1330	2305
Backfill	0-10.6	734	1469

TABLE 2-4.

FRACTIONS OF CRITICAL VISCOUS DAMPING FROM

FREE VIBRATION ANALYSES OF BURIED ARCH

Case	Cycles 1-2	Cycles 2-3	Average
Soil properties based on 2 X tangent moduli; friction included	.14	.26	20
Soil properties based on 2 X tangent moduli	.12	.21*	17
Soil properties based on tangent moduli	.17*	.06	12
Soil properties based on secant moduli	.12*		

*If these cases are selected as being most representative, a trend of increasing damping with increasing soil stiffness is obtained. Including friction increases damping to the level which suppressed resonance in the frequency sweep simulation using modal analysis.

SECTION 3

INTERPRETATION OF EXPERIMENTAL DATA AND CORRELATION WITH ANALYSIS

3.1. INTRODUCTION

The purpose of this section is to discuss the experimental measurements on the arch in light of the analyses described in the previous section and to explain why at least one of the buried rectangular structures exhibited strong resonance whereas in the buried arch, resonance was suppressed.

3.2. ESTIMATE OF DAMPING IN TESTS ON BURIED ARCH AND COMPARISON WITH CALCULATIONS

One method of estimating the equivalent fraction of critical viscous damping of the covered arch from experimental data is to regard it as a single degree-of-freedom oscillator. Although this is not the case it is a reasonable idealization because the frequency sweep tends to excite each normal mode in turn and that mode temporarily dominates all others. For steady state forced vibration of a single degree-of-freedom oscillator we have:

$$\frac{V_{max}}{F_{max}} = \frac{\omega/k}{\sqrt{(1 - p^2/\omega^2)^2 + 4\eta^2 p^2}} \qquad (3\text{-}1)$$

where

V_{max} = peak velocity

F_{max} = peak harmonic exciting force

p = frequency of excitation

ω = natural frequency of system

k = static stiffness

η = fraction of critical damping

If the arch is subjected to excitation of its natural frequency (for example, $p = \omega = 150$ Hz), the impedance, taken from Figure 1-2, is 1.5×10^4 lb.-sec./in. (vibrations in-phase) or 3.0×10^4 lb.-sec./in. (vibrations 180^o out-of-phase).

The static stiffness of the arch, defined by the force required to produce a unit deflection at the crown, is $k \approx 5 \times 10^7$ lb./ft.

Simplifying Equation 4-1 we obtain

$$\eta = \frac{2F_{max}/V_{max}}{k} p \qquad (3\text{-}2)$$

Substituting experimentally measured values of F_{max}/V_{max} into this expression, the results presented in Table 3-1 are obtained. Equation 3-2 has been evaluated at p = 105 Hz and 222 Hz because resonance is observed in the uncovered arch in this range and because p = 105 Hz is in the center of the range considered by the modal analysis, Section 2.3, which indicated that 25 percent critical damping is the minimum needed to suppress resonance. The results presented in the table are not reasonable except in the case of vibrators in phase at ω = 105 Hz where the uncovered structure with only 6 percent critical damping would exhibit resonance whereas the covered structure with 41 percent would not. The other values are apparently too high. This exercise illustrates the difficulty of evaluating the fractions of critical damping from the experiments. It is only slightly easier to estimate the effective damping in the calculations, as is described in Section 2.5.

The failure of this approach to yield reasonable values for damping in the experiments was unfortunate since it meant that there was no method of comparing quantitatively the measured and calculated fractions of critical damping. Instead, it must be argued that since the modal analysis indicates that *about 25 percent critical damping suppresses* resonance and since this amount can be accounted for in the finite element simulation if wave speeds are based on 2 X tangent moduli, it is possible that the fundamental phenomena observed in the tests are accounted for in the calculation.

3.3. DIFFERENT RESPONSES OF ARCH AND RECTANGULAR STRUCTURES

The buried rectangular structure 3D (L/h = 4) clearly exhibited resonance in the experiments as shown in Figure 1-4. The buried rectangular structure 3B (L/h = 10) less clearly exhibited resonance in the experiments

as shown in Figure 1-6, but WES considers that there was weak resonance over a broad, low frequency range, Ref. 1. In contrast, the arch structure is considered to have exhibited no resonance. A major factor contributing to higher damping for the arch than for the rectangular structures is different backfill conditions. The arch structure was placed in native backfill which was compacted dynamically in stages. The resulting material had a stress-strain curve which was initially concave to the strain axis and which, as a result, had a high seismic wave velocity. The calculations described above have clearly demonstrated that this situation leads to strong coupling between structure and the backfill and surrounding soil and to relatively high radiation damping. The rectangular structures were excavated after the main ESSEX-V event, and new sand backfill was rained into place. The properties of the sand backfill were not measured directly, but they are considered by WES to be about the same as Cook's Bayou sand. This sand has a stress-strain curve which is convex to the strain axis and has, as a result, a relatively low seismic wave velocity. The uniaxial stress-strain curve for Cook's Bayou sand is shown in Figure 2-6 along with the initial tangent modulus (measured) and 2 X initial tangent modulus for the arch backfill. The initial tangent modulus for Cook's Bayou sand is about the same as the secant modulus used in case 1 for the arch, Table 2-3, which produced small values of radiation damping. It is also possible that the procedure of raining backfill alongside a structure with vertical walls, such as the rectangular structures, may not produce strong coupling between backfill and structure during vibration testing.

To summarize the different backfill conditions, the arch was well coupled to a relatively high wave speed backfill whereas the rectangular structures were emplaced in lower wave speed backfill. The net result was that radiation damping was certainly higher in the arch than in the rectangular structures, and possibly it was much higher.

TABLE 3-1.

FRACTIONS OF CRITICAL DAMPING ESTIMATED FROM THE

EXPERIMENTAL DATA ON ARCH USING EQUATION 3-1

	Covered		Uncovered	
P	In Phase	Out of Phase	In Phase	Out of Phase
105	.41	.81	.06	.27
222	2.2	4.2	.55	1.1

SECTION 4

SINGLE DEGREE-OF-FREEDOM PARAMETERS FROM FORCED VIBRATION TESTS

The value of forced vibration tests in developing parameters for highly simplified structural models, such as SDOF oscillators, appears limited in light of experimental and analytic findings. These tests are probably a good way to obtain data on frequencies in the elastic regime so long as the frequencies show up (unlike the arch case) and so long as the backfill of the model is tamped similarly to that of the prototype. The possibility of lessened participation of soil mass due to loose backfill must be recognized both for test and target or prototype structures. Table 2-2 shows that the frequencies of covered and uncovered structures differ significantly; these represent lower and upper bounds, respectively, on the effect of soil mass participation. The analyst who intends to use forced vibration test data must either know where the backfill conditions of his target structure place it in the frequency range shown in Table 2-2, or he must be prepared to assume upper and lower bounds for the frequency of his model and conduct at least two analyses in order to bound the response.

The test data and analysis also show that the contribution of radiation to the total damping depends significantly on the wave speeds in the soil. Here again the backfill stiffness in the test must be like that of the prototype to be sure that this effect is properly accounted for. Since forced vibration tests generate stresses much lower than weapons effects loading, the effective wave speeds in the test are either higher or lower than in the prototype depending on whether the uniaxial stress-strain curve is stiffening or softening in the range of interest.

Another point related to different stress levels in vibration tests and weapons effects loading is the effect of hysteresis in soil stress-strain relations. The role of hysteresis in damping structural vibrations is at present unknown and should be investigated. If hysteresis were significant, it would be another deficiency of the forced vibration tests.

One way in which tests like those on the arch and box structures could be made more valuable is to concentrate more heavily than is done currently on transient, free vibration behavior. This would give another, perhaps clearer, picture of damping.

SECTION 5

SUMMARY AND CONCLUSIONS

A finite element simulation of the forced vibration tests on the buried arch structure at ESSEX-V was developed. The model of the structure surrounded by a finite amount of soil was qualified by calculating natural frequencies and mode shapes and, for the uncovered structure, comparing them with measurements. Modal analysis of the soil-structure system showed that drive point motions increased dramatically in both covered and uncovered cases when the frequency of the oscillating force at the crown approached a natural frequency of the system. Modal analysis of the covered structure was repeated using different assumed fractions of critical viscous damping. The resonant behavior of the structure was suppressed when about 25 percent critical damping in all modes was assumed.

Radiation damping, friction, hysteresis in the surrounding medium and structural damping were identified as possible mechanisms for absorbing the energy of vibration in the physical test. To evaluate the contributions of radiation damping and friction, transient, free vibration of the buried structure was simulated using a direct integration approach. Nonreflecting boundary conditions were used on the subsurface boundaries of the soil island to simulate a semi-infinite soil domain. It was found that the amount of radiation damping varies significantly, depending on the wave speeds assumed in the backfill and surrounding media. In order to establish a reasonable upper bound on radiation damping, it was assumed that the initial tangent constrained modulus of the backfill was two times the value recommended by WES on the basis of laboratory tests. This produced damping due to radiation effects of about 21 percent of critical; evaluation of the percentage is somewhat subjective. A friction model was developed which added about 5 percent to the radiation damping, leading to a total of about 26 percent of critical. The model used in the calculations probably overestimates the damping due to friction effects because signs and magnitudes of friction forces are based on absolute rather than relative velocities. Hysteresis in the soil was not

considered quantitatively, but it is believed capable of contributing less than 3 to 5 percent. Structural damping was not considered.

An attempt was made to evaluate damping from the physical test. This led to larger values of damping than appear reasonable and was considered unsuccessful.

Unlike the case of the arch, forced vibration of rectangular structures produced resonance. This is partly explained by the backfill conditions, which differed significantly between the two types of structures. The arch had a compacted backfill of native soil whose uniaxial stress-strain curve was initially concave to the strain axis. In contrast, the rectangular structures had sand backfill which was placed by raining. The uniaxial stress-strain curve for the sand was initially convex to the strain axis, which leads to lower seismic wave speeds than for the arch. The parametric series of calculations on the arch shows that its radiation damping is greater than for the rectangular structures and could be about two times greater. The result of the different backfill conditions is that the rectangular structures were closer to in vacuuo conditions than was the arch.

It is concluded that effective damping can be increased from 10 to 12 percent critical to 20 to 25 percent critical and possibly higher by increasing the wave speed in the backfill and surrounding soil by a factor of three to four. Damping due to friction is at most one-fifth that due to radiation effects in the present study. In cases where the active earth pressure due to overburden is less, the influence of friction is likely to be less. It is concluded further that a large part of the difference between the responses of the arch and the rectangular structures is due to the different backfill materials and methods of placement.

SECTION 6

RECOMMENDATIONS

The following recommendations are divided into categories of analysis, testing and development of single degree-of-freedom models of complex structures.

1. Analysis--the model of the arch with friction and high wave speed backfill (case 3, Table 2-4) should be used to simulate a portion of the frequency sweep in which quasi-steady state conditions are reached at a number of closely-spaced frequencies. This would clarify whether resonance is apparent when radiation and friction effects are explicitly included in the model rather than being lumped as in modal damping. Their values should be the maximum that can be reasonably assumed.

2. Testing--future tests on large model structures should be performed with the same thoroughness, including soil testing in the backfill and vibrations at different levels of maximum force, as were the ESSEX-V tests. The possibility of measuring relative displacements at the soil-structure interface tangential to the structure surface should be investigated; this would indicate whether friction should be included in the calculations. It appears that much information might be also derived from smaller scale model tests; a series of parallel vibration tests and shock loading tests in the Blast Load Generator would show whether the forced vibration tests include the same damping phenomena that are present in shock response. Finally, attention should be given to a free vibration phase of the tests in which damping could be estimated by observing the log decrement of the amplitude.

3. Development of SDOF Models--if incorporating 20 to 30 percent critical damping in SDOF models has a significant impact on targeting decisions, new methods of evaluating the equivalent fraction of critical viscous damping from test data on complex structures should be developed. Those who use such models should become aware that backfill conditions can affect damping significantly and that, if they do not know the backfill conditions in the structures they are analyzing, they should assume a range of damping values from about 12 to 15 percent to 25 to 30 percent.

REFERENCES

1. Crowson, R., and Kiger, S., "Vibration Tests and Analysis to ESSEX-V Model Structures," USAEWES report to be published.

2. Hartog, Den, J. P., "Mechanical Vibrations," 4th Edition, McGraw-Hill Book Company, New York, New York, 1956, p. 373.

3. Huck, Peter J., et al., "Dynamic Response of Soil/Concrete Interfaces at High Pressure," IIT Research Institute, AFWL-TR-73-264, April 1974.

4. Kolsky, H., "Stress Waves in Solids," Dover Publications, New York, 1963.

5. Idriss, I. M., and Seed, H. B., "Seismic Response of Soil Deposits," Journal of the Soil Mechanics and Foundation Division, Proceedings, ASCE, Vol. 96, No. SM2, March 1970.

6. Seed, H. B., and Idriss, I. M., "Soil Moduli and Damping Factors for Dynamic Response Analyses," Report No. EERC 70-10, University of California EERC, Berkeley, California, December 1970.

7. Lysmer, J., and Kuhlemeyer, R. L., "Finite Dynamic Model for Infinite Media," Proceedings, ASCE, Engineering Mechanics Division, EM4, August 1969.

8. Ehrgott, J. Q., "Recommended Profile and Representative Constitutive Properties for ESSEX-I, Phase 3," Soil and Pavements Lab., USAEWES, 6 February 1976.

9. Isenberg, J., and Pang, Steven S. H., "Analysis of Soil-Structure Interaction on Site Defense (SD) Type Semi-Buried Structures. Part II: Soil Structure Interaction and Dynamic Structural Response," HNDTR-75-20-ED-CS, Weidlinger Associates, 1 March 1976.

10. Sandler, I., "Parameter Studies of Mixed Company; Influence of Constitutive Properties on Ground Motion Calculations," Weidlinger Associates, Consulting Engineers, Contract Report S-75-2 to U. S. Army Engineer Waterways Experiment Station, June 1975.

11. Geers, T. L., Presented at the 14th International Congress of Theoretical and Applied Mechanics, Delft, The Netherlands, August 30 to September 14, 1976, In Preparation for Publication.

APPENDIX I

MODE SHAPES OF ARCH STRUCTURE WITH AND WITHOUT BACKFILL

Natural frequencies and mode shapes of the arch structure were calculated with and without backfill in place. The soil and backfill properties were based on secant moduli up to 10 psi. Although it was subsequently found that using initial tangent moduli improved the dynamic simulation using direct integration methods, the modal extraction analyses were not repeated. Previous experience (Ref. 9) indicates that the frequencies would not be significantly increased (less than 10-15 percent) by basing the soil stiffness on tangent moduli and that the mode shapes would not be changed at all. An end-on elevation view of the structure and surrounding soil is shown in Figure 2-1. For the modal analysis, all subsurface boundaries of the soil island were fixed except nodes on the plane of symmetry (parallel to the plane shown in Figure 2-1), which were constrained to move in the plane. The mode shapes of the structure are shown with soil stripped away. Figure I-1 shows the undeformed structure. Figures I-2 through I-11 show mode shapes of the uncovered structure. Figures I-12 through I-21 show mode shapes of the covered structure.

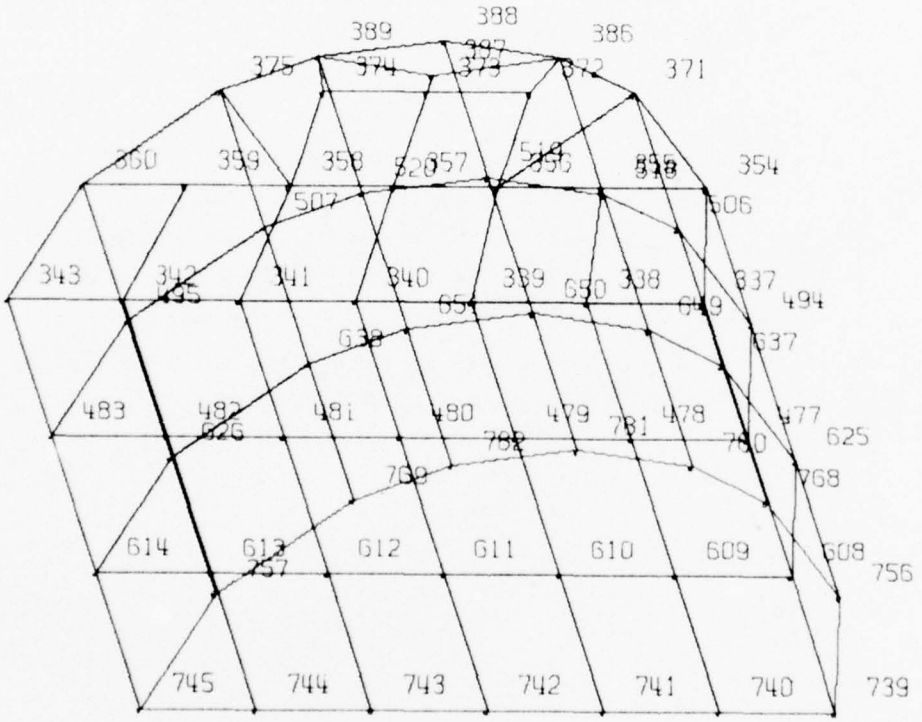

Figure I-1. Initial Undeformed Configuration of Arch.

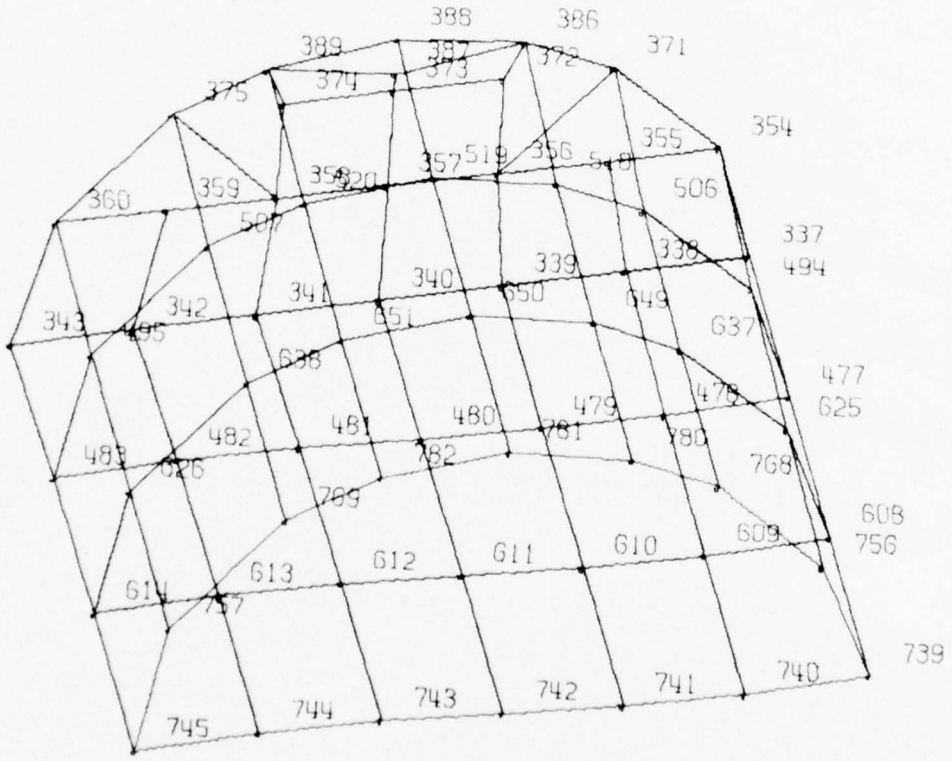

Figure I-2. Mode 1, Uncovered Arch, ω = 10.8 Hz.

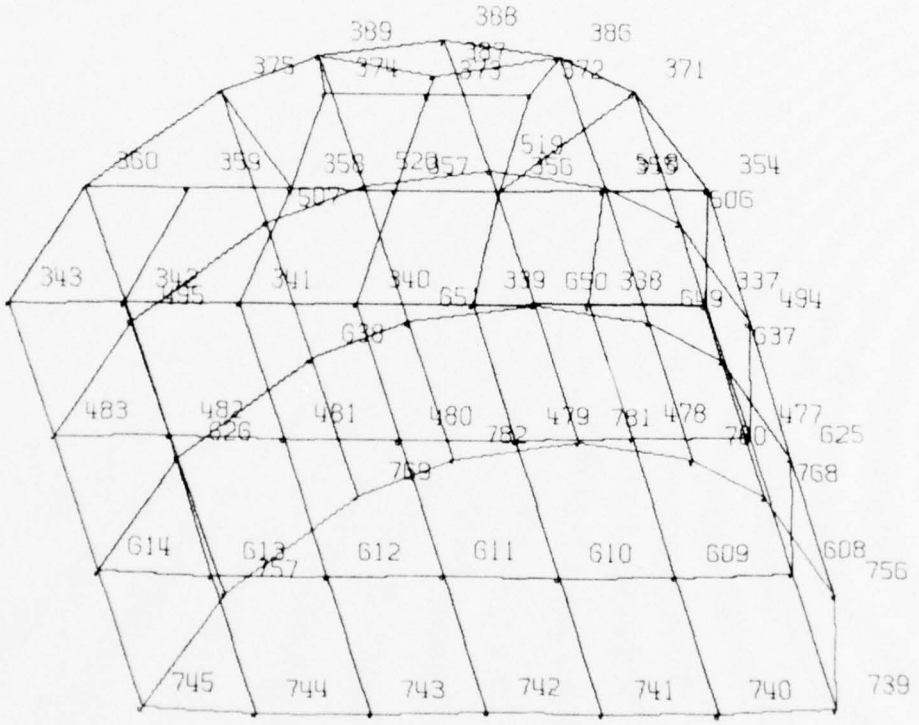

Figure I-3. Mode 2, Uncovered Arch, ω = 13.7 Hz.

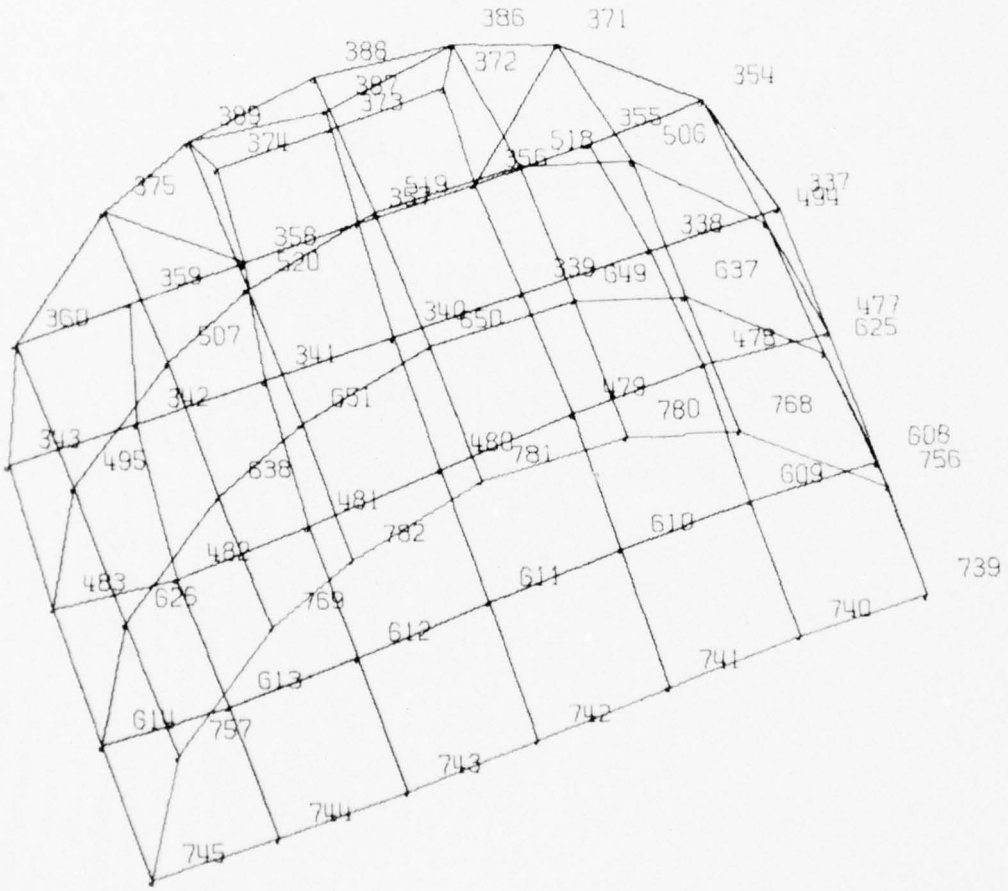

Figure I-4. Mode 3, Uncovered Arch, ω = 16.1 Hz.

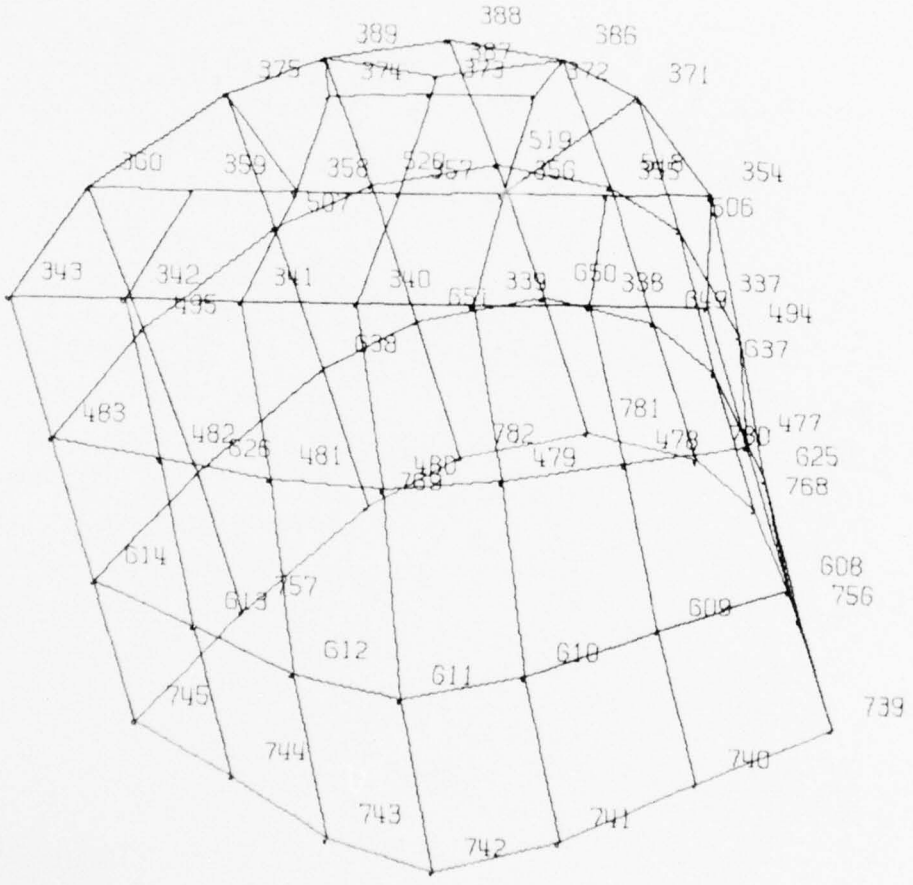

Figure I-5. Mode 4, Uncovered Arch, ω = 33.0 Hz.

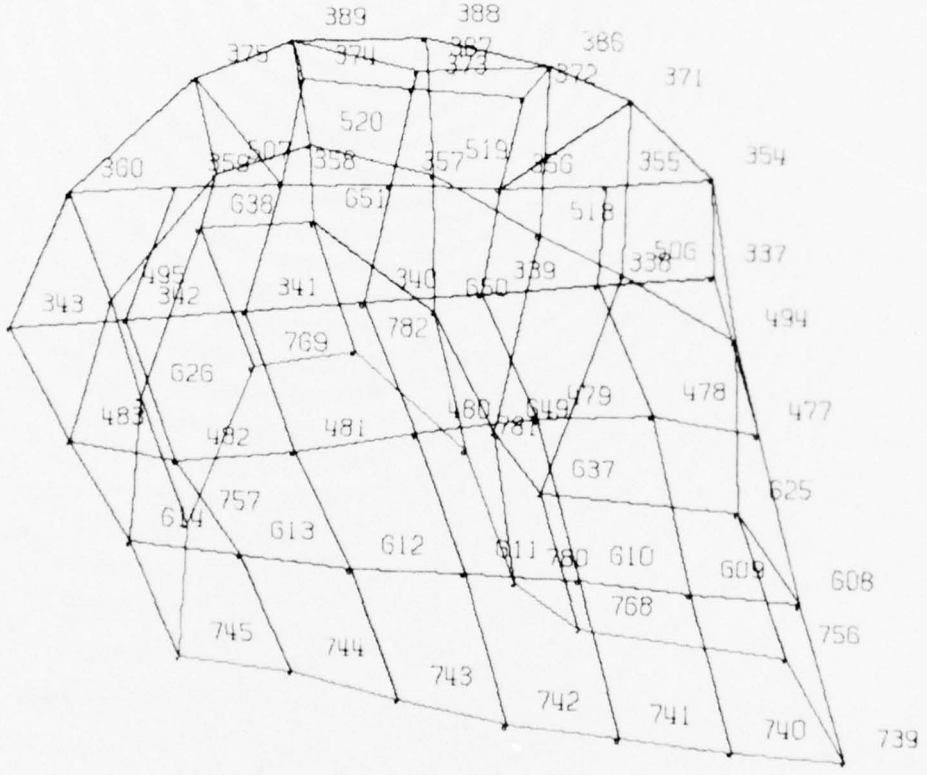

Figure I-6. Mode 5, Uncovered Arch, ω = 70.7 Hz.

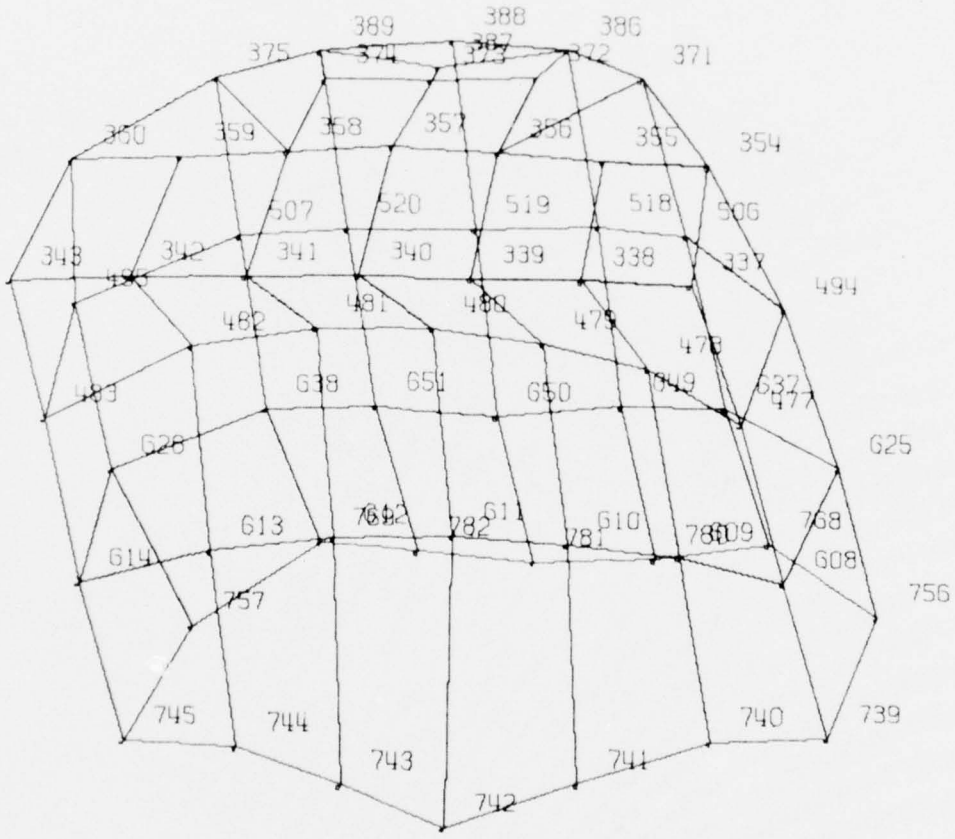

Figure I-7. Mode 6, Uncovered Arch, ω = 84.2 Hz.

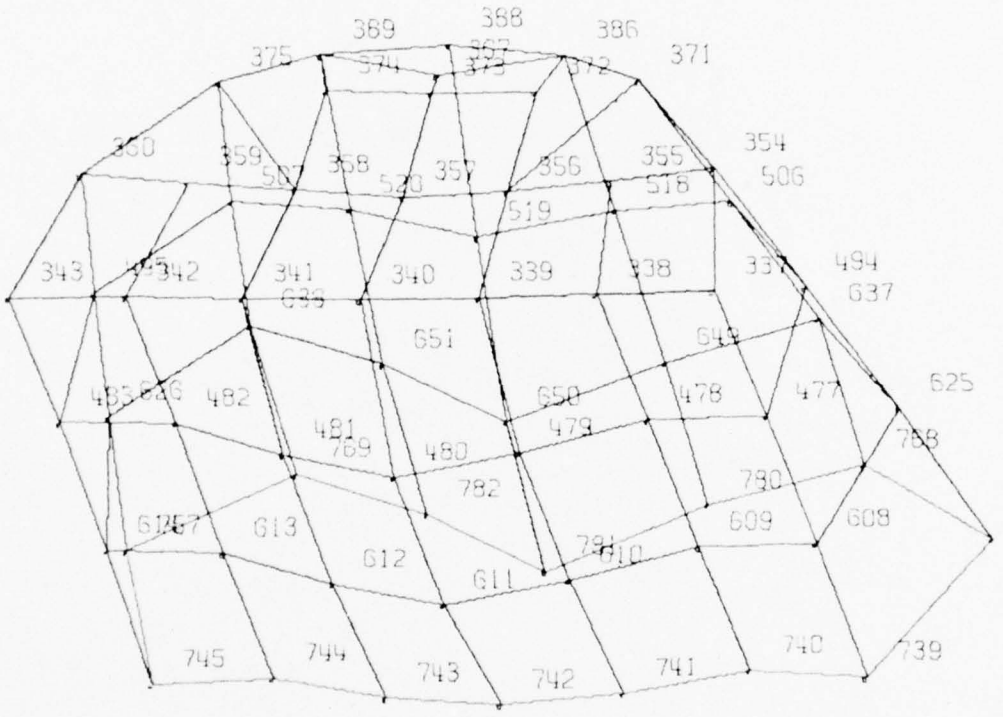

Figure I-8. Mode 7, Uncovered Arch, ω = 100.1 Hz.

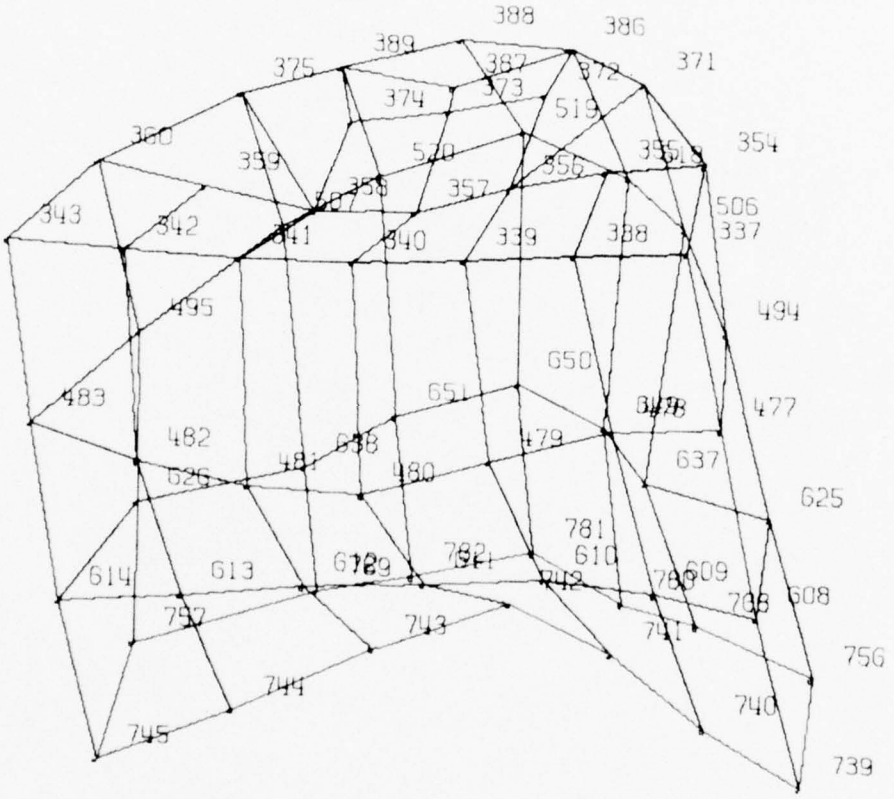

Figure I-9. Mode 8, Uncovered Arch, ω = 119.9 Hz.

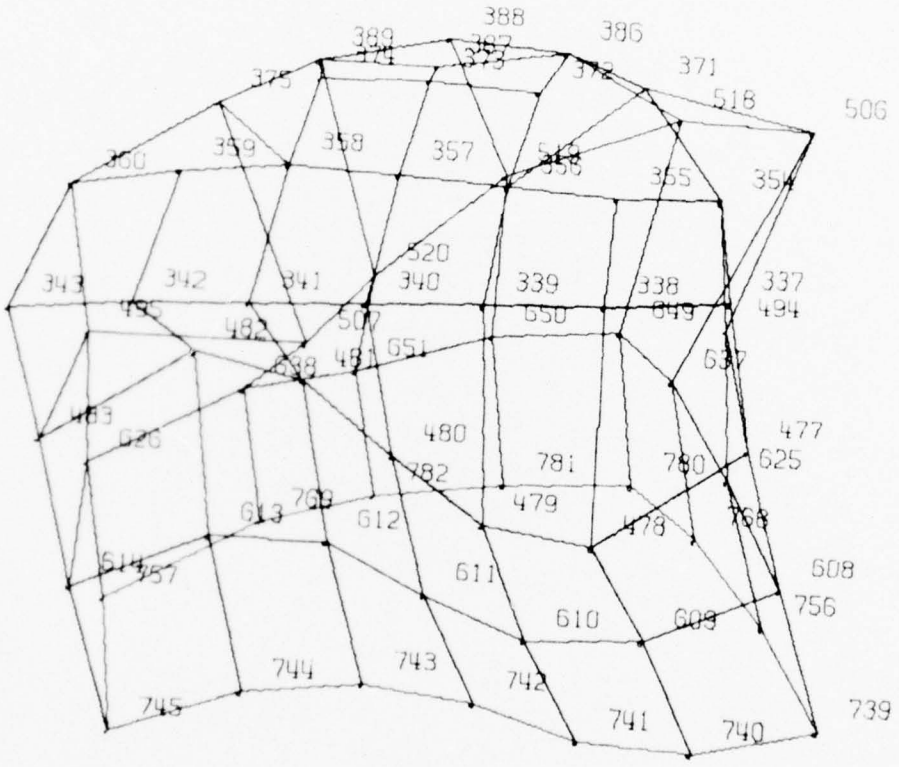

Figure I-10. Mode 9, Uncovered Arch, ω = 148.7 Hz.

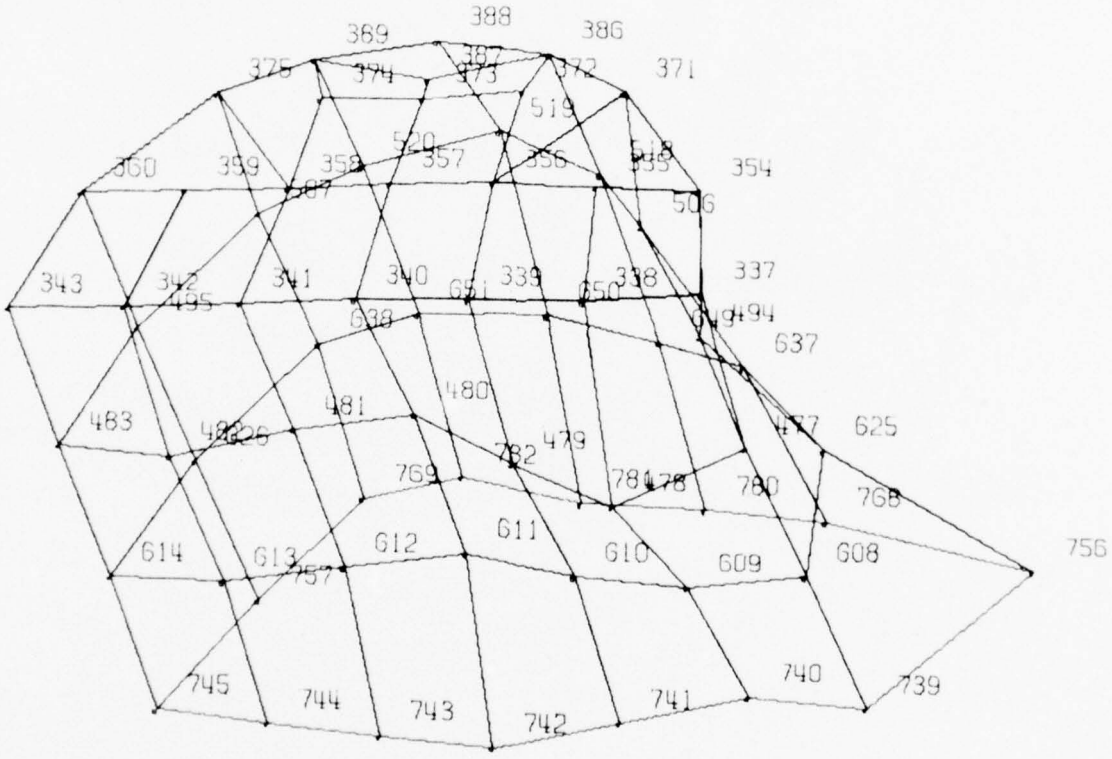

Figure I-11. Mode 10, Uncovered Arch, ω = 185.4 Hz.

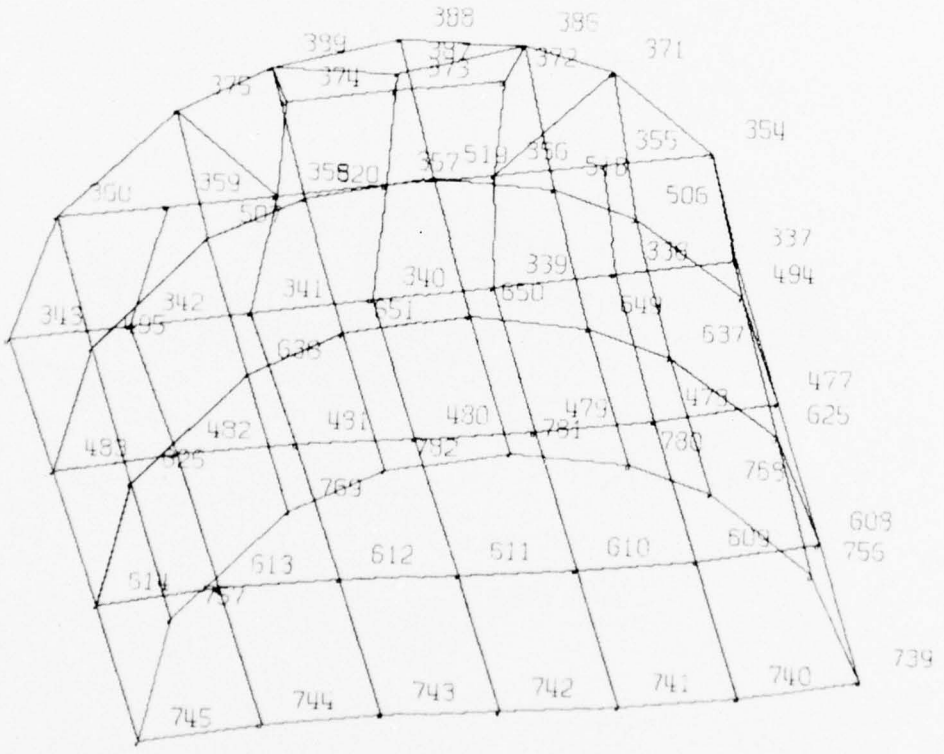

Figure I-12. Mode 1, Covered Arch, ω = 10.1 Hz.

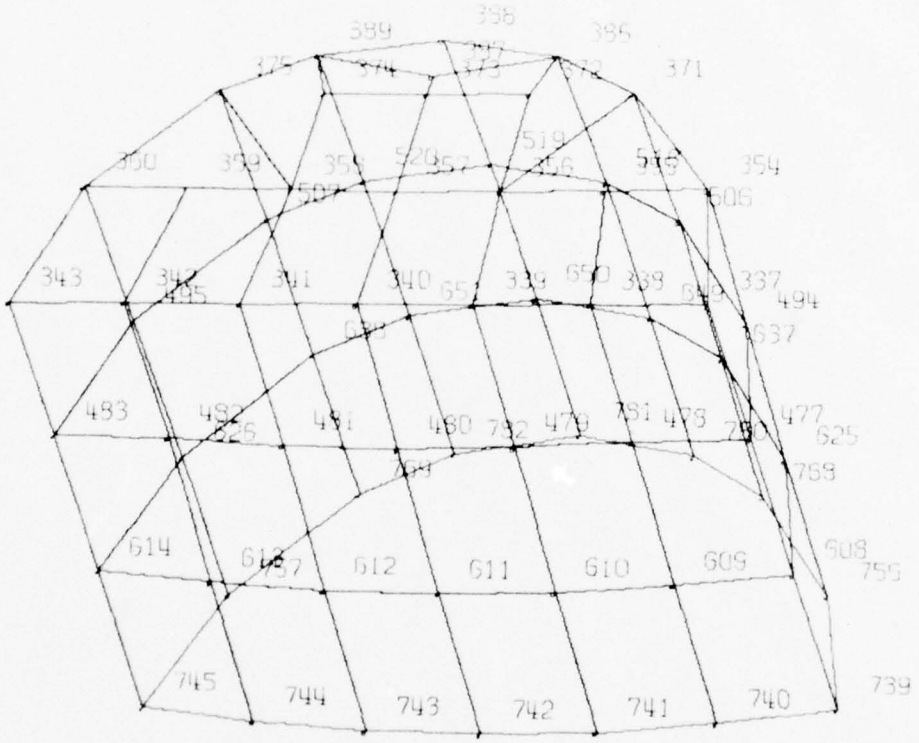

Figure I-13. Mode 2, Covered Arch, ω = 10.4 Hz.

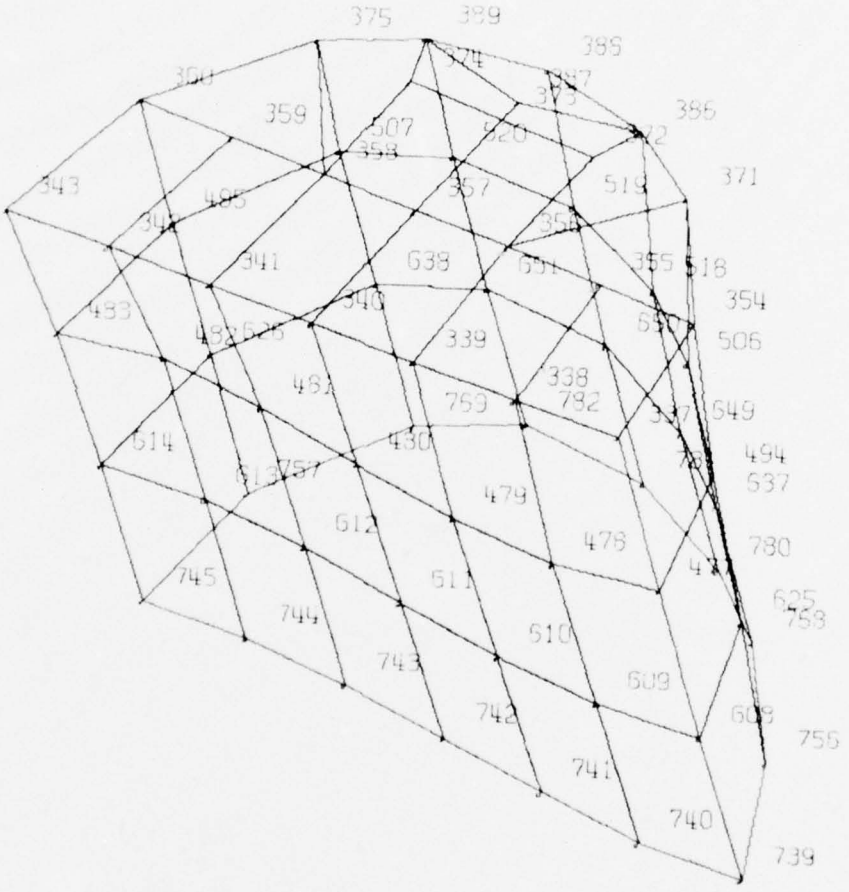

Figure I-14. Mode 3, Covered Arch, ω = 13.8 Hz.

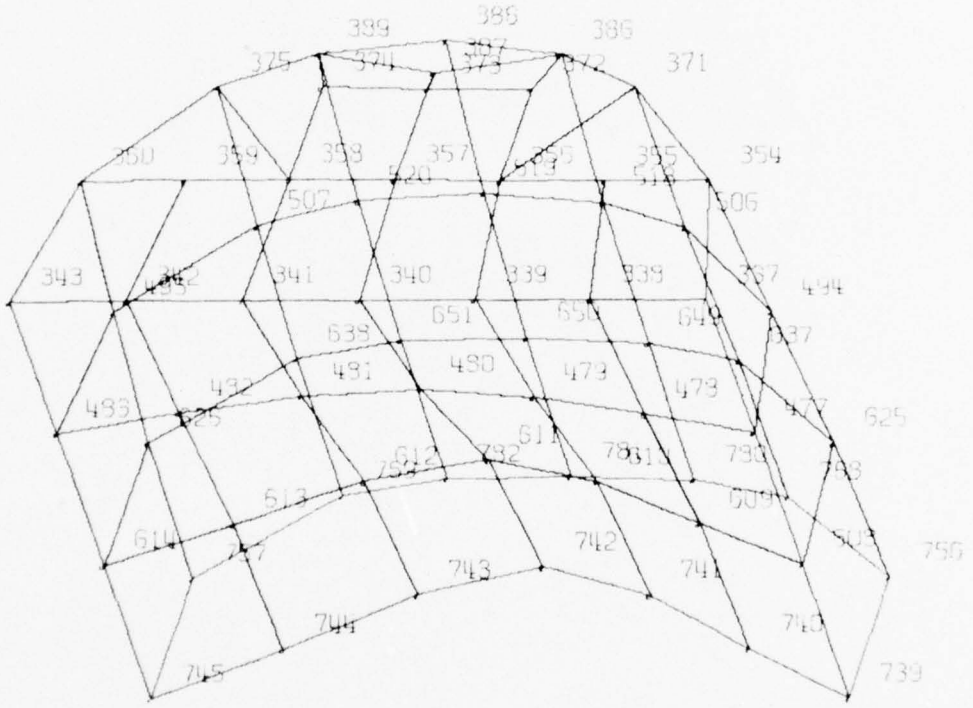

Figure I-15. Mode 4, Covered Arch, ω = 29.3 Hz.

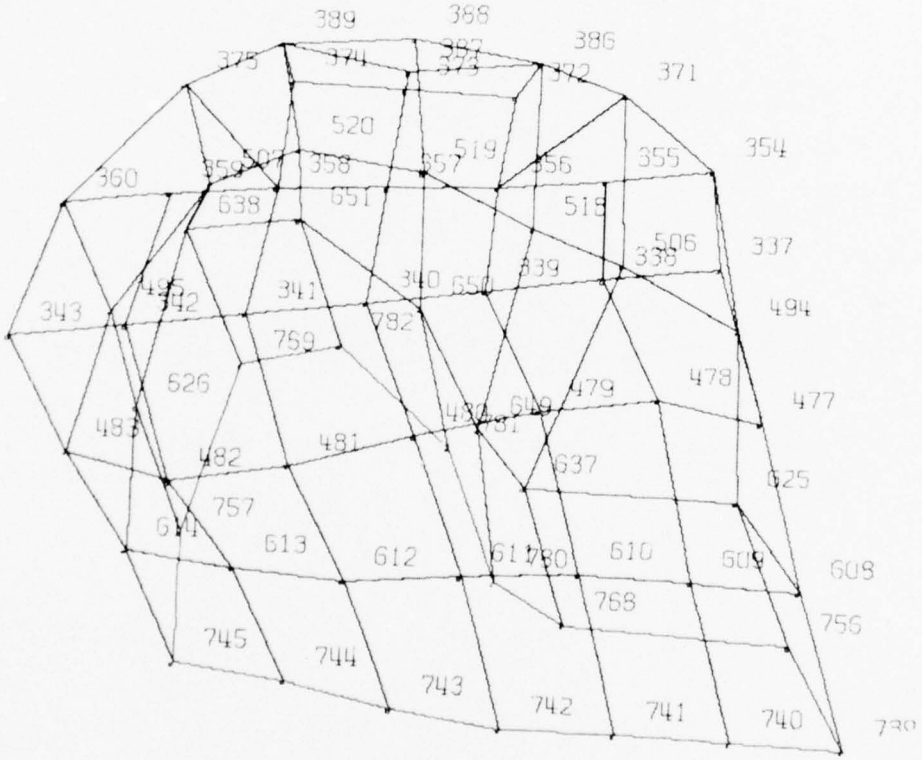

Figure I-16. Mode 5, Covered Arch, ω = 42.1 Hz.

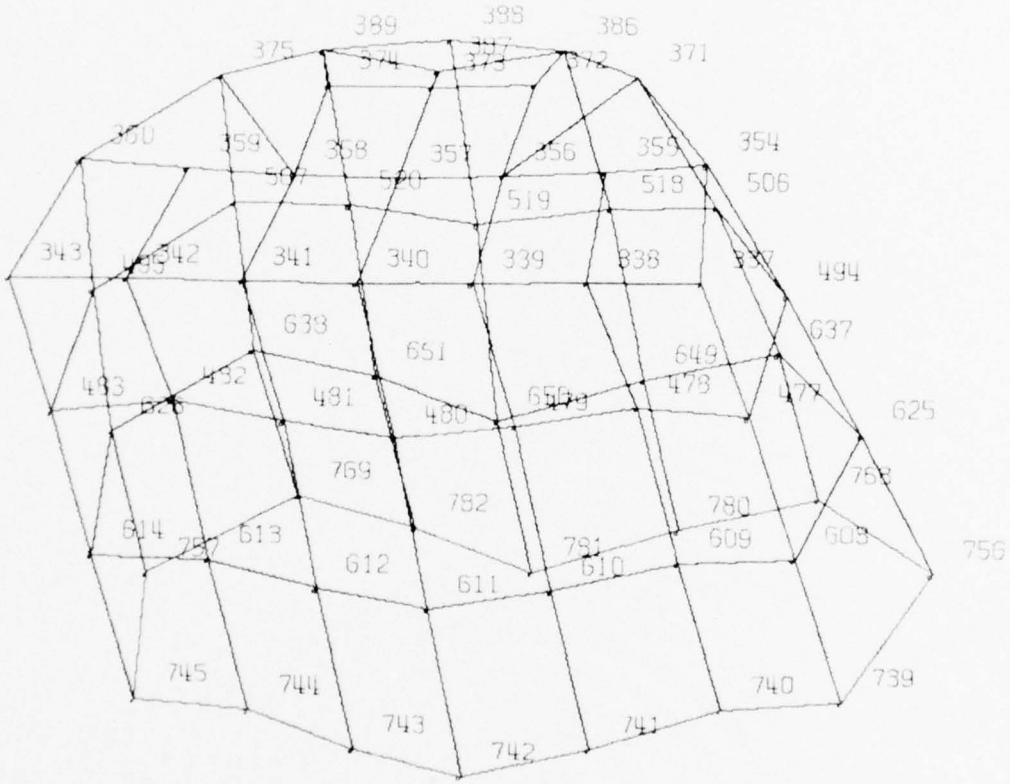

Figure I-17. Mode 6, Covered Arch, ω = 51.8 Hz.

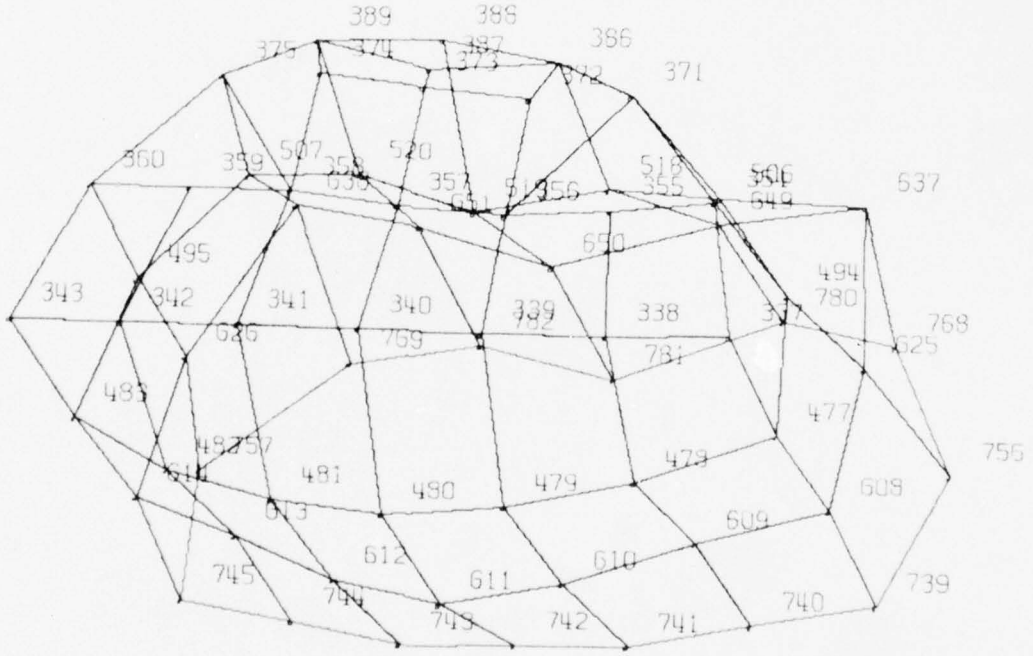

Figure I-18. Mode 7, Covered Arch, ω = 62.5 Hz.

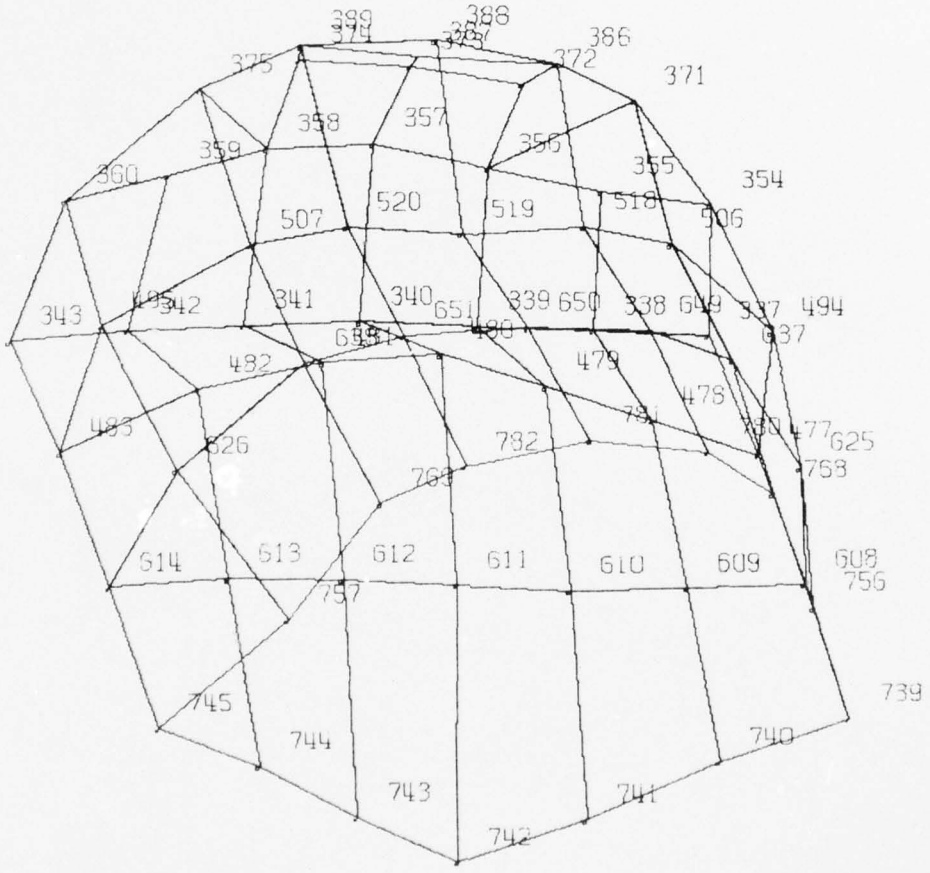

Figure I-19. Mode 8, Covered Arch, ω = 83.8 Hz.

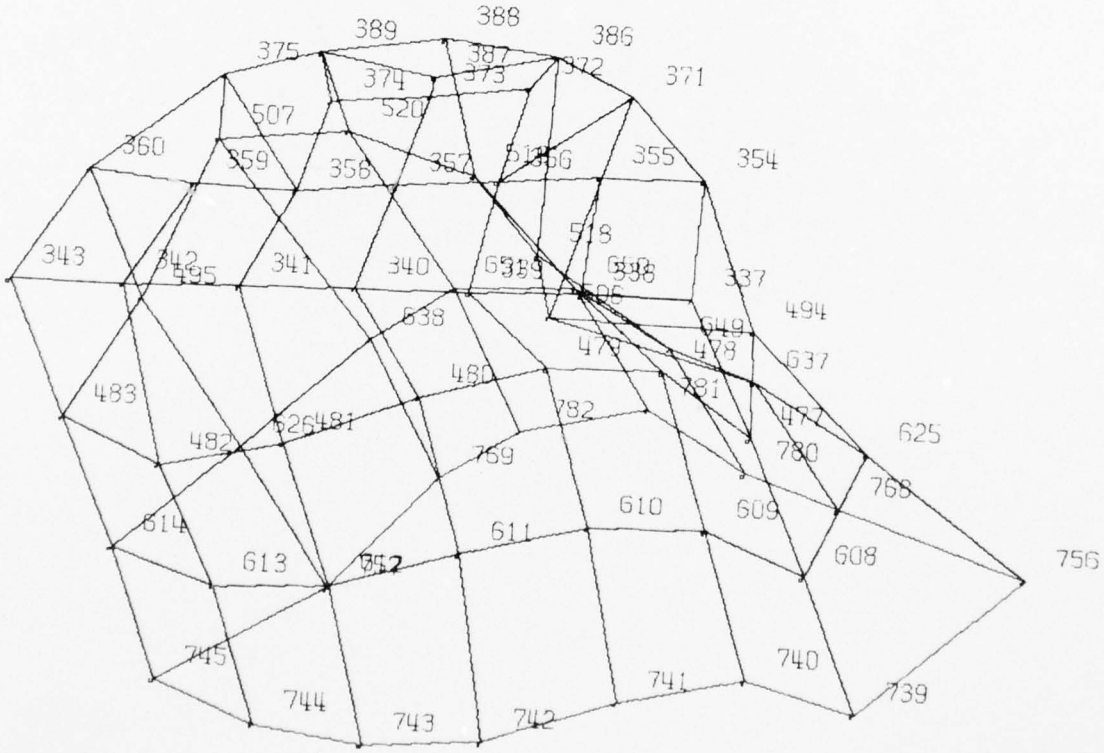

Figure I-20. Mode 9, Covered Arch, ω = 100.7 Hz.

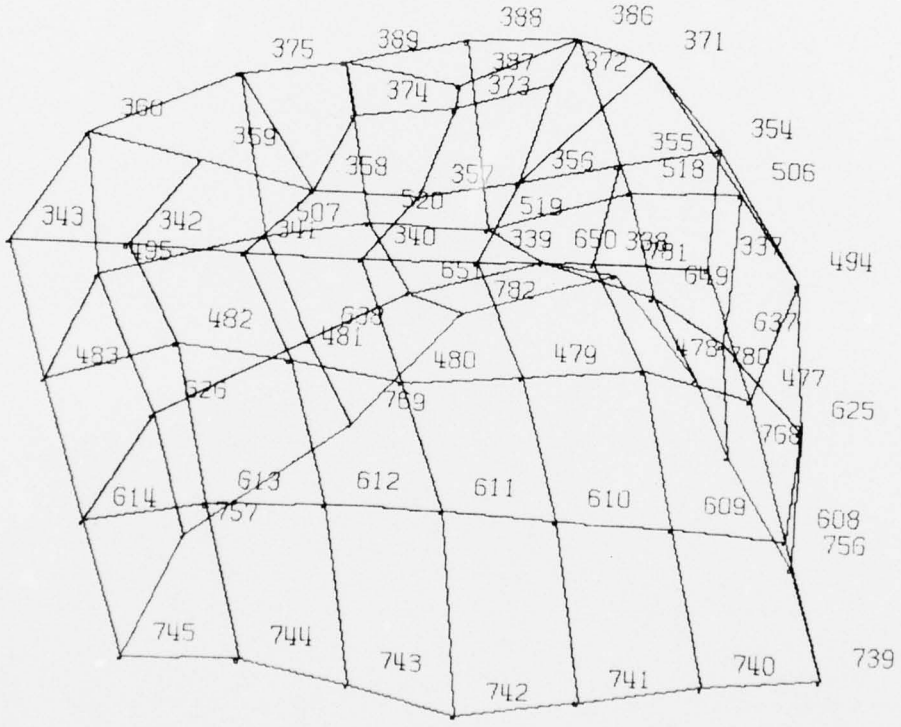

Figure I-21. Mode 10, Covered Arch, ω = 110.3 Hz.

APPENDIX II

RADIATION DAMPING ASSOCIATED WITH DEFORMATIONAL MODES OF A CIRCULAR CYLINDER EMBEDDED IN AN INFINITE ELASTIC DOMAIN

It is shown in Section 3 that radiation damping associated with vibration of the covered arch increases significantly as the stiffness of the surrounding soil increases. It appears that, in the range of uncertainty with which wave speeds in the surrounding soil are known, significant variation in radiation damping can occur. This finding suggests that backfill conditions, such as degrees of compaction and contact with the structure, may need to be considered in developing damping parameters for the idealized, single degree-of-freedom analytic models used in targeting analysis.

To confirm the trend obtained in the finite element calculations, Weidlinger Associates requested that another DNA contractor, Lockheed Palo Alto Research Laboratory, apply a closed-form analysis technique (Ref. 11) to obtain free vibration, modal response of an infinitely long cylinder embedded in an infinite elastic domain. The principal investigator at Lockheed, Dr. T. L. Geers, supplied the responses for three problems in which the shell parameters were held constant while the wave speeds in the soil varied in the ratio 1:2:4. The geometry and material properties of the cylindrical shell and soil, defined by following non-dimensional ratios, are roughly the same as those of the arch.

$$\alpha = \frac{h^2}{12a^2} = .0017$$

$$\mu_o = \frac{\rho_o h}{\rho_m a} = .17$$

$$\beta_s = \frac{c_s}{c_p} = 1/2$$

where

h, a = thickness, radius, respectively, of the shell

ρ_o, ρ_m = mass density of the shell and soil medium, respectively

c_s, c_p = shear and dilatational wave speeds, respectively, in the soil medium

The wave speeds in the soil are defined through a further dimensionless ratio

$$\beta_o = \frac{c_o}{c_p}$$

where

c_o = bar velocity in the shell, $c_o^2 = \frac{E_o}{\rho_o (1 - \nu^2)}$, where

E_o, ν_o are Young's Modulus and Poisson's ratio, respectively, for the shell material.

In the three cases considered, β_o was varied by varying c_p the dilatational wave speed in the soil. The range of parameters was as follows:

Case	β_o
1	47.6 (softest soil)
2	23.8
3	11.9 (stiffest soil)

The time histories of radial displacement are presented in Figures II-1 through II-4 for modes n = 0 through n = 3 for an impulsive excitation of the extensional modes. The radial displacement w for mode n and the time t are normalized to a and c_p/a, respectively. The normalization parameter for time makes it appear in the figures as if the natural frequencies of the shell are drastically reduced if the shell is placed in stiffer soil. This is mainly an illusion caused by the nondimensional parameter, as can be seen by dividing the time scale in cases 2 and 3 in Figure II-1 by 2 and 4, respectively. Some reduction of natural frequency occurs, however, apparently due to large effective damping ratios; see case 3, Figure II-4.

The main purpose of performing these calculations is to see how the equivalent fraction of critical viscous damping varies with wave speed in the

soil. In these cases, damping is entirely of the radiation type. There is no ambiguity in evaluating the log decrement for each displacement-time history because each represents the oscillation in one mode only, and the decay rates for deformational modes are negative exponentials. The fractions of critical damping are shown in Table II-1. The table shows a trend of higher damping with increasingly stiffer soil, which is the same trend exhibited by the finite element calculations of the arch. When the properties of the system are fixed, the amount of damping is highly dependent on the mode number. For example, in case 2, mode 1 is lightly damped, mode 2 is about critically damped and mode 4 is highly, yet subcritically, damped. This clearly illustrates the frequency dependence of structure-medium interaction. The n = 1 mode involves rigid body motion only and hence the normalized response appears to be independent of wave speed in the soil. The damping for this mode is logarithmic in nature, unlike that for the deformational modes which is exponential. Damping in the rigid body mode is very large and no oscillation occurs.

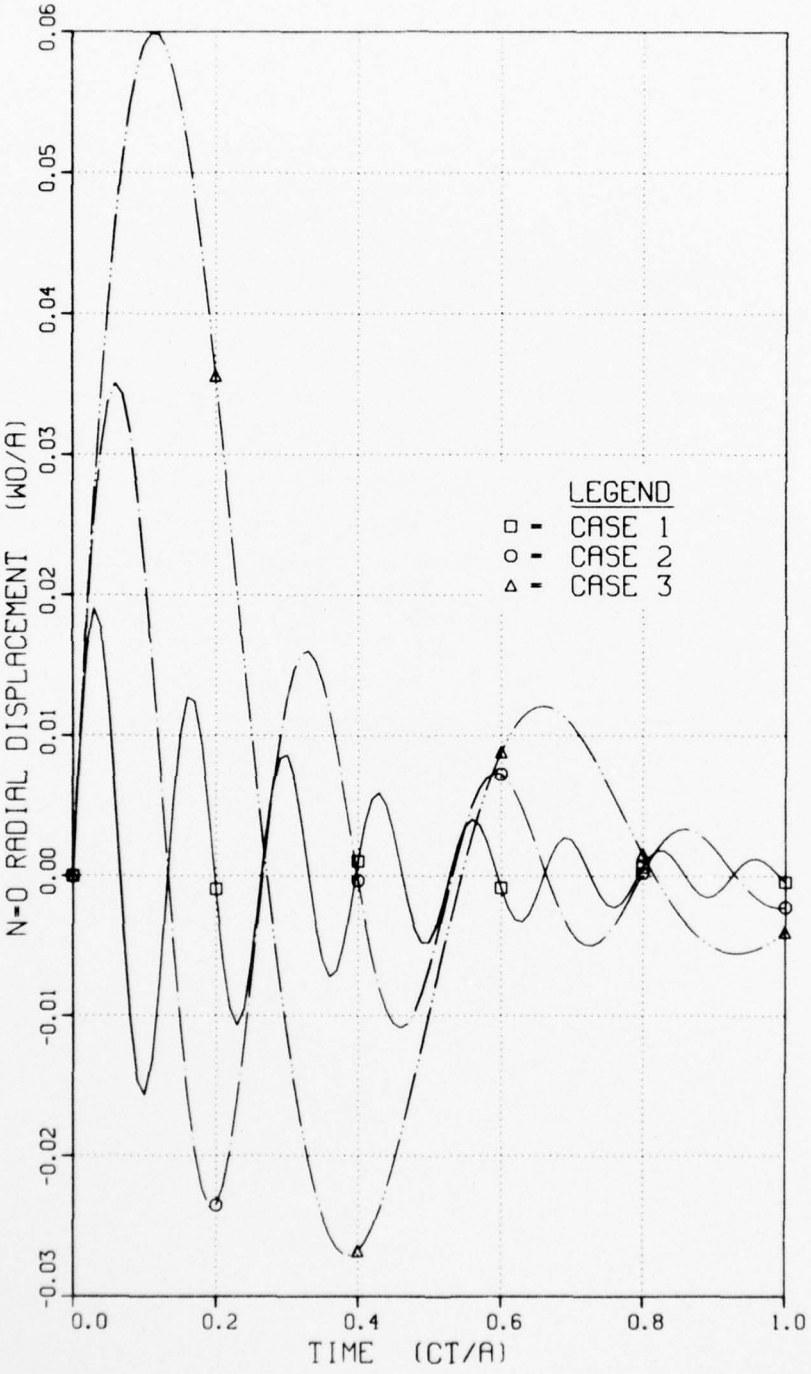

Figure II-1. Normalized Modal Displacement for n = 0 Mode Versus Normalized Time for a Shell Embedded in Three Different Elastic Soils.

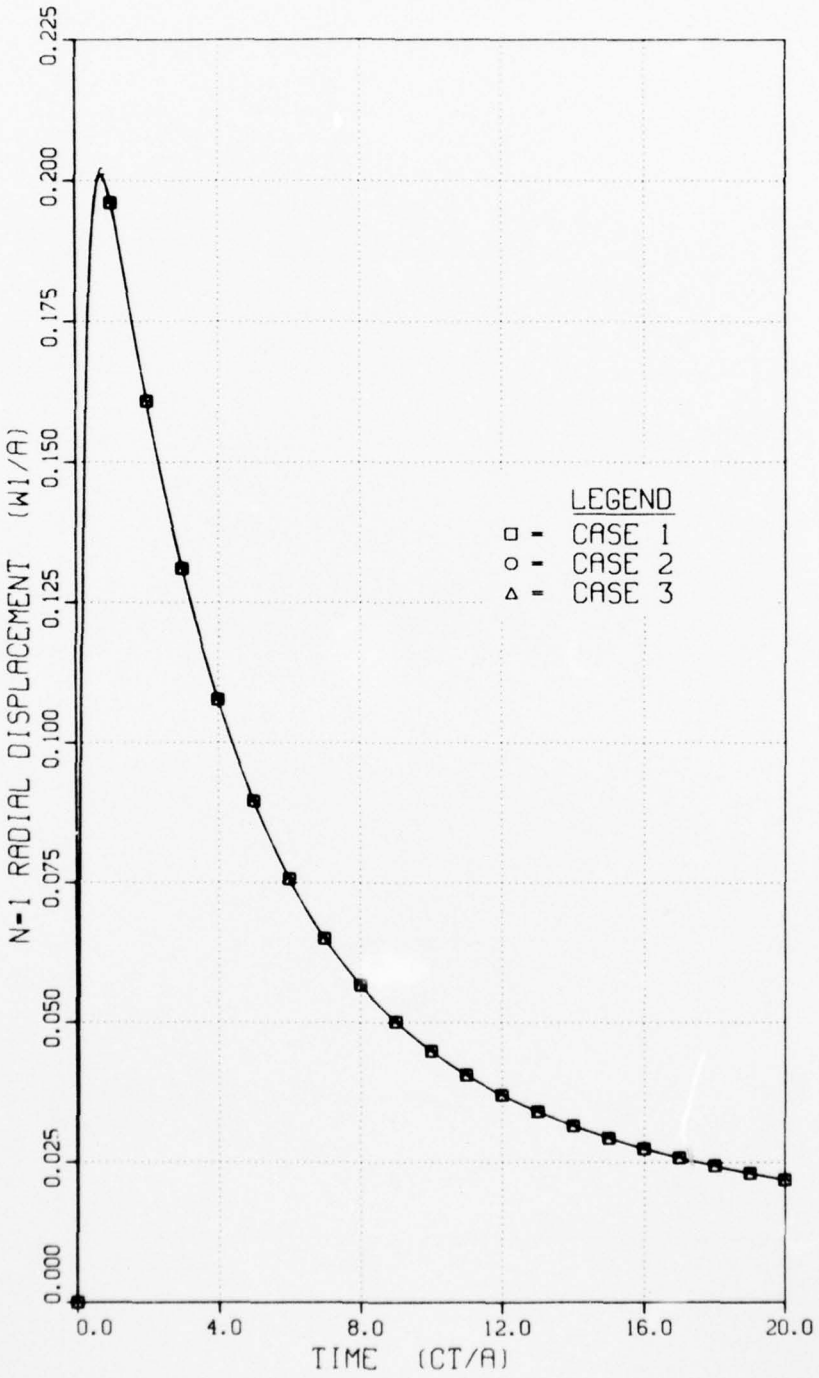

Figure II-2. Normalized Modal Displacement for n = 1 Mode Versus Normalized Time for a Shell Embedded in Three Different Elastic Soils.

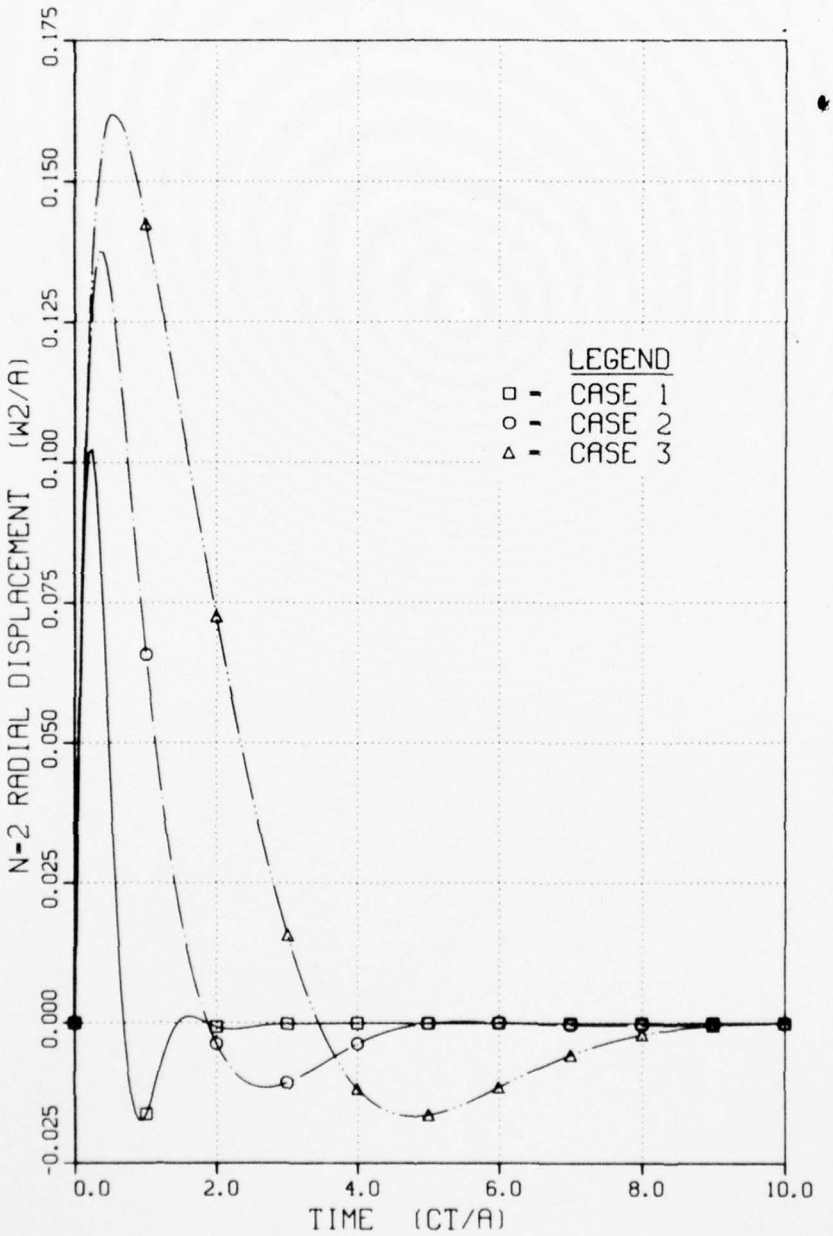

Figure II-3. Normalized Modal Displacement for n = 2 Mode Versus Normalized Time for a Shell Embedded in Three Different Elastic Soils.

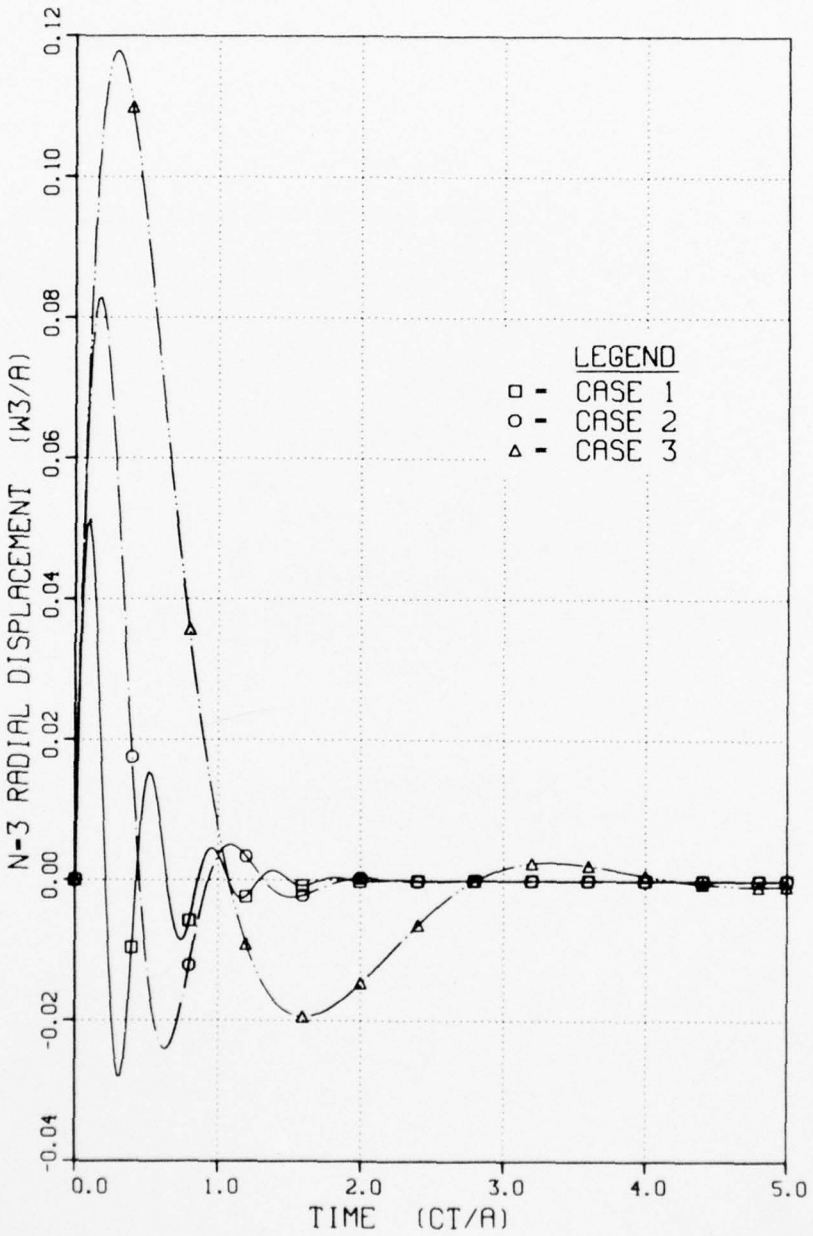

Figure II-4. Normalized Modal Displacement for n = 3 Mode Versus Normalized Time for a Shell Embedded in Three Different Elastic Soils.

TABLE II-1.

EQUIVALENT FRACTIONS OF CRITICAL VISCOUS DAMPING FOR INFINITELY LONG CYLINDER IN INFINITE SOIL MEDIUM SUBJECTED TO IMPULSIVE LOADING

Mode	n	Case 1 (soft soil)	Case 2	Case 3 (stiff soil)
1	0	.06	.13	.24
2*	1	>1.0	>1.0	>1.0
3	2	.61	∿1.0	∿1.0
4	3	.19	.41	.51

*Mode 2 (n = 1) is a rigid body translation mode for which damping is large.

APPENDIX III

CHECK PROBLEMS FOR IMPLEMENTATION OF FRICTION IN THREE-DIMENSIONAL, LINEAR FINITE ELEMENT CODE

The implementation of a friction model in GENSAP required numerous coding changes, and two check problems were devised to test the new model. These are illustrated in Figure III-1. The simulation of the block sliding on the plane is the same problem for which Den Hartog (Ref. 2) derived equivalent viscous and Coulomb damping. The friction coefficients in the expression

$$f = \mu N$$

was chosen such that $\mu = 0.20$. This produces 10 percent equivalent critical viscous damping. Initially, a force having rise and decay times each equal to a quarter of the natural period of the system was applied to the block to set it in motion. Displacement-time histories for the block with and without friction are shown in Figures III-2 and III-3. Eliminating the damping due to the integration algorithm, which accounts for the decrease in amplitude in Figure III-2, indicates that the friction is responsible for approximately 8 percent damping.

A more ambitious check solution was then obtained for the two-dimensional arch subjected to a point load at the crown, which is illustrated in Figure III-1. The dimensions of this arch and the three-dimensional one of ultimate interest are identical. However, the mass and stiffness properties of the soil were omitted from the two-dimensional example. In this calculation, the frictional forces F were computed separately for each node.

$$F = (\mu\sigma_n)A$$

where

σ_n = the normal stress at each node, respectively, due to overburden stress

The value of σ_n varies due to variable depth of a hypothetical overburden and to varying angle between the normal to the arch and the vertical.

Another detail in implementing the model is to decide on the direction of the friction force. It must lie along the tangent to the arch at each node, but there are two possible directions. The choice is made by comparing the direction of the velocity vector with the normal and requiring the friction force vector to lie on the opposite side of the normal. This is illustrated in Figure III-1.

As in the other example, the effect of damping is evaluated by applying an impulsive force to the crown and noticing the decrement in amplitude of the crown with successive cycles. The cases shown in Figures III-4 and III-5 have $\mu = 0.4$ and zero friction, respectively. As in the case of the block sliding on a frictionless plane, there is significant decrease in amplitude. In this case, it is partly due to the integration algorithm and partially due to the nature of the dynamic response. The decrement in the case with friction is much greater.

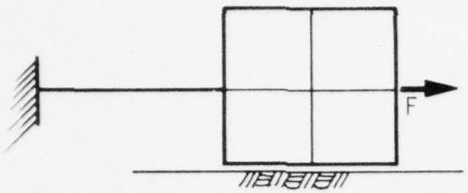

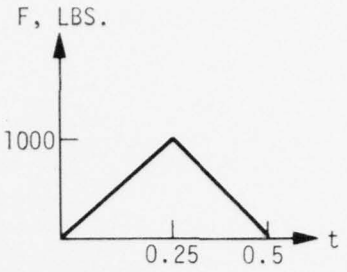

ω_o = 1 CPS

W = 816 LBS.

k = 1000 LBS/FT.

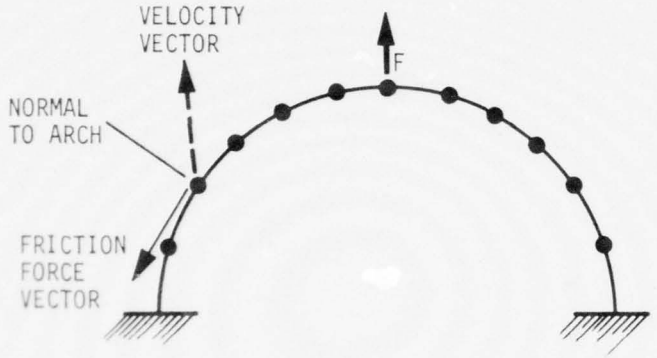

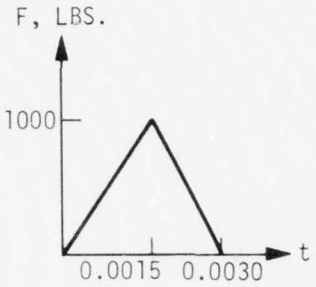

EI = 5.52×10^7 LB-FT.^{2}

THICKNESS = 1 FT.

ω_o = 338 CPS

w = 150 LB/FT.^{3}

Figure III-1. Test Problems for Viscous Friction (cont.)

AD-A047 386 WEIDLINGER ASSOCIATES MENLO PARK CALIF F/G 13/13
NUMERICAL SIMULATION OF FORCED VIBRATION TESTS ON A BURIED ARCH--ETC(U)
MAR 77 J ISENBERG, H S LEVINE, S H PANG DNA001-76-C-0110
UNCLASSIFIED 7712 DNA-4281F NL

2 OF 2
AD
A047386

END
DATE FILMED
1-78
DDC

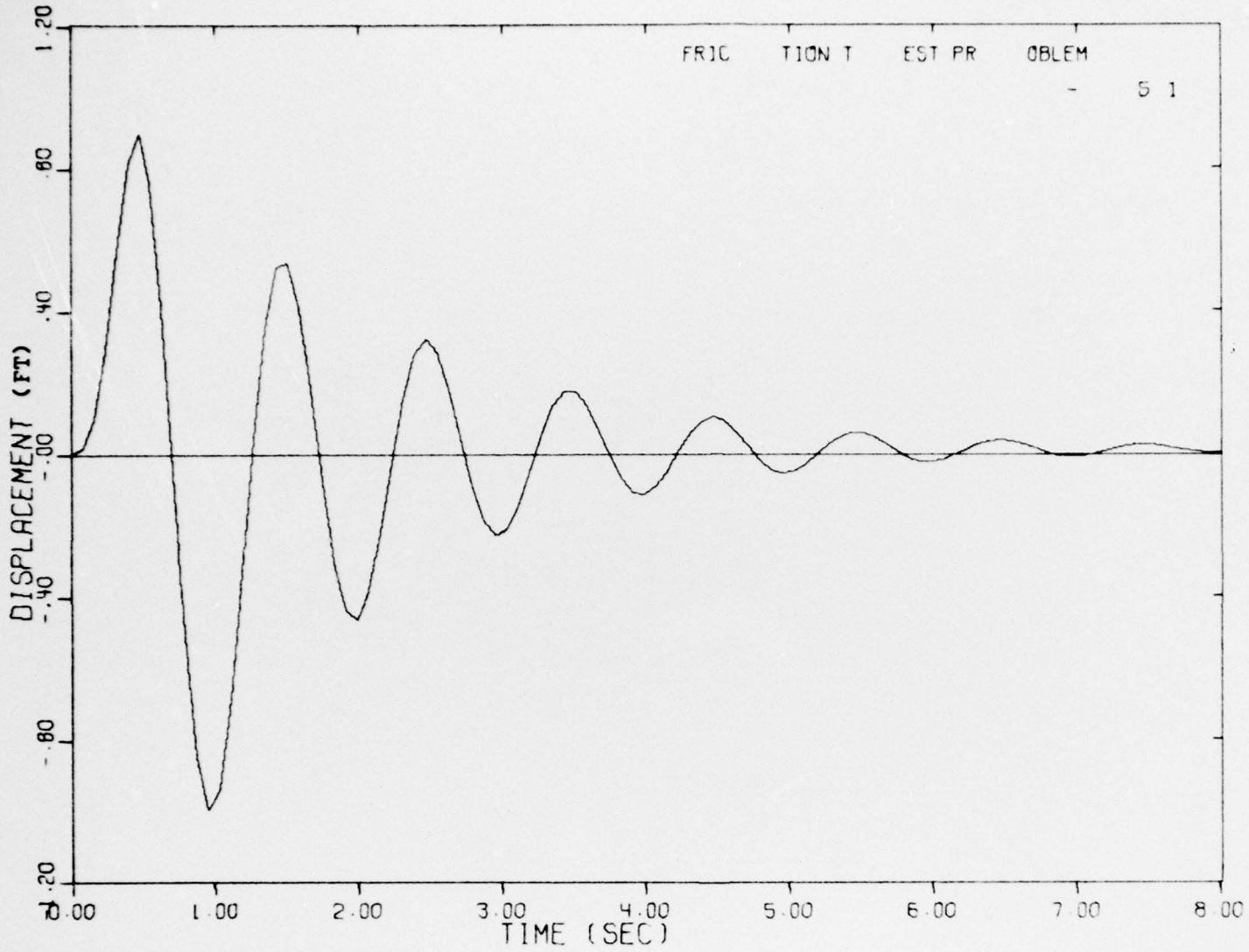

Figure III-2. Displacement-Time History of Block Sliding on Plane with Coulomb Friction Damping.

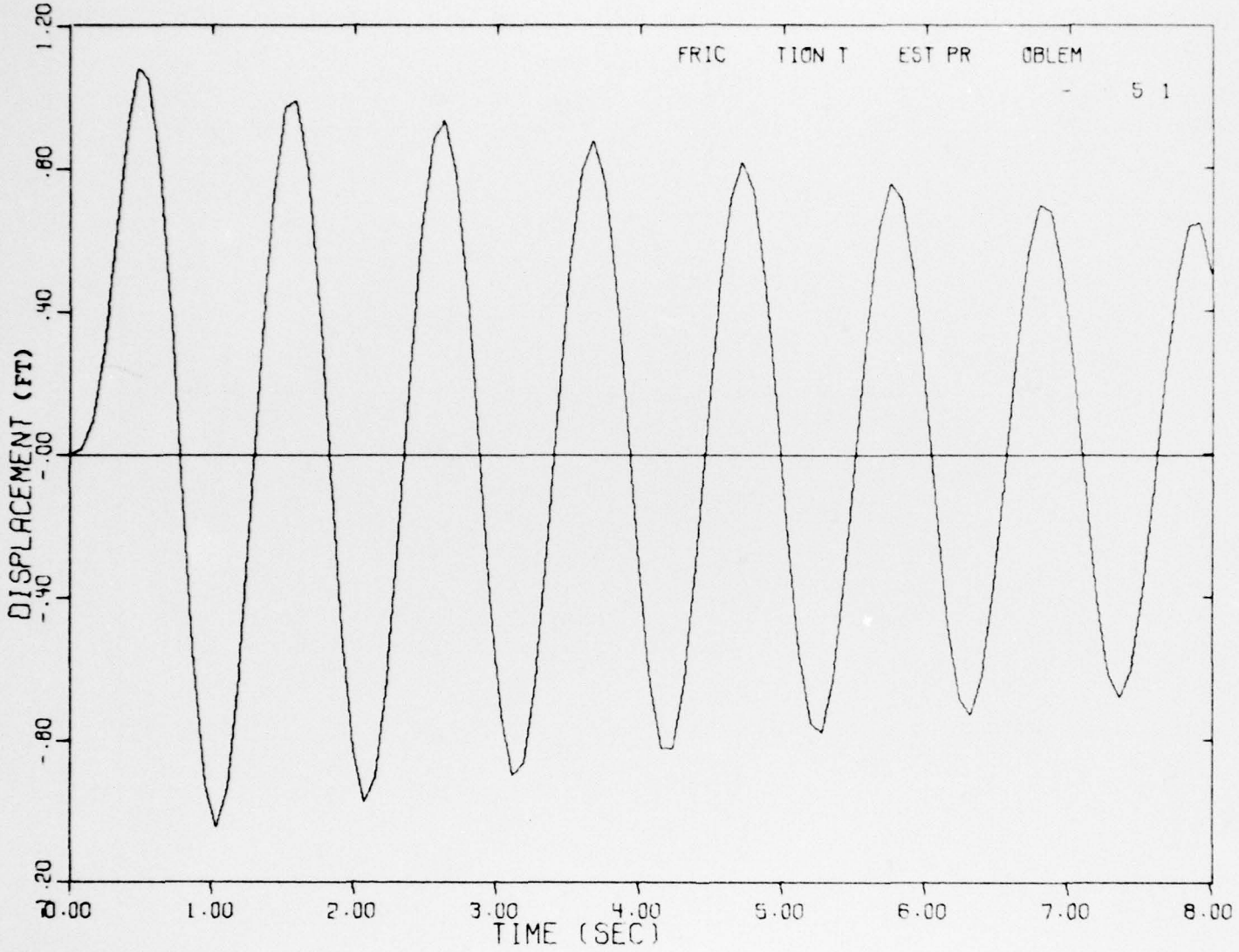

Figure III-3. Displacement-Time History of Block Sliding on Frictionless Plane.

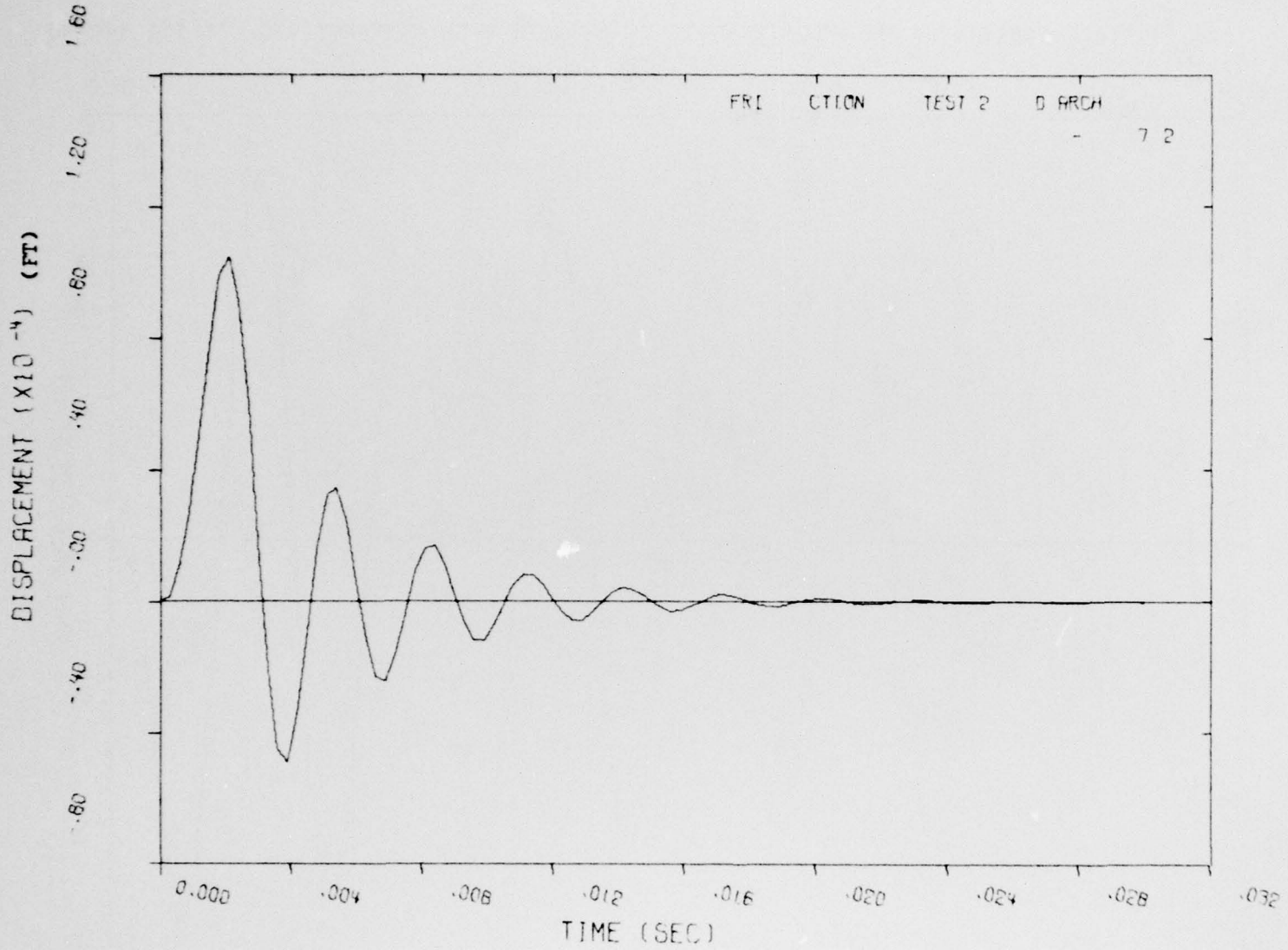

Figure III-4. Displacement-Time History at the Crown of Two-Dimensional Arch with Friction on Surface. Impulsive Load at Crown.

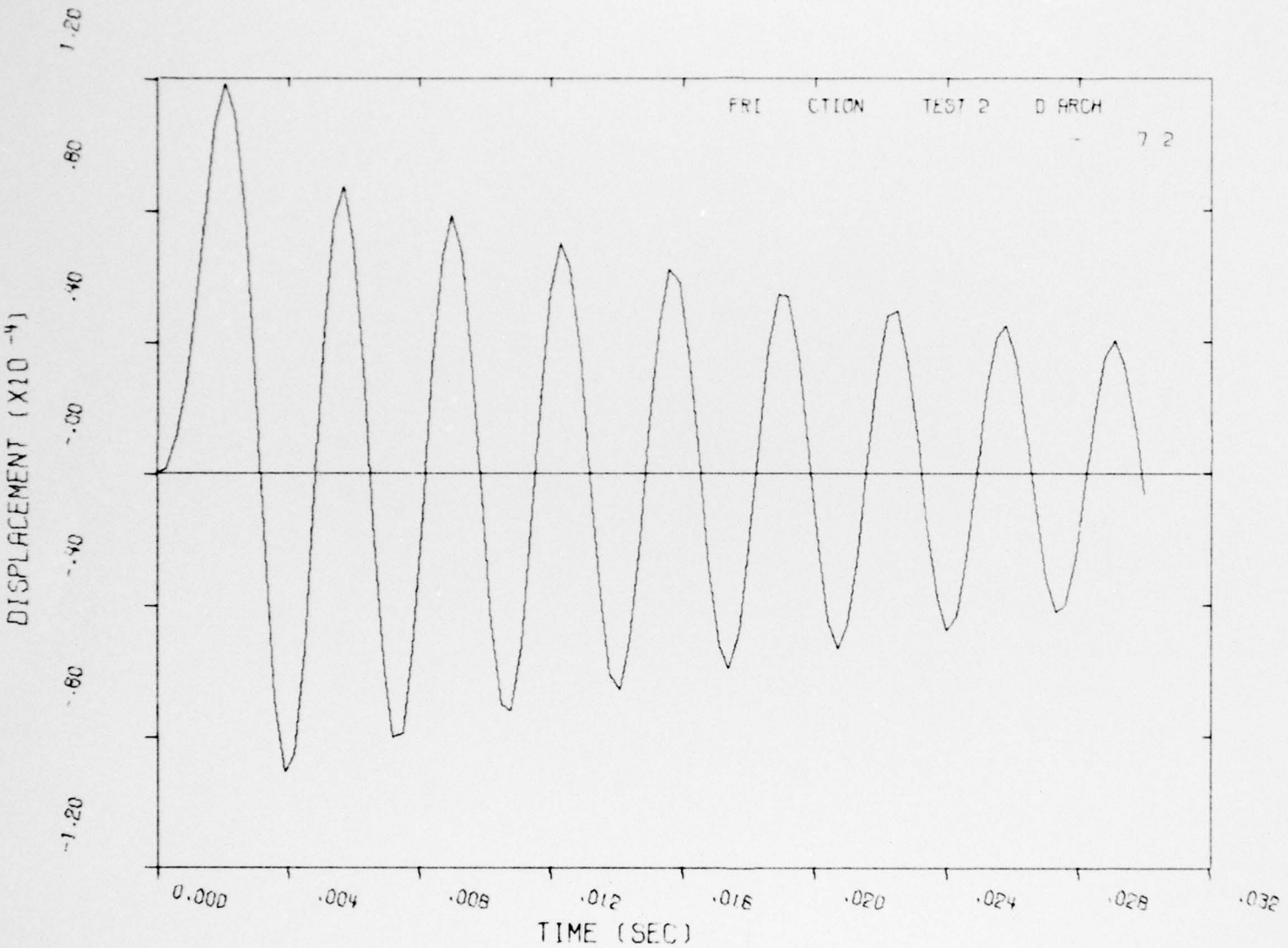

Figure III-5. Displacement-Time History at the Crown of Two-Dimensional Arch without Friction. Impulsive Load.

DISTRIBUTION LIST

DEPARTMENT OF DEFENSE

Assistant to the Secretary of Defense
Atomic Energy
Department of Defense
ATTN: Honorable Donald R. Cotter

Director
Defense Advanced Research Proj. Agency
ATTN: NMRO
ATTN: PMO
ATTN: STO
ATTN: Technical Library

Director
Defense Civil Preparedness Agency
Assistant Director for Research
ATTN: Admin. Officer
ATTN: Staff Dir. Resr., George N. Sisson

Defense Communications Agency
WWMCCS System Engineering Org.
ATTN: Thomas Neighbors

Defense Documentation Center
Cameron Station
12 cy ATTN: TC

Director
Defense Intelligence Agency
ATTN: Technical Library
ATTN: DB-4C, Edward O'Farrell
ATTN: DT-2, Wpns. & Sys. Div.

Director
Defense Nuclear Agency
2 cy ATTN: SPSS
ATTN: DDST
ATTN: TISI, Archives
3 cy ATTN: TITL, Tech. Library

Dir. of Defense Rsch. & Engineering
Department of Defense
ATTN: S&SS (OS)

Commander
Field Command
Defense Nuclear Agency
ATTN: FCTMOF
ATTN: FCPR

Director
Interservice Nuclear Weapons School
ATTN: Document Control

Director
Joint Strat. Target Planning Staff, JCS
ATTN: STINFO, Library

Chief
Livermore Division, Field Command, DNA
Lawrence Livermore Laboratory
ATTN: FCPRL

DEPARTMENT OF THE ARMY

Director
BMD Advanced Tech. Center
Huntsville Office
ATTN: CRDABH-X
ATTN: CRDABH-S

Director
Construction Engineering Research Lab.
ATTN: CERL-SL

Dep. Chief of Staff for Rsch. Dev. & Acq.
Department of the Army
ATTN: Technical Library

Chief of Engineers
Department of the Army
ATTN: DAEN-MCE-D
ATTN: DAEN-RDM

Deputy Chief of Staff for Ops. & Plans
Department of the Army
ATTN: Technical Library

Commander
Harry Diamond Laboratories
ATTN: DRXDO-TI, Tech. Lib.
ATTN: DRXDO-NP

Commander
Redstone Scientific Information Center
US Army Missile Command
ATTN: Chief, Documents

Director
US Army Ballistic Research Labs.
ATTN: DRXBR-X, Julius J. Meszaros/W. Taylor
ATTN: Tech. Lib., Edward Baicy

Commander
US Army Communications Command
ATTN: Technical Library

Commander
US Army Engineer Center
ATTN: ATSEN-SY-L

Division Engineer
US Army Engineer Div. Huntsville
ATTN: HNDED-SR

Division Engineer
US Army Engineer Div. Ohio River
ATTN: Technical Library

Director
US Army Engr. Waterways Exper. Sta.
ATTN: Technical Library
ATTN: William Flathau/James Ballard

Commander
US Army Mat. & Mechanics Rsch. Center
ATTN: Technical Library

DEPARTMENT OF THE ARMY (Continued)

Commander
US Army Materiel Dev. & Readiness Command
ATTN: Technical Library

Commander
US Army Mobility Equip. R & D Center
ATTN: Technical Library

Commander
US Army Nuclear Agency
ATTN: Tech. Lib.
ATTN: ATCA-NAW

DEPARTMENT OF THE NAVY

Chief of Naval Material
Navy Department
ATTN: MAT 0323

Chief of Naval Operations
Navy Department
ATTN: OP 981
ATTN: OP 03EG

Chief of Naval Research
Navy Department
ATTN: Code 464, Jacob L. Warner/T. P. Quinn
ATTN: Technical Library
2 cy ATTN: Nicholas Perrone

Officer in Charge
Civil Engineering Laboratory
Naval Construction Battalion Center
ATTN: Technical Library
ATTN: Stan Takahashi/R. J. Odello

Commander
David W. Taylor, Naval Ship R & D Center
ATTN: Code L42-3, Library

Commander
Naval Electronic Systems Command
Naval Electronic Systems Command Hqs.
ATTN: PME 117-21A

Commander
Naval Facilities Engineering Command
Headquarters
ATTN: Technical Library
ATTN: Code 04B
ATTN: Code 03A

Superintendent (Code 1424)
Naval Postgraduate School
ATTN: Code 2124, Tech. Rpts. Librarian

Director
Naval Research Laboratory
ATTN: Code 2600, Tech. Lib.
ATTN: Code 8440, F. Rosenthal

Commander
Naval Sea Systems Command
Navy Department
ATTN: Code 03511
ATTN: ORD-91313, Lib.

DEPARTMENT OF THE NAVY (Continued)

Commander
Naval Ship Engineering Center
Department of the Navy
ATTN: Technical Library
ATTN: NSEC 6105G

Commander
Naval Ship Rsch. & Development Center
Underwater Explosive Research Division
ATTN: Code 17, William W. Murray
ATTN: Technical Library

Officer in Charge
Naval Surface Weapons Center
ATTN: Code WA501, Navy Nuc. Prgms. Off.

Commander
Naval Surface Weapons Center
Dahlgren Laboratory
ATTN: Technical Library

Commanding Officer
Naval Underwater Systems Center
ATTN: Code EM, Jack Kalinowski

Director
Strategic Systems Project Office
Navy Department
ATTN: NSP-43, Tech. Lib.

DEPARTMENT OF THE AIR FORCE

AF Geophysics Laboratory, AFSC
ATTN: SUOL, Research Lib.
ATTN: LWW, Ker C. Thompson

AF Institute of Technology, AU
ATTN: Library AFIT, Bldg. 640, Area B

AF Weapons Laboratory, AFSC
ATTN: SUL
ATTN: DEP, Jimmie L. Bratton
ATTN: DES-S, M. A. Plamondon

Headquarters
Air Force Systems Command
ATTN: DLCAW
ATTN: Technical Library

Commander
Foreign Technology Division, AFSC
ATTN: NICD, Library

Hq. USAF/IN
ATTN: INATA

Hq. USAF/PR
ATTN: PRE

Hq. USAF/RD
ATTN: RDQSM

Commander
Rome Air Development Center, AFSC
ATTN: EMTLD, Doc. Library

SAMSO/MN
ATTN: MNN

DEPARTMENT OF THE AIR FORCE (Continued)

Commander in Chief
Strategic Air Command
ATTN: NRI-STINFO, Library

ENERGY RESEARCH & DEVELOPMENT ADMINISTRATION

University of California
Lawrence Livermore Laboratory
ATTN: Tech. Info. Dept. L-3
ATTN: Larry W. Woodruff, L-96

Los Alamos Scientific Laboratory
ATTN: Doc. Con. for Reports Lib.

Sandia Laboratories
Livermore Laboratory
ATTN: Doc. Con. for Tech. Library

Sandia Laboratories
ATTN: Doc. Con. for 3141, Sandia Rpt. Coll.
ATTN: L. Hill

US Energy Rsch. & Dev. Admin.
Albuquerque Operations Office
ATTN: Doc. Con. for Tech. Library

US Energy Rsch. & Dev. Admin.
Division of Headquarters Services
Library Branch G-043
ATTN: Doc. Con. for Class Tech. Lib.

US Energy Rsch. & Dev. Admin.
Nevada Operations Office
ATTN: Doc. Con. for Tech. Lib.

Union Carbide Corporation
Holifield National Laboratory
ATTN: Doc. Con. for Tech. Lib.
ATTN: Civil Def. Res. Proj.

OTHER GOVERNMENT AGENCIES

Department of the Interior
Bureau of Mines
ATTN: Tech. Lib.

DEPARTMENT OF DEFENSE CONTRACTORS

Aerospace Corporation
ATTN: Tech. Info. Services

Agbabian Associates
ATTN: M. Agbabian/F. Safford

Applied Theory, Inc.
2 cy ATTN: John G. Trulio

Avco Research & Systems Group
ATTN: Research Lib., A830, Rm. 7201

Battelle Memorial Institute
ATTN: Technical Library

The BDM Corporation
ATTN: Technical Library

The Boeing Company
ATTN: Aerospace Library

DEPARTMENT OF DEFENSE CONTRACTORS (Continued)

California Research & Technology, Inc.
ATTN: Technical Library
ATTN: Sheldon Shuster
ATTN: Ken Kreyenhagen

Calspan Corporation
ATTN: Technical Library

Civil/Nuclear Systems Corp.
ATTN: Robert Crawford

University of Dayton
Industrial Security Super KL-505
ATTN: Hallock F. Swift

University of Denver
Colorado Seminary
Denver Research Institute
ATTN: Sec. Officer for Fred P. Venditti
ATTN: Sec. Officer for J. Wisotski

EG&G, Inc.
Albuquerque Division
ATTN: Technical Library

The Franklin Institute
ATTN: Zenons Zudans

Gard, Incorporated
ATTN: G. L. Neidhardt

General Electric Company
TEMPO-Center for Advanced Studies
ATTN: DASIAC

IIT Research Institute
ATTN: Milton R. Johnson
ATTN: R. E. Welch
ATTN: Technical Library

Institute for Defense Analyses
ATTN: IDA Librarian, Ruth S. Smith

Kaman AviDyne
Division of Kaman Sciences Corp.
ATTN: Technical Library
ATTN: E. S. Criscione/N. P. Hobbs

Kaman Sciences Corporation
ATTN: Library

Lockheed Missiles & Space Company, Inc.
ATTN: Tech. Infor. Center, D/COLL
ATTN: Tom Geers, D/52-33, Bldg. 205

Lovelace Foundation for Medical Education & Rsch.
ATTN: Technical Library
ATTN: Asst. Dir. of Res., Robert K. Jones

McDonnell Douglas Corporation
ATTN: Robert W. Halprin

Merritt Cases, Incorporated
ATTN: Technical Library

The Mitre Corporation
ATTN: Library

DEPARTMENT OF DEFENSE CONTRACTORS (Continued)

Nathan M. Newmark
Consulting Engineering Services
B106A Civil Engineering Building
University of Illinois
ATTN: Nathan M. Newmark

Physics International Company
ATTN: Doc. Con. for E. T. Moore
ATTN: Doc. Con. for Dennis Orphal
ATTN: Doc. Con. for Larry A. Behrmann
ATTN: Doc. Con. for Robert Swift
ATTN: Doc. Con. for Tech. Lib.
ATTN: Doc. Con. for Charles Godfrey

R & D Associates
ATTN: William B. Wright, Jr.
ATTN: Henry Cooper
ATTN: Albert L. Latter
ATTN: Harold L. Brode
ATTN: J. G. Lewis
ATTN: Technical Library
ATTN: Robert Port

Science Applications, Inc.
ATTN: David Bernstein
ATTN: D. E. Maxwell

Science Applications, Inc.
ATTN: Technical Library

Southwest Research Institute
ATTN: A. B. Wenzel
ATTN: Wilfred E. Baker

Stanford Research Institute
ATTN: George R. Abrahamson/B. R. Gasten

Systems, Science & Software, Inc.
ATTN: Thomas D. Riney
ATTN: Donald R. Grine
ATTN: Technical Library
ATTN: Ted Cherry

Terra Tek, Inc.
ATTN: Sidney Green
ATTN: Technical Library

Tetra Tech., Inc.
ATTN: LI-San Hwang
ATTN: Technical Library

DEPARTMENT OF DEFENSE CONTRACTORS (Continued)

TRW Defense & Space Sys. Group
ATTN: Pravin Bhutta, R1-1104
ATTN: Tech. Info. Center/S-1930
2 cy ATTN: Peter K. Dai, R1/2170

TRW Defense & Space Sys. Group
San Bernardino Operations
ATTN: E. Y. Wong, 527/712

Universal Analytics, Inc.
ATTN: E. I. Field

URS Research Company
ATTN: Technical Library

The Eric H. Wang Civil Engineering Rsch. Fac.
University Station
ATTN: Neal Baum

Washington State University
Administrative Organization
ATTN: Arthur Miles Hohorf for George Duval

Weidlinger Assoc. Consulting Engineers
ATTN: Melvin L. Baron

Weidlinger Assoc. Consulting Engineers
4 cy ATTN: J. Isenberg
ATTN: H. S. Levine
ATTN: S. H. Pang

Westinghouse Electric Corp.
Marine Division
ATTN: W. A. Volz